MATERIAL AND DEVICE DESIGN FOR ORGANIC OPTOELECTRONICS

Jack W. Levell

A Thesis Submitted for the Degree of PhD
at the
University of St Andrews

2011

Material and Device Design for Organic Optoelectronics

Jack W. Levell

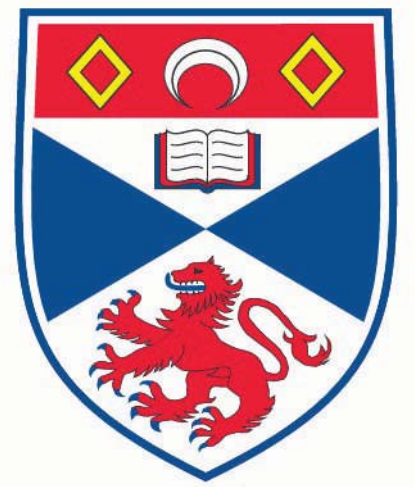

This thesis is submitted in partial fulfilment for
the degree of PhD
at the
University of St Andrews

May 2011

Abstract

This thesis describes investigations into the photophysical properties of luminescent materials and their application in optoelectronic devices such as light emitting diodes and photodetectors. The materials used were all solution processable because of the interest in low cost processing of organics.

I have investigated the photophysics of 1,4,5,8,9,12-hexamethyltriphenylene, a triphenylene derivative which has its luminescence enhanced by the addition of methyl groups. These groups change the planar shape of the triphenylene molecule into a twisted one, changing the symmetry of the molecule and increasing its dipole moment in absorption and emission by ~4 fold. This increased its rate of radiative de-excitation by ~20 times. In addition, the twisted shape of the molecule prevents intermolecular interactions and concentration effects from affecting the luminescence. This results in an efficient solid-state photoluminescence quantum yield of 31%.

This thesis also includes an investigation into phosphorescent polymer dendrimers, designed to have suitable viscosities in solution for inkjet printed OLED applications. A photophysical study of the intra-chain aggregation effects on the luminescence was undertaken in both homopolymers and copolymers with high energy gap spacer units. Using double dendrons to increase the steric protection of the luminescent cores, the best homopolymers achieved 12.1% external quantum efficiency (39.3 cd/A) at 100 cd/m^2 brightness and the best co-polymer achieved 14.7% EQE (48.3 cd/A) at 100 cd/m^2. This compares favourably with 11.8% EQE for the best phosphorescent polymer and 16% for the best solution processed dendrimer OLED previously reported.

Finally I have applied a solution processed enhancement layer to silicon photodiodes to enhance their ultraviolet response. Using a blend of materials to give favourable absorption and emission properties, 61% external quantum efficiency was achieved at 200 nm, which is better than the 20-30% typical for vacuum deposited lumogen enhancement layers used commercially.

1. Candidate's Declarations

I, Jack William Levell, hereby certify that this thesis, which is approximately 45,000 words in length, has been written by me, that it is the record of work carried out by me and that it has not been submitted in any previous application for a higher degree.

I was admitted as a research student in September 2007 and as a candidate for the degree of Doctor of Philosophy in September 2007 the higher study for which this is a record was carried out in the University of St Andrews between 2007 and 2011.

Date: 18/05/10 Signature of candidate: Jack W. Levell

2. Supervisor's Declarations

I hereby certify that the candidate has fulfilled the conditions of the Resolution and Regulations appropriate for the degree of Doctor of Philosophy in the University of St Andrews and that the candidate is qualified to submit this thesis in application for that degree.

Date: 18/05/10 Signature of supervisor: Ifor D. W. Samuel

3. Permission for Electronic Publication:

In submitting this thesis to the University of St Andrews I understand that I am giving permission for it to be made available for use in accordance with the regulations of the University Library for the time being in force, subject to any copyright vested in the work not being affected thereby. I also understand that the title and the abstract will be published, and that a copy of the work may be made and supplied to any bona fide library or research worker, that my thesis will be electronically accessible for personal or research use unless exempt by award of an embargo as requested below, and that the library has the right to migrate my thesis into new electronic forms as required to ensure continued access to the thesis. I have obtained any third-party copyright permissions that may be required in order to allow such access and migration, or have requested the appropriate embargo below.

The following is an agreed request by candidate and supervisor regarding the electronic publication of this thesis:

Access to all of printed copy but embargo of all of electronic publication of thesis for a period of 1 year on the following ground: Publication would preclude future publication

Date: 18/05/10 Signature of candidate: Jack W. Levell

Date: 18/05/10 Signature of supervisor: Ifor D. W. Samuel

Acknowledgements

This thesis and the work within it would literally not have been possible without the help of a large number of people, some of whom I've listed below.

Everyone within the organic semiconductor optoelectronics (OSO) group has been very helpful and has made my time here a pleasure. I'd like to thank Ruth Harding and Stuart Stevenson for training me in experimental techniques. Arvydas Ruseckas was lots of help with photophysics problems, in particular on the HMTP project. Graham Turnbull has been an excellent second supervisor and his constant cheerfulness has been reassuring throughout. Most of all I'd like to thank Mario Giardini. The photodiodes project was based on his original idea but he has also shown me that solving problems for a living is great fun.

Thanks go to Yi Wang and Trent Galow at the University of Edinburgh for letting me work on their fascinating HMTP material. The phosphorescent polymer work would not have happened without Paul Burn's vision and the hard work of Jack Gunning in Oxford, and Wen-Yong Lai and Shih-Chun Lo in Queensland. Wen-Yong in particular worked tirelessly and those materials presented in this thesis are only a small fraction of his total output! I wish him all the best at his new posting in Nanjing.

I'd also like to thank George Robb and Steve Balfour, without whom nothing would ever work in the cleanroom. I'm sorry about that fire alarm but if George could have a look at the health and safety considerations concerned with throwing people into the physics pond I would be very grateful.

Outside of work I've been kept sane by many people including my family, Ken Armstrong, Saif Ur-Rehman, Tosca Lynch, Nick Drewett and Fiona Howe. Life would also have been quite dull without my gaming group: Steve Grant, Alasdair Lymer, George Crossley and Joseph Collins who've helped with the other ~200 page document I've produced during my time here.

Finally I'd like to thank Ifor Samuel, my supervisor, for putting up with me and carefully reading through the many hundreds of pages of terrible English, red pen in hand.

To my parents, Bruce and Sally.

For everything.

"Understanding is a three-edged sword."

- Ambassador Kosh, Babylon 5

Table of Contents

1. Introduction

The word plastic is originally Greek and refers to materials that are easily shaped or moulded such as wax or clay. Today plastic normally refers to organic (carbon based) polymers which have these properties. By injection moulding, stamping or extruding these materials can be used for making many of low cost mass produced items in our daily lives. However, in addition to allowing low cost manufacturing, polymers can also provide us with unique materials properties. Poly-paraphenylene terephthalamide, better known as Kelvar is such a polymer which has a yield stress per unit weight more than 5 times higher than steel. It has been crucial for the development of modern body armour as well as being useful in many engineering applications. Polytetrafluoroethylene (PTFE) or teflon is highly resistant to chemical attack, making it useful for laboratory equipment, but this also leads to having non-stick properties allowing it to be used to lubricate joints without the need for oil and in non-stick cookware. These materials have properties that mean that instead of merely responding to an existing need, they have helped to define the products and applications they have been applied to.

Organic semiconductors, sometimes referred to as plastic electronics, are another revolutionary set of materials. They come in the form of conjugated polymers or small molecules that can conduct electrical currents and absorb and re-emit light. They can be applied in many of the applications of traditional inorganic semiconductors such as transistors [1], light emitting diodes [2] and photovoltaics [3]. However, unlike their inorganic counterparts they are amorphous and can be deposited from solution [4]. This means that they can be deposited over large areas quickly and at low cost but also that they can take advantage of technologies including ink jet, screen, flexographic and gravure printing for patterned deposition of optoelectronic devices. When combined with the fact their amorphous structure makes them flexible this opens up new areas of application.

Progress in the field of organic semiconductors has resulted from improved device design but also from improvements in the materials used. Organic chemistry is very flexible and capable of producing an almost endless variety of molecules which can

be used to drive progress. Much of the work in this thesis would not have been possible without the efforts of synthetic chemists who provided many of the new materials for photophysical investigation and device fabrication.

Given the large number of possible materials one clearly needs to adopt a systematic approach to material design. Dendrimers which consist of a core, dendrons and surface groups, are one example of such an approach [5]. These molecules are designed primarily for light emission and so they use a highly emissive central core. However, without isolation from neighbouring molecules, the emission from the core can be quenched. In addition the chosen cores are optimised for their emissive properties and so are often only sparingly soluble. These issues are addressed by using sterically bulky dendrimer arms with solubilising groups. As the core and dendrons can be changed independently of one another this allows us to optimise both parts of the molecule independently.

The research in this thesis explores how organic semiconductors interact with light, in particular their luminescent properties. A major theme of the work (Chapters 6 and 7) is focused on the development of materials for organic light emitting diodes (OLEDs) for display and lighting applications. The photophysics of the molecules determine their maximum effectiveness these applications, as well as adding to our basic scientific understanding. It is thus important to understand them both as isolated molecules in solution and in solid thin films that can be used to make devices.

In Chapter 2 I present an overview of organic semiconductors and many of their applications including transistors, solar cells, lasers and optical amplifers. Chapter 3 then focuses in on organic light emitting diodes in more detail. Chapter 4 covers the experimental methods used to investigate the photophyics of the materials studied and the fabrication of OLED devices.

I begin the experimental chapters in Chapter 5 with an investigation of the photophysical properties of a planar molecule triphenylene in comparison to a twisted counterpart, 1,4,5,8,9,12-hexamethyltriphenylene. Triphenylene naturally only has weak emission and absorption because its symmetry means that it does not couple strongly to light via the dipole transistion. Planar molecules also have a strong

tendency to stack on top of one another due to their shape. I show that a simple substitution to the molecule can dramatically enhanced its emissive properties by changing the symmetry of the molecule and by preventing planar π stacking in the solid state.

Chapters 6 and 7 introduce phosphorescent polymer-dendrimers, which have been developed for ink-jet printed OLED applications. Phosphorescence is important for electroluminescent materials as it allows the emission from all excited states regardless of their spin state, whereas most organic materials are fluorescent and are limited to only harvesting a fraction of these states. This limits the efficiency of most OLEDs based on fluorescent conjugated polymers. These two chapters follow the development of a class of phosphorescent polymers which aim to take advantage of the higher viscosity of polymer solutions, which is required for ink-jet printing, while also increasing emission efficiency using phosphorescence. These materials take the form of a polymer backbone with pendant dendimers and so I also investigate the effects of the dendrimer structure on the photophysics of the materials.

Chapter 6 focuses on homo-polymers, which all have the same emissive repeat unit, while Chapter 7 focuses on copolymers, where some higher energy spacer units have been introduced. These higher energy spacers help to separate the emissive cores, reducing concentration quenching, and can also be chosen to improve charge transport through devices.

In Chapter 8 I apply luminescent polymers to the problem of enhancing the ultra-violet response of silicon photodiodes. As the UV response of silicon photodetectors is very poor silicon photodiodes and charge-coupled devices (CCDs) are often coated with luminescent layers to down convert incident light to longer wavelengths. Normally these layers are deposited by high cost vacuum deposition techniques but in this chapter I show that good performance can be achieved through lower cost solution processing. By optimising a blended organic layer to provide even UV absorption, along with emission at a wavelength where the photodiode is more sensitive I take advantage of the well understood and efficient silicon technology combined with the adaptability and low cost processing of an organic semiconductor

blend. This is an example of a hybrid semiconductor device that exploits the complementary properties of organic and inorganic semiconductors [6, 7].

This thesis therefore explores the photophysical properties of solution processable luminescent materials and their use in devices. Much of this work puts an emphasis on controlling aggregation in order to produce efficient emission in the solid state. The other main themes are the systematic study of new families of materials and new applications were easily processed organic semiconductors could have a significant impact.

1. Yan, H., et al., *A high-mobility electron-transporting polymer for printed transistors.* Nature, 2009. **457**(7230): p. 679.
2. Grimsdale, A.C., et al., *Synthesis of Light-Emitting Conjugated Polymers for Applications in Electroluminescent Devices.* Chemical Reviews, 2009. **109**(3): p. 897-1091.
3. Spanggaard, H. and F.C. Krebs, *A brief history of the development of organic and polymeric photovoltaics.* Solar Energy Materials and Solar Cells, 2004. **83**(2-3): p. 125-146.
4. Forrest, S.R., *The path to ubiquitous and low-cost organic electronic appliances on plastic.* Nature, 2004. **428**: p. 911.
5. Burn, P.L., S.C. Lo, and I.D.W. Samuel, *The development of light-emitting dendrimers for displays.* Advanced Materials, 2007. **19**(13): p. 1675-1688.
6. Yang, Y., G.A. Turnbull, and I.D.W. Samuel, *Hybrid optoelectronics: A polymer laser pumped by a nitride light-emitting diode.* Applied Physics Letters, 2008. **92**(16): p. 163306.
7. Currie, M.J., et al., *High-efficiency organic solar concentrators for photovoltaics.* Science, 2008. **321**(5886): p. 226-228.

2. Organic Semiconductors

2.1 Overview

This chapter contains an overview of the importance of semiconductor technology and the development of organic semiconductors together with a discussion of the desired properties of these materials for applications in solution-processed light-emitting diodes. Section 2.2 outlines the applications of semiconductor technology and section 2.3 introduces organic semiconductors, which are promising materials for low cost and high efficiency semiconductor devices. Charge transport organic semiconductors is discussed Section 2.4, which is critical for organic electronics, and emissive excited states or excitons are discussed in Section 2.5. Finally an overview of many possible types of organic devices is given in Section 2.6.

2.2 Semiconductors

Semiconductors are extremely useful materials that are named for their capacity to function as either conductors or insulators depending on the conditions they are placed under. This property arises because they have a band gap, an energy gap where there are no allowed electronic states.

Conductors, such as metals, have a continuous electronic density of states meaning that an electron can easily be promoted to an effectively infinitesimally higher energy state with a different momentum allowing conduction even at very small applied fields. For semiconductors to conduct, either sufficient energy must be put in (in the form of heat or light) to excite carriers across the energy gap, or the carrier density

must be changed by moving the Fermi level away from the centre of the band gap by doping or injecting carriers from the electrodes. These properties allow semiconductors to be used as temperature sensors, photodetectors or switches. Taken together with the fact that they can be formed into compact and reliable solid state devices they have created a revolutionary technology. By allowing the development of the transistor by John Bardeen and Walter Brattain in 1947 [1] and subsequently the development of the microchip these materials have changed the shape of the modern world.

The majority of this thesis concerns the interactions of semiconductors with light. When a semiconductor absorbs a photon above the band gap energy, it promotes an electron to a state above the band gap and leaves behind an unfilled energy state. In semiconductor terminology this excited electron is simply called an “electron” and the empty state is called a “hole”. As the remainder of the electrons in the material, and the nuclei whose charges they screen, can be seen as a passive background we normally consider only these two entities and their properties.

By separating the electron and hole and extracting them from different sides of the device (the cathode and anode respectively) a current and voltage can be produced allowing electrical power to be generated. Using heat to produce this electron-hole pair allows thermoelectric devices [2] via the Seebeck effect [3] and using light allows us to make solar cells [4]. These are extremely useful for addressing the world’s current energy needs as well as the demand for portable energy sources. Any device that produces electrical current in response to a stimulus can also be used as a sensor. In this way semiconductors can be used as compact temperature sensors or photodetectors. Combined with the ability of semiconductors to act as transistors and logic gates, this allows the manufacture of compact imaging devices such as the now ubiquitous charge-coupled device or CCD.

Instead of separating charges produced by an incident photon we can instead make a device where electrons and holes are injected and light is emitted when the carriers of opposite polarity meet up and recombine. This allows us to produce a light source. Typically this takes the form of a light-emitting diode or LED [5] however light-emitting transistors are also possible [6]. In photovoltaic devices it is important that

the charges are separated quickly before they have a chance to recombine and decay either radiatively or non-radiatively. In a light-emitting device the priority is instead that the charge carriers recombine efficiently and that radiative decay dominates over wasteful non-radiative decay processes. Due to these different requirements different materials and device structures are used for photovoltaic and light-emitting applications. For much of this thesis I will concentrate on light-emitting materials, and in particular how their radiative properties can be enhanced so they can be used in devices.

In materials which are good emitters strong coupling to light via an electric dipole transition means that they are often also efficient absorbers of light. By using higher energy photons than the bandgap the material can be excited and then it can relax again by emitting a lower energy photon. This effect is called photoluminescence and is the basis of “day glow” and fluorescent paints which absorb ultra-violet or blue light and then emit it at longer wavelengths and so appearing to glow with their own light. Photoluminescent materials can be used for all optical devices because of stimulated emission. This is when the emissive electronic transition is induced by light of the same energy as the emitted light. If the emitted light is passed further through the material even more emission can be induced. This allows us to create medium in which there is optical gain allowing optical amplifiers or, if feedback is introduced to allow the light to pass through the material multiple times, lasers.

2.3 Organic Semiconductors

Organic chemistry refers to the chemistry of carbon based systems. Carbon is tetravalent meaning it requires four pairs of bonding electrons to complete its outmost shell. Carbon can therefore form single, double and triple bonds as well as forming conjugated systems. This makes carbon an excellent building block to form to form long polymer chains and macromolecules.

Carbon also easily forms strong bonds with nitrogen and oxygen, due to similar atomic size and well matched energy levels. This allows for functionalistion of the bare carbon skeleton. The increased electro-negativity of these elements allows the creation of dipoles for hydrogen bonding which increases solubility in water as well

as intra-molecular bonds that are critical for biological molecules in aqueous environments such as proteins, enzymes and deoxyribonucleic acid (DNA). Finally carbon is a readily available material with a well understood chemistry. Carbon compounds can readily be made from oil and extensive investigations into it's chemistry have been make in order to understand life and produce pharmaceuticals as well as making plastics for a wide variety of applications.

The electrons in a carbon atom are organised into the orthogonal 1s, 2s, and 2p orbitals. The two electrons in the 1s orbital have the lowest energy and sit closest to the carbon's nucleus meaning they have has no significant overlap with the orbitals of neighbouring atoms and so do not contribute to bonding. The second and outermost shell of orbitals contain the four electrons that allow carbon to bond to other atoms. For an isolated atom these electrons can be said to occupy the 2s zero orbital angular momentum and the three 2p orbitals (which have one unit of orbital angular momentum each in one of three orthogonal directions). The electrons are distributed with 2 in the 2s orbital and two spread among different p orbitals. When carbon is bonded to 4 atoms by σ single bonds, as in the case of diamond or methane, it forms a tetrahedral structure in which all the bonds are equivalent. In this state the orbitals are said to be hybridised into degenerate sp^3 orbitals formed from linear combinations of the 2s and 2p orbitals. Each of these sp^3 orbitals contains one electron and allows the correct symmetry for tetrahedral bonding. In a double bonded system the carbon atoms form three single bonds at 120 degrees in one plane and the double bonding occurs between the 2p orbital that lies out of the plane. The three single bonding orbitals are said to be sp^2 hybridised as they are formed from combinations of the s orbital and 2 of the p orbitals leaving the remaining p orbital free to form π double bonds and contribute to a conjugated system. The tetrahedral arrangement of sp^3 carbon and the planar arrangement of sp^2 carbon are illustrated by the 3D diagrams of ethane and ethene, respectively, in Figure 2.1. An illustration of how the p orbitals overlap in a π double bond system is shown below in Figure 2.2. When the p orbitals are in phase a π bond is formed that is filled by the 2 electrons left over from the single bonds. In ethane this is the highest occupied molecular orbital or HOMO. When the two p orbitals are out of phase they create a higher energy π* anti-bonding

orbital which is empty in ethene making it the lowest unoccupied molecular orbital or LUMO.

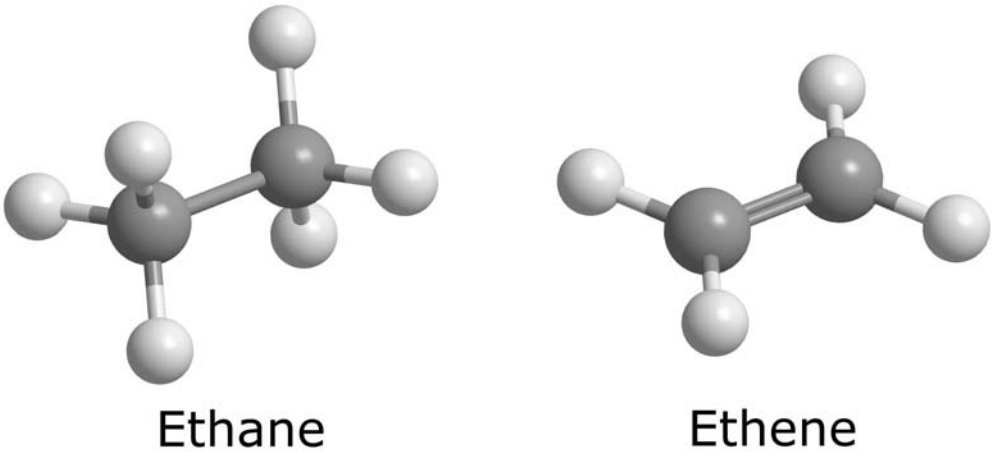

Figure 2.1 The molecular structures of ethane and ethene illustrating tetrahedral and planar bonding for sp3 and sp2 hybridised carbon respectively. This graphic was created using Chem3D Pro 12.0.

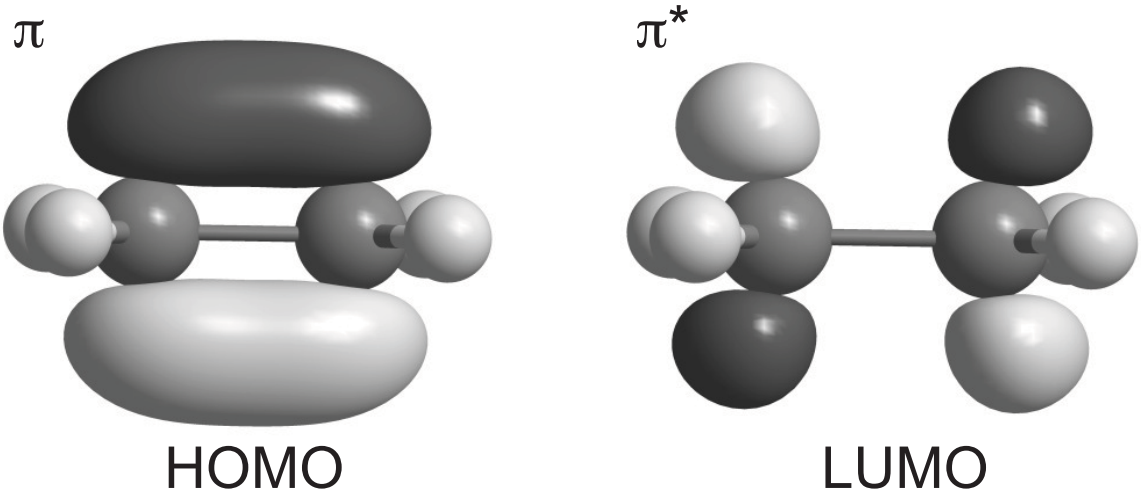

Figure 2.2 An illustration of the π bonding Highest Occupied Molecular Orbital (HOMO) and π anti-bonding Lowest Occuptied Molecular Orbital (LUMO) in ethene. This graphic was created using Chem3D Pro 12.0.*

By adopting a configuration of alternating single and double bonds, carbon atoms can form conjugated chains (such as polyacetylene) or rings (such as benzene, or larger systems like perylene) which are shown below in Figure 2.3. Conjugated systems do not in fact actually consist of alternating fixed double bonds and single bonds, instead

the p orbitals from the double bonds are delocalised over the length of the conjugated system. This is shown in Figure 2.4. This delocalisation means that if the molecule is charged by the addition or removal of an electron (known as reduction or oxidation) that charge is said to be stabilised. This is because there is a lower electrostatic energy associated with a charge if it is spread over a larger area in the same way that the capacitance of a metal plate increases with its size.

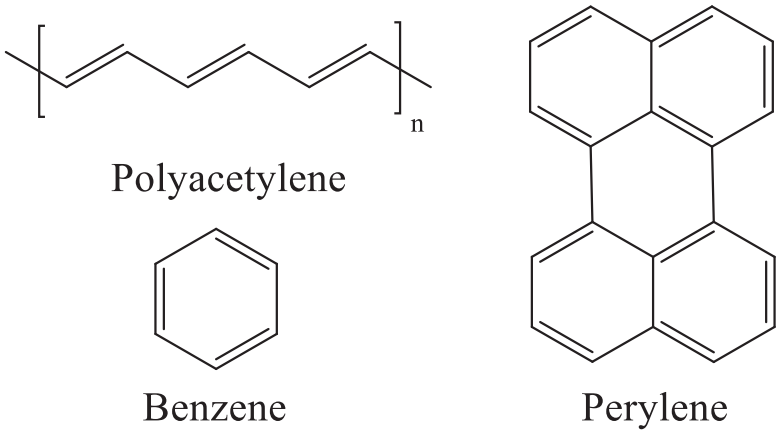

Figure 2.3 The molecular structures of the conjugated molecules polyacetylene, benzene and perylene.

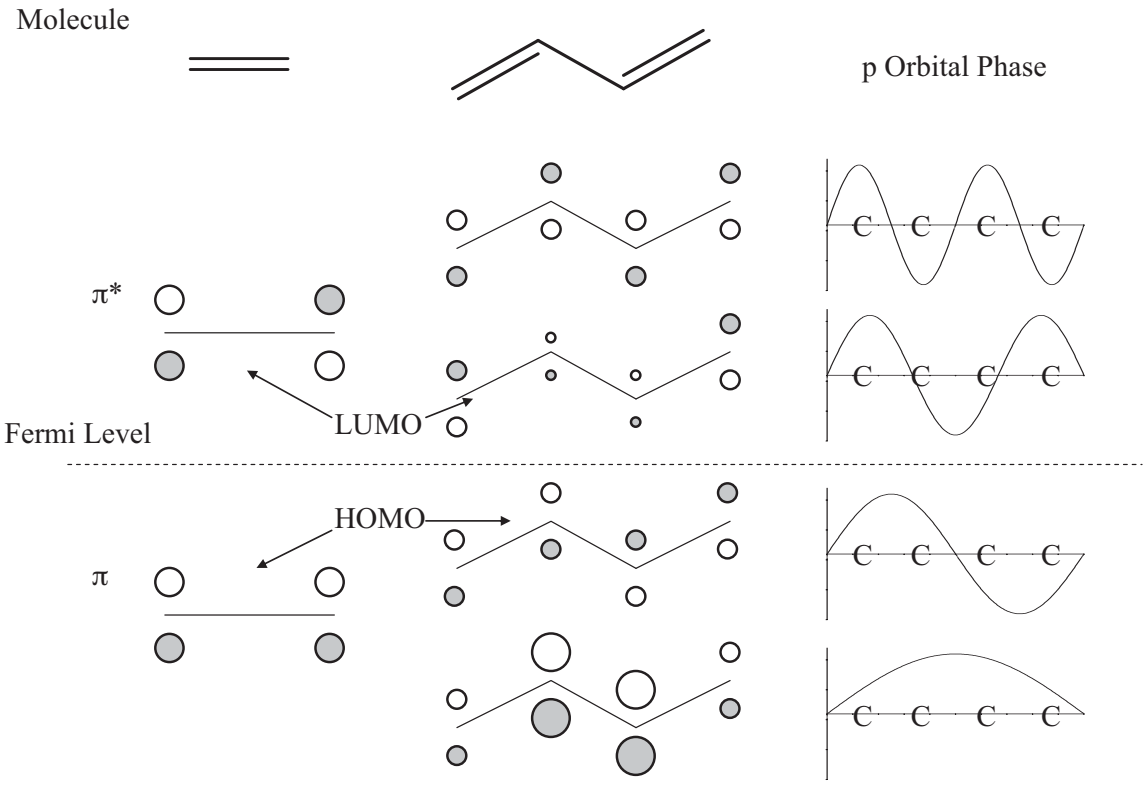

Figure 2.4 The phase relationship between p orbitals in ethene and in a short conjugated chain of 4 carbon atoms (1,3-butadiene). Each molecular orbital can

hold 2 electrons and each carbon contributes 1 electron meaning that half the π orbitals are filled.

π bonds between adjacent atoms have are formed from atomic p orbitals, which have lower orbital overlap than the s orbitals that make up σ bonds. This means that when the energy levels of the p orbitals are split by the interaction between the neighbouring atoms the energy gap between in phase π and out of phase π* orbitals is smaller than for σ and σ* orbitals. As a result there is a lower energy cost associated with promoting a π electron to a π* orbital than there would be for σ and σ* electrons. It also lowers the energy cost of adding or removing an electron from the system meaning the molecule can be reduced or oxidised more easily. Crucially the fact that the π electrons sit above and below the line between the nuclei also means that the anti-bonding repulsive interaction is weaker in π* systems than σ* systems which means that electrons can be promoted into these anti-bonding orbitals without causing the molecule to break apart. In conjugated systems these advantages are increased as the phase between individual p orbitals can be varied more slowly than between two atoms as is the case in ethene. This is illustrated in Figure 2.4 above.

The phase difference between the p orbitals of each individual carbon determine the energy level of the orbitals and whether there is an attractive (bonding) or a repulsive (anti-bonding) force between the atoms. From Schrödinger's equation we know that the second derivative of the wave function is related to the kinetic energy of the orbital from Schrödinger's equation. This is shown in Equation 2.1 where ψ is the wavefuntion, E is the energy of the wavefunction, $\hat{H}$ is the Hamiltonian, $\hbar$ is the reduced Plank constant, m is the mass of the electron and V is the electrostatic potential at a position r.

$$E\psi = \hat{H}\psi = \left(-\frac{\hbar}{2m}\nabla^2 + V(r)\right)\psi \qquad [2.1]$$

This means that the greater the phase difference between p atomic orbitals there is, in a given molecular orbital, the higher its kinetic energy is likely to be. This also means the more nodes there are in a conjugated system the higher the energy of the orbital.

As a node is a point where the wavefunction has opposite phase on either side, these imply a larger phase difference along the molecule. In addition the nodes in the wavefunction are regions where there is no electron density as the modulus of the wavefunction is zero here. With low electron density between the atomic nuclei there is reduced screening of the positive nuclear charges and less attraction of both nuclei towards the electron cloud between them. This reduces the attractive interaction between nuclei and can leave an overall repulsive force resulting in an anti-bonding orbital.

In conjugated systems, like the one in Figure 2.4, as the length of the conjugated chain increases the difference in the phases of neighbouring atoms between the HOMO and the LUMO decreases. This means a smaller band-gap and less repulsive force between the atoms in the LUMO, making the excited or charged states more stable. In addition the extended conjugated system stabilises charged states by spreading out the net charge. Taken together this leads to organic conjugated molecules being able to act like semiconductors. This was first demonstrated in perylene in 1954 by Hideo Akamatu et al. [7] and later in polyacetylene in 1977 by Hideki Shirakawa et al. [8]. These researchers found that by doping these molecules with halogens they could introduce free charge carriers into the materials and increase the conductivity by several orders of magnitude.

2.4 Charge Transport

Charge transport in organic semiconductors occurs when a molecule in a charged state transfers its charge to one of its neighbours or when one part of a polymer chain transfers the charge to the next segment. This charged state is called a polaron after the distortion introduced in the lattice of a dielectric crystal in response to a charge, an idea developed by Landau [9]. This distortion occurs as like charged ions in the structure move away from the free charge and oppositely charge ions to move towards it. This has the effect of screening the free charge and also reducing the energy of the charged system. As the energy cost of this distortion must be paid again if the charge moves this creates a local potential well that must be overcome every time the charge

moves from site to site. The energy required to overcome this barrier comes from thermal vibrations of the molecules and the electric field across the organic device. This leads to temperature and electric field dependence of the mobility in organic materials.

The ease with which charge carriers can move from site to site is determined partly by this polaron energy but also by the extent to which the polaron's wave function overlaps with that of the site it is hopping to [10]. Although the quantum mechanics of calculating the overlap of the charged state and the uncharged site may be complicated, in general this means the shorter the distance between sites the higher the hopping rate [11]. It is also important where exactly the polaron sits on the molecule and that the molecules are correctly oriented [12]. This means that charge transport in polymers can be strongly dependent on the chain alignment [13] as a result of processing conditions and subsequent annealing. It also means that the mobility is likely to be anisotropic in polymers as the polymer chains tend to lie horizontally in the plane of the substrate. More broadly, as most organic systems are disordered, the orientation and distance dependence greatly complicates any attempt to model charge mobility although recent efforts have attempted to take it into account explicitly [14, 15].

In addition to the positional disorder, organic systems contains molecules in many different conformations and environments. This creates shifts in the HOMO and LUMO levels of the individual molecules and some energetic disorder from site to site. In addition some of the sites may be chemically different, for example due to the presence of oxidised polymer units or impurities. Together these broaden the density of states for electron and hole transport and add to the temperature dependence of the mobility. The presence of trap sites, that can potentially be filled at higher carrier concentrations, also leads to a charge carrier density dependent mobility [16].

All of these effects taken together mean that it is important to measure the charge transport of materials for organic devices under the conditions they are expected to operate as the mobilties for electrons or holes may vary markedly depending on whether a device is a transistor making use of low electric fields and high carrier

densities with charges flowing horizontally, parallel to the substrate, or an LED which has higher fields and lower charge densities flowing vertically [17].

Typical mobilities in amorphous semiconductor materials, such as those used in Chapters 6 and 7 in the range of 10^{-3} to 10^{-6} cm^2/Vs. Highly ordered crystalline organic semiconductors can reach values of up to 50 cm^2/Vs. This is still low compared to crystalline inorganic semiconductors which have mobilities of about 10^3 cm^2/Vs [18].

2.5 Excited States: Excitons

As was described in Section 2.2, when light is absorbed by a semiconductor promoting an electron from the conduction to the valance band an electron and a hole are formed. These charged quasi-particles attract each other electrostatically and can form a bound state (called an exciton) in which they orbit one another [19, 20]. In typical inorganic semiconductors the dielectric constant of the material is high and so the binding energy of the electron hole pair is relatively low, meaning that the initial photon energy or thermal vibrations can easily dissociate the exciton and form free charges. Exciton formation in these materials can be seen when the material is excited below the bandgap energy at low temperatures. As the binding energy reduces the required photon energy for absorption, “excitonic” absorption bands can be seen in the region where the photon does not have quite enough energy to cross the bandgap.

When these exictons are formed the high dielectric constant means that the electron and hole orbit each other at a large radius, several times the lattice spacing. This means the electrostatic force between the particles can be thought of as resulting from the averaged lattice and thus the bulk dielectric constant can be used. These excitons are said to be Mott – Wannier excitons and they have a binding energy simply given by the binding energy for charges in a dielectric medium. This is similar to the formula for the energy levels of the hydrogenic atom in free space and is given below in Equation 2.2. Where $E_{binding}$ is the exciton binding energy, e is the electronic charge, m_* is the reduced effective mass of the electron-hole system, h is Planck’s

constant, ε is the dielectric constant and n is an integer which represents the various possible allowed exciton orbital states.

$$E_{binding} = \frac{e^4 m_*}{2\varepsilon^2 h^2 n^2} \quad [2.2]$$

In materials with lower dielectric constants the exciton radius is smaller due to the higher binding energy and so the crystal lattice cannot simply be averaged over and this simple model cannot be used. These are referred to as Poole - Frenkel excitons.

Organic semiconductors have low dielectric constants and they are not extended systems with periodic lattices. This means that the emissive state is not free electron holes recombining but localised excitons. Their excitations are related to the molecular orbitals described more fully in Section 2.3. The exciton is not well described as an electron and hole orbiting each other but instead as an excited state of the entire molecule. A third intermediate type of excition exists in donor-acceptor molecular blends, like those used in organic photovoltaics, called a charge transfer (CT) exciton. CT excitons are delocalised across a pair of donor acceptor molecules.

When the light is first absorbed it can be thought of as an instantaneous transition from the HOMO to the LUMO of the molecule. However once the molecule is excited, the nuclei will relax in a manner similar to a polaron described in Section 2.5 to a new more energetically favourable conformation. This is illustrated using the Franck–Condon diagram shown below in Figure 2.5. Both the ground state and the excited state have vibronic energy levels, which are oscillations about their preferred geometry. As the LUMO of the molecule is calculated using the ground state positions for the nuclei it is not the preferred excited state geometry and it is coupled to it by movements of the nuclei or vibronic modes. Once the exciton has settled in this state it can decay back to the electronic ground state, however the nuclei are now out of position for the preferred ground state and the molecule once again ends up in a vibrationally excited state and the nuclei have to relax back.

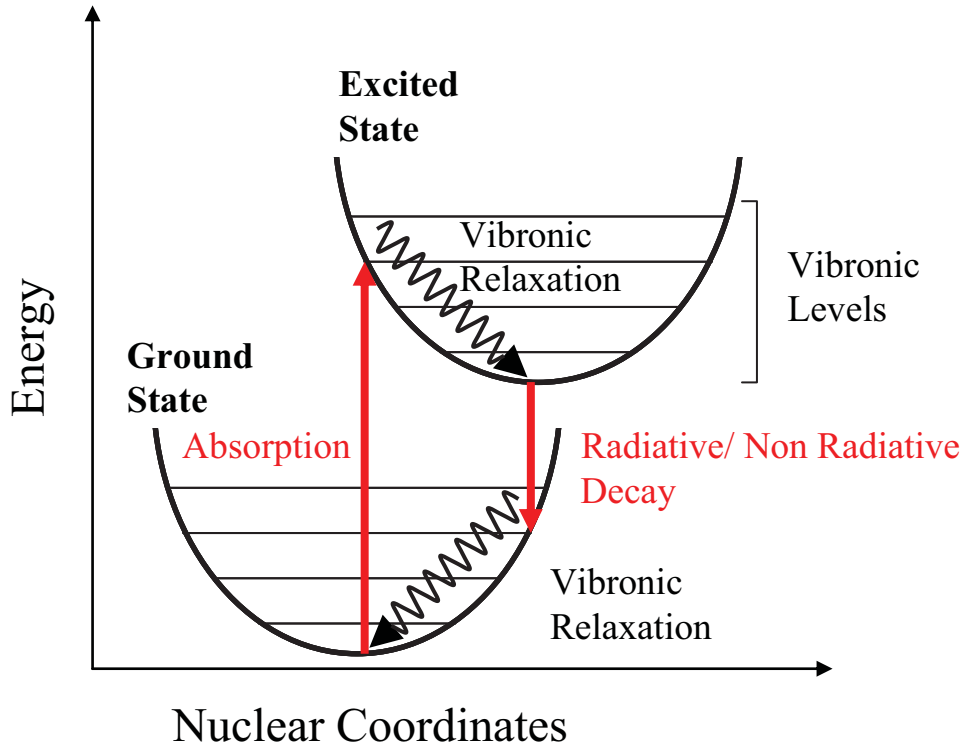

Figure 2.5 The Frank-Condon diagram illustrating the vibronic modes of the ground and excited electronic states and the transitions between them.

The result of these molecular relaxations is that the energy of the emitted light from an organic semiconductor will be lower than the excitation energy from absorbed photons. The difference between the optical absorption of a material and its emission is known as its Stokes shift.

2.6 Organic Semiconductors for Devices

Organic semiconductors have a band gap energy that naturally lies close to the visible part of the spectrum. For this reason organic molecules have long been used as dyes. An example of an organic dye is porphyrin which derives its name from the Greek word for purple and in the form of the iron complex haem is responsible for the colour of red blood cells. The black colour of coal and pencils comes from extended conjugated graphene type systems which have a small enough band gap that they efficiently absorb right across the visible spectrum. The favourable band gap energy of organic semiconductors combined with strong dipole moments, which allow

efficient coupling to light, make them attractive materials for applications involved in inter-converting light and electricity, also known as optoelectronics.

Another key advantage of organic semiconductors is that they can be readily functionalised or modified using the wide range of techniques available from synthetic organic chemistry. This allows excellent control over light-emitting and physical properties by modifying the structure of the molecules to suit the needs of the application. Organic synthetic techniques can produce the desired materials in large quantities. In addition organic materials do not require carefully grown defect free crystals that are commonly used in inorganic semiconductors. Large quantities of the material can easily be produced and stored without the final substrate even being in sight allowing the construction of separate facilities for synthesis and device fabrication.

Finally some organic molecules can be readily dissolved in organic solvents, which in addition to being a boon for organic chemists, allows easy processing of materials. The semiconductor can be dissolved in a volatile solution and coated by spin casting, doctor blading or even ink-jet printing [21] in a manner that is far lower cost than sophisticated chemical vapour deposition or molecular beam epitaxy techniques required for growing inorganic semiconductor crystals. The fabrication of entire arrays of light-emitting diodes to form a single display of usable size [22] become possible via ink-jet printing in a way that wouldn't be economical for inorganic devices. Solution-processing also allows compatibility with a wider range of substrates, which together with the flexibility of organics allows fully flexible electronic devices [22].

Not all organic molecules are soluble in common solvents or suitable for solution processing. Today much work is done using organic molecules that are only sparingly soluble in most solvents and do not form good films when spin cast. These small molecules tend to be deposited by thermal evaporation in high vacuum which is a relatively high cost processing technique. Small molecules have also been used to form high purity single crystals however the slow growth of these crystals means that they are not really suited for solution-processing on a large scale. The majority of solution processable organic semiconductors take the form of much higher molecular

weight polymers and oligomers, however solution processible dendrimers have also been developed. These molecules use a small molecule core surrounded by dendron arms which help protect the core from quenching interactions with its neighbours and help solubilise it. They are discussed in detail in Chapter 3.

Organic semiconductors have been successfully used in a wide range of semiconductor devices including transistors [23, 24], light-emitting diodes [25, 26], solar cells [27, 28] and lasers [29]. Organic transistors, LEDs and solar cells are now being produced commercially and organic lasers are now efficient and compact enough to be pumped by a single inorganic LED [30]. Organic light-emitting diodes are described in detail in chapter 3 but a basic overview of the other devices is given below.

Organic field effect transistors work by using a gate electrode that is insulated by a dielectric to populate the organic layer with charge carriers. A typical device structure is shown in Figure 2.6. Once populated the material is conducting and charge carriers can easily flow between source and drain. Aside from the obvious use of this device as a switch or amplifier OFETs are also used to study charge transport in organic semiconductors. The charge density in the organic layer is known (as it is balanced by the charge on the gate electrode) and so by measuring the source to drain current the carrier mobility in the plane of the substrate can be measured.

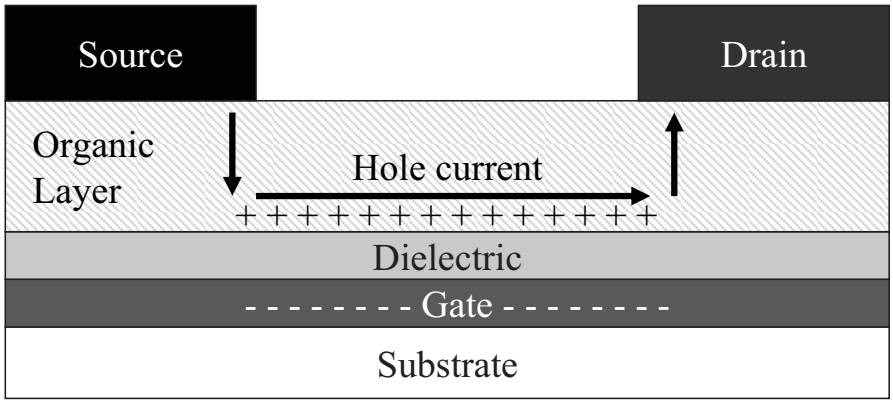

Figure 2.6 A typical p-type organic field effect transistor architecture.

Organic solar cells make use of a pair of materials called a donor and an acceptor. The purpose of the donor and acceptor is to have a mismatched HOMO and LUMO level

to split the excitons resulting from the absorbed phonons. The excited electron will transfer to the material with the lower LUMO (the acceptor) and the resulting hole will transfer to the material with the higher HOMO level (the donor). This is shown in Figure 2.7(a). An advantage of solution-processed organic semiconductors is that they can interpenetrate one another creating a bulk hetrojunction with a larger surface area, where excitons can be split, compared to evaporated organic devices. A typical device structure is shown in Figure 2.7(b).

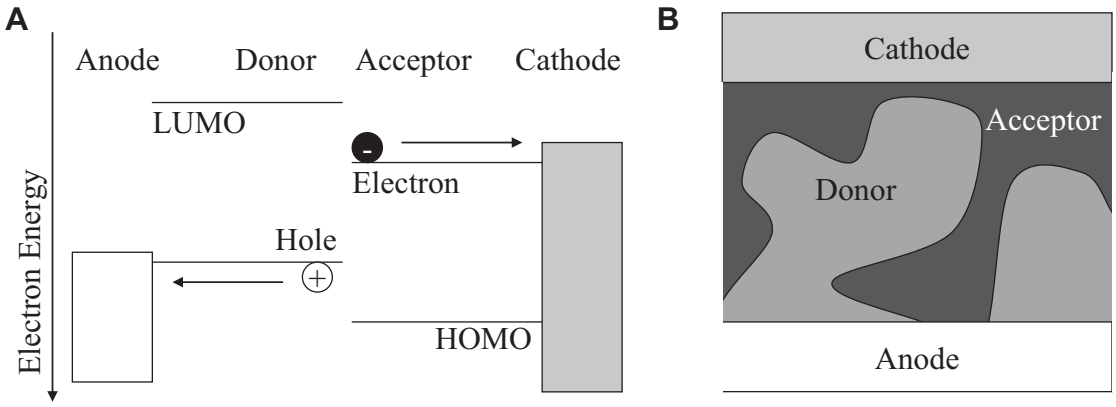

Figure 2.7 The band structure (a) and device structure (b) of a typical bulk hetrojunction organic solar cell

The key requirement for lasing is a material that can produce optical gain. This is achieved in a laser through stimulated emission, when a photon passing through the medium increases the rate at which other photons of the same wavelength are emitted. In a two level system the molecules that are unexcited will also absorb light at this wavelength thereby attenuating the light. This means that unless more molecules are in the excited state and ready to emit than are in the final state and ready to absorb the light, the material will not provide gain. This required distribution of molecular states is called a population inversion and cannot be achieved in a two level system. Fortunately, as shown in Figure 2.5, the vibronic relaxations of the excited state and ground state after transistions create a four level system in organic semiconductors and thus gain is possible. This allows the creation of optical amplifiers [31] and, by using a light pulse to depopulate the emissive level for short periods of time, optical switches [32].

If feedback can be provided so that the gain from each pass can be recycled then a laser can be produced. In organics we can take advantage of the fact that the organic layer typically has a refractive index of ~1.8, which is higher than a glass substrate, and allows waveguiding within the sample. Feedback can be introduced by etching a Bragg grating structure onto the substrate or by pressing the pattern into the lasing layer using a soft lithographic stamp this is shown in Figure 2.8. The Bragg grating is of a period choosen so that the first order scattering outcouples the laser beam and the second order scattering provides in plane feedback. This has allowed compact, solution processable lasers to be made in a range of colours [29].

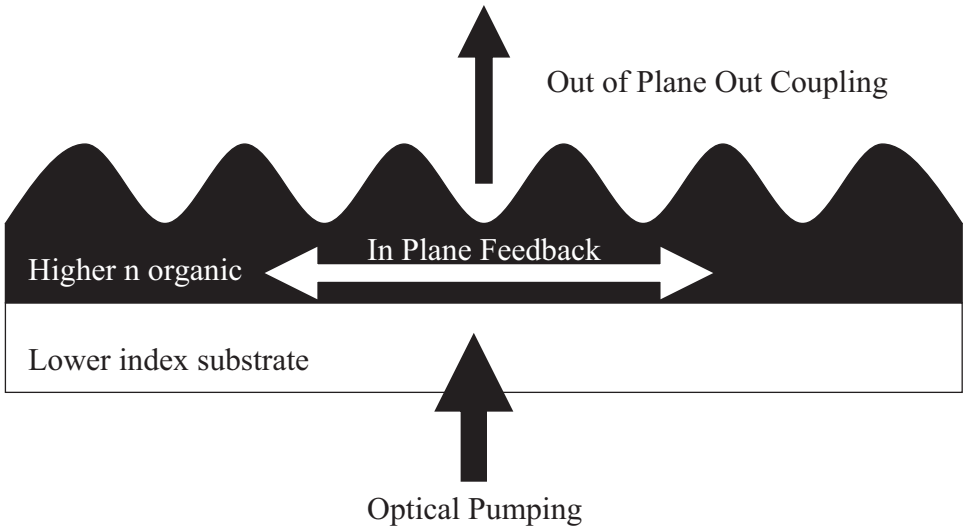

Figure 2.8 A typical organic laser using an in plane Bragg grating to provide feedback.

2.7 Conclusion

In this chapter we have highlighted the versatility of existing inorganic semiconductor technology and its importance to the modern world. We have also introduced organic semiconductors as a new class of materials that offer much of the same functionality as conventional inorganic semiconductors, together with many advantages in terms of flexibility and low cost processing.

Much of the reason for the success of organics is that modifications to the chemistry allows the development of new materials. Both solution-processing and thermal

evaporation allow emissive guests to be blended with charge transport hosts for greater OLED efficiency or acceptors to be blended with donors for efficient charge separation in solar cells. In polymers solar cells, for example, much attention is also paid to phase separation and ways to control it by varying solvent mixture and thermal annealing regimes.

This flexibility, combined with ease of solution-processing means that organic electronics is an area that is likely to have many commercial applications.

1. Brattain, W.H. and J. Bardeen, *The Transistor, A Semi-Conductor Triode.* Physics Review, 1948. **74**: p. 230.
2. Mahan, G.D., *Good thermoelectrics*, in *Solid State Physics, Vol 51*1998, Academic Press Inc: San Diego. p. 81-157.
3. Seebeck, T.J., *Ueber die magnetische Polarisation der Metalle und Erze durch Temperatur-Differenz.* Annalen der Physik, 1826. **82**(2): p. 160.
4. Chapin, D.M., C.S. Fuller, and G.L. Pearson, *A New Silicon p-n Junction Photocell for Converting Solar Radiation into Electrical Power.* 1954. **25**(5): p. 677.
5. Holonyak, J.N. and S.F. Bevacqua, *Coherent (Visible) Light Emission From Ga(As $_{1-x}$ P $_{x}$) Junctions.* Applied Physics Letters, 1962. **1**(4): p. 83.
6. Genoe, J., et al., *pnp Resonant Tunneling Light-Emitting Transistor.* Applied Physics Letters, 1992. **61**(9): p. 1051-1053.
7. Akamatu, H., H. Nokuchi, and Y. Matsunga, *Electrical Conductivity of the Perylene–Bromine Complex.* Nature, 1954. **173**: p. 168.
8. Shirakawa, H., et al., *Sythesis of Electically Conducting Organic Polymers - Halogen Derivatives of Polyacetylene, (CH)x.* Journal of the Chemical Society-Chemical Communications, 1977(16): p. 578-580.
9. Landau, L.D., *On the motion of electrons in a crystal lattice'.* Phys. Z. Sowjetunion, 1933. **3**: p. 884.
10. Bredas, J.L., et al., *Organic semiconductors: A theoretical characterization of the basic parameters governing charge transport.* Proceedings of the National Academy of Sciences of the United States of America, 2002. **99**(9): p. 5804-5809.
11. Markham, J.P.J., et al., *Charge transport in highly efficient iridium cored electrophosphorescent dendrimers.* Journal of Applied Physics, 2004. **95**(2): p. 438-445.
12. Yamada, T., et al., *Revealing bipolar charge-transport property of 4,4'-N,N'-dicarbazolylbiphenyl (CBP) by quantum chemical calculations.* Organic Electronics, 2011. **12**(1): p. 178.
13. Sirringhaus, H., et al., *Two-dimensional charge transport in self-organized, high-mobility conjugated polymers.* Nature, 1999. **401**(6754): p. 685-688.
14. Vukmirovic, N. and L.W. Wang, *Carrier hopping in disordered semiconducting polymers: How accurate is the Miller-Abrahams model?* Applied Physics Letters, 2010. **97**(4): p. 043305.

15. MacKenzie, R.C.I., J.M. Frost, and J. Nelson, *A numerical study of mobility in thin films of fullerene derivatives.* Journal of Chemical Physics, 2010. **132**(6): p. 064904.
16. Tanase, C., et al., *Charge carrier density dependence of the hole mobility in poly(p-phenylene vinylene).* Physica Status Solidi a-Applied Research, 2004. **201**(6): p. 1236-1245.
17. Tanase, C., et al., *Unification of the hole transport in polymeric field-effect transistors and light-emitting diodes.* Physical Review Letters, 2003. **91**(21): p. 216601.
18. Coropceanu, V., et al., *Charge transport in organic semiconductors.* Chemical Reviews, 2007. **107**(4): p. 926-952.
19. Liang, W.Y., *Excitons* Physics Education 1970. **4**: p. 226.
20. Wannier, G.H., *The Structure of Electronic Excitation Levels in Insulating Crystals.* Physics Review, 1937. **52**(3).
21. Forrest, S.R., *The path to ubiquitous and low-cost organic electronic appliances on plastic.* Nature, 2004. **428**: p. 911.
22. Zhou, L.S., et al., *All-organic active matrix flexible display.* Applied Physics Letters, 2006. **88**(8): p. 083502.
23. Newman, C.R., et al., *Introduction to organic thin film transistors and design of n-channel organic semiconductors.* Chemistry of Materials, 2004. **16**(23): p. 4436-4451.
24. Sirringhaus, H., *Device physics of Solution-processed organic field-effect transistors.* Advanced Materials, 2005. **17**(20): p. 2411-2425.
25. Geffroy, B., P. Le Roy, and C. Prat, *Organic light-emitting diode (OLED) technology: materials, devices and display technologies.* Polymer International, 2006. **55**(6): p. 572-582.
26. Grimsdale, A.C., et al., *Synthesis of Light-Emitting Conjugated Polymers for Applications in Electroluminescent Devices.* Chemical Reviews, 2009. **109**(3): p. 897-1091.
27. Spanggaard, H. and F.C. Krebs, *A brief history of the development of organic and polymeric photovoltaics.* Solar Energy Materials and Solar Cells, 2004. **83**(2-3): p. 125-146.
28. Scharber, M.C., et al., *Design rules for donors in bulk-heterojunction solar cells - Towards 10 % energy-conversion efficiency.* Advanced Materials, 2006. **18**(6): p. 789.
29. Samuel, I.D.W. and G.A. Turnbull, *Organic semiconductor lasers.* Chemical Reviews, 2007. **107**(4): p. 1272-1295.
30. Yang, Y., G.A. Turnbull, and I.D.W. Samuel, *Hybrid optoelectronics: A polymer laser pumped by a nitride light-emitting diode.* Applied Physics Letters, 2008. **92**(16): p. 163306.
31. Amarasinghe, D., et al., *Broadband solid state optical amplifier based on a semiconducting polymer.* Applied Physics Letters, 2006. **89**(20): p. 201119.
32. Amarasinghe, D., et al., *Picosecond gain switching of an organic semiconductor optical amplifier.* Applied Physics Letters, 2008. **92**(8): p. 083305.

3. Organic Light Emitting Diodes

3.1 Introduction

In the previous chapter on organic electronics I discussed the basics of light emission and charge transport in organic materials. By placing a thin ~100 nm layer of an emissive, semiconducting material between two electrodes we can electrically excite its luminescence and create an Organic Light Emitting Diode (OLED) [1]. Like their inorganic LED counterparts, OLEDs have significant practical applications. At present OLEDs are being developed commercially and have been deployed to replace

liquid crystal displays in mobile phones, cameras and televisions. The first OLEDs for lighting products are available commercially and in the near future are likely to offer an alternative to fluorescent and halogen lights.

In Section 3.2, I will discuss how to characterise an OLED and determine its fitness for display and lighting applications. In Section 3.3 I will introduce an overview of light emission in OLEDs and the parameters that result in good OLED efficiency. The development of materials for OLEDs is discussed in Section 3.4 and the design of OLED device structures is covered in Section 3.5.

3.1.2 OLEDs vs. LCD Displays

The main flat screen display technology in use at the moment is the liquid crystal display (LCD). Colour LCDs work by having a series of colour filters in front of a backlight and modulating the light transmission through each pixel. This is achieved by using electric fields to change the orientation of the molecules in the liquid crystal and their birefringence properties. This allows variable amounts of light to be transmitted through crossed polarising filters. This scheme is shown below in Figure 3.1. Unfortunately this means that there are significant loses in the light from the back light: half of the light is lost at the first polariser, assuming the liquid crystal is 100% efficient and rotating the transmitted light there are no losses there or at the second polariser but a minimum of 2/3^{rds} of the light must be lost at the colour filter. This means in optimal cases and when the screen is showing white only 1/6th of the light emitted by the backlight can reach the viewer.

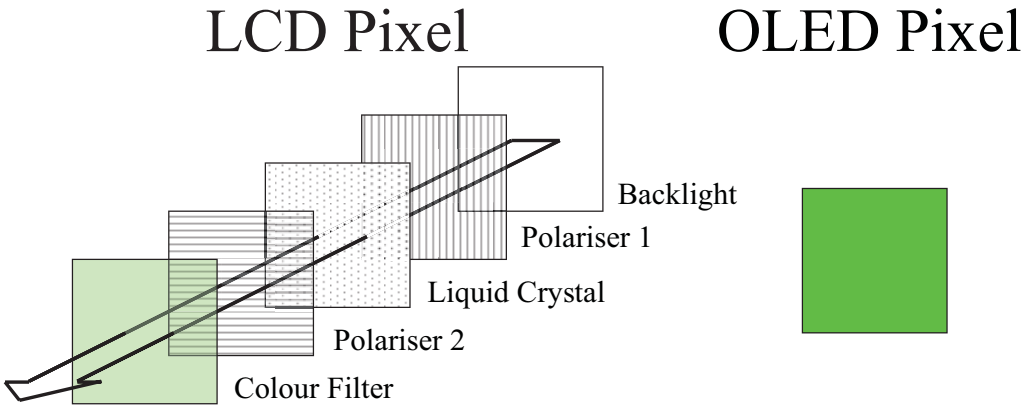

Figure 3.1 A comparison of the structure of an LCD pixel to an OLED pixel.

In addition if a white (rather than narrow line width red, green and blue LED) backlight is used the narrower the colour filters, and greater the colour purity, the more light is lost. This makes LCD displays intrinsically less bright and more limited in their colour purity than OLED displays which control the brightness of the pixel directly.

The LCD system is thick and this limits the possible viewing angle and takes up space in compact devices. By contrast the OLED device can be less than a micron thick and so has no viewing angle issues. Finally when showing blacks the LCD display is wasting the backlight power as it simply shutters off the backlight. This process is also imperfect allowing some light to leak through and limiting the contrast ratio. OLEDs are off when the pixels are not required, saving power and giving better contrast ratios. OLEDs can achieve ratios of 1,000,000:1 compared in the dark to only 10,000:1 for LCDs and commercial LCD displays can have a ratio less than 1,000:1. Contrast ratios for OLED screens in practice are limited mostly by reflected light [2]. Performing well when showing black is a significant advantage when viewing movies as darkness and shadow are often used to provide drama in cinema releases. It is less important when viewing text, which tends to be black on white.

Another advantage of OLEDs over LCDs is that the liquid crystal can take time to re-orient in response to the applied field. This can lead to response times of 15-25 milliseconds per frame. OLEDs can be turned on and off much faster than this and have been pulsed as quickly as ~100 ns [3]. In practice the fastest switching speed is determined by the capacitances in the pixel and the speed at which the pixels can be addressed. In any case this allows faster refresh rates with OLED displays for high performance applications where motion tracking is important, for example in computer games or watching sport.

Finally OLEDs and organic transistors are compatible with flexible substrates allowing flexible displays. This might allow concepts such as flexible “e-paper” but also means that the devices are less vulnerable to sudden impacts than rigid LCD displays. These are both features that are attractive for portable applications.

3.1.3 OLEDs for Lighting

White OLEDs have advantages over fluorescent lighting in power efficiency [4] and producing more aesthetically pleasing orange "warm" white colours [5, 6] (see section 3.2 below). They also have the advantage that they are available in thin layers that provide an even light over a large area. This in particular reduces glare and so does not require luminaires or light fittings to provide uniform illumination. This means the light fittings require less space and avoid efficiency losses associated with luminaires. These panels could even be flexible conforming to curved surfaces allowing more choices to architects or making it easier to fit lighting to vehicle interiors. The large OLED lighting panels move in the opposite direction to inorganic LED lighting which uses expensive chips driven at very high brightnesses, due to their high cost of fabrication per unit area, increasing glare and the requirement for luminaires.

3.2 Characterising OLEDs: Device Parameters

An overview of the parameters on which OLEDs are assessed is given here, while the experimental details of the determination of the various device parameters are given in Chapter 4.

3.2.1 Power Efficiency

The simplest device parameter to understand is power efficiency. Clearly for any given application it is better if a given amount of light can be produced for the smallest possible amount of electrical power.

When calculating the useful amount of light put out by a light source we cannot simply measure its output in Watts because the human eye is not equally sensitive to all wavelengths (as shown in Figure 3.2). We instead need a new unit that measures the amount of useful light based on the eye's perceptions. This perceived brightness is measured in lumens or lm and so the power efficiency is measured in lumens per Watt or lm/W of electrical power.

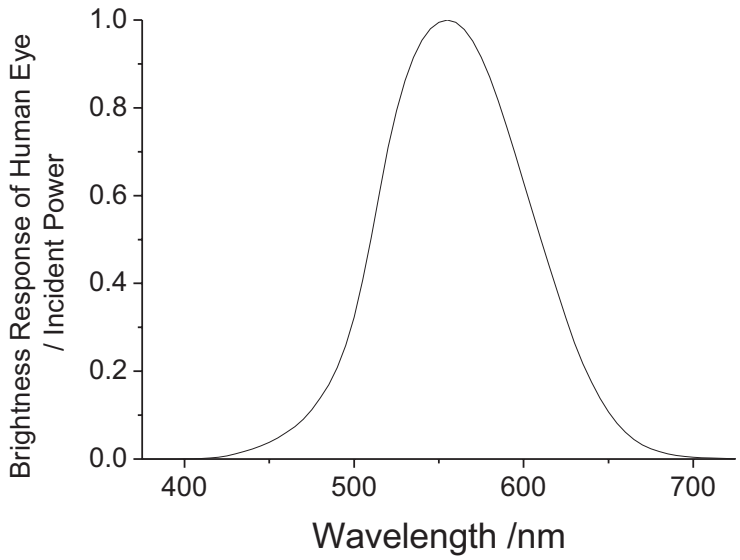

Figure 3.2 The brightness response of the human eye to incident power at a given wavelength.

Like their inorganic counterparts OLEDs are capable of high power efficiency. While "energy efficient" fluorescent lighting tubes typically have power efficiencies 60-70 lm/W, white OLEDs have been demonstrated with over 90 lm/W [4]. OLEDs have an advantage because fluorescent lights work by producing blue or ultraviolet light and then use fluorescent coatings convert some of this light to longer wavelengths, producing overall white light. By contrast a white OLED works by producing white emission directly. This is often from multiple emissive materials working together in the same device. This means that narrower energy gap materials can be used in OLEDs lowering the voltage required to operate the devices and thus the power requirements.

3.2.2 Brightness

The brightness of a device being viewed directly is measured in the number of lumens they radiate per steradian in the viewing direction. One lumen per steradian is known as a candela. For a point light source viewed from a distance (like a navigation light) the brightness is best described in candela using all the light emitted for the device, however for extended objected viewed from nearby (like a display) the best measure of brightness is in cd/m^2. This unit is also referred to as the "nit". For displays a

brightness of 200-300 cd/m^2 is a typical maximum brightness and 100 cd/m^2 is typical of normal usage and so it is best to assess the performance of OLEDs for displays at this brightness.

3.2.3 CIE Colour Co-ordinates

For OLEDs for display applications it is important to describe what colour the display will appear to be to the viewer. This is normally expressed as the Commission internationale de l'éclairage (CIE) x and y coordinates which measure the relative amount of red and green between, 0 and 1, in the spectrum of a device respectively [7]. The amount of blue is whatever fraction remains, thus low x and y coordinates correspond to blue, low x and high y is green and high x and low y is red. The possible colours that can be produced using this coordinate system are plotted on the 1931 CIE colour diagram below.

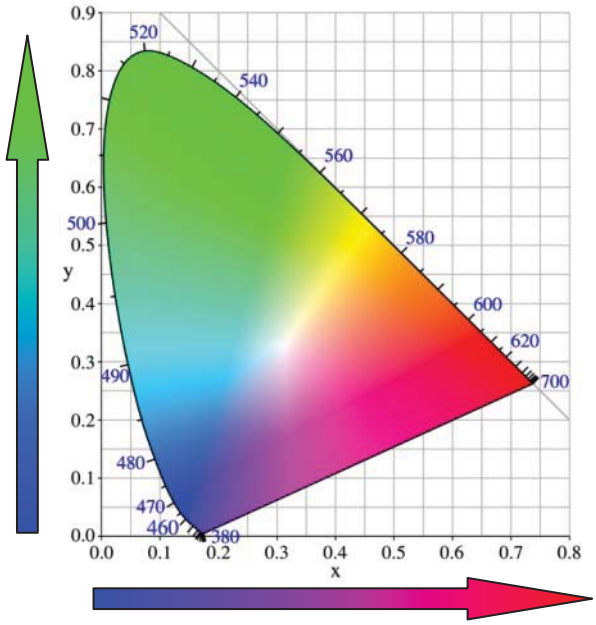

Figure 3.3 The CIE 1931 colour diagram. The x-axis corresponds the fraction of red and the y axis corresponds to the fraction of green in a given colour.

The CIE coordinates of a given light source are found by multiplying its power spectrum of the source by three functions, $\bar{x}(\lambda)$, $\bar{y}(\lambda)$ and $\bar{z}(\lambda)$, which correspond to the colours red, green and blue respectively. These functions are plotted below in

Figure 3.4. The green response $\bar{y}(\lambda)$ also happens to correspond the eye's brightness response described above in Section 3.2.1.

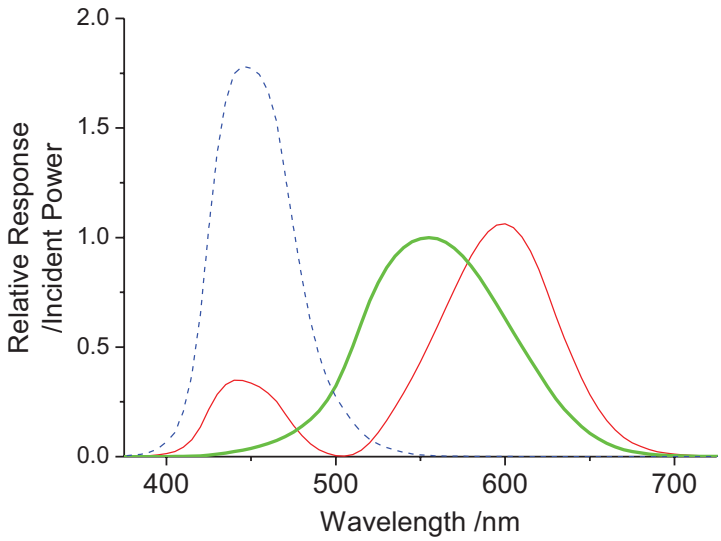

Figure 3.4 The CIE 1931 colour matching functions $\bar{x}(\lambda)$ (dashed blue line), $\bar{y}(\lambda)$ (thick green line) and $\bar{z}(\lambda)$ (thin red line).

Using the $\bar{x}(\lambda)$, $\bar{y}(\lambda)$ and $\bar{z}(\lambda)$ functions the amounts of red (X), green (Y) and blue (Z) can be determined using the integrals 3.1, 3.2 and 3.3 below. Here $\beta(\lambda)$ is the emission spectrum in units of photons per unit wavelength that has been converted into the power per unit wavelength by dividing by the wavelength λ.

$$X = \int \frac{\bar{x}(\lambda)\beta(\lambda)}{\lambda} d\lambda \qquad [3.1]$$

$$Y = \int \frac{\bar{y}(\lambda)\beta(\lambda)}{\lambda} d\lambda \qquad [3.2]$$

$$Z = \int \frac{\bar{z}(\lambda)\beta(\lambda)}{\lambda} d\lambda \qquad [3.3]$$

Ignoring the brightness of the source the fraction of green and red response gives the CIE x and y coordinates respectively using Equations [3.4] and [3.5] below. This allows the colour of the OLED to be plotted on the CIE colour diagram shown in Figure 3.3.

$$x = \frac{X}{X + Y + Z} \quad [3.4]$$

$$y = \frac{Y}{X + Y + Z} \quad [3.5]$$

For colour displays pixels should have the most saturated possible colours possible so that they can be used in combination to show the widest possible array of colours. It has been a challenge to produce deep blue emitting devices because it can be difficult to find suitably high energy band gap materials [8, 9]. This means achieving pure blue emission, as well as high efficiency is a key requirement for OLEDs for displays.

3.2.4 Colour Rendering Index

The faithfulness with which colours are reproduced when illuminated by a light source is measured by a number called the colour rendering index or CRI. A value of 100 is the best possible CRI and corresponds to a reference good quality white source. A light which does not have even light emission across the visible may appear white when looking directly at it while still being not be useful for trying to illuminate coloured objects because parts of the objects reflection spectrum can fall into gaps in the emission spectrum of the light source. For displays and signs the colour rendering index is not important as the devices will not be used to illuminate objects but are designed to be viewed directly.

The phosphors for down conversion in fluorescent lights often give imperfect white emission and don't evenly cover the spectrum. OLEDs typically use materials with relatively broad emission spectra giving a more even coverage. The phosphors can also let though a relatively large amount of blue light leading to "cold" white light which can be less aesthetically pleasing than the "warm" emission that is more weighted towards the red from black body emitters like older incandescent light bulbs or the sun. As OLEDs do not rely on these phosphors it is easier to modify their emission to give a more pleasing neutral or warm orange white. One way of quantifying this factor is to try to fit the spectrum to that of the nearest black body spectrum to give a "colour temperature" for the light source in Kelvin. Ironically this

means that “cool” bluish emission is assigned a high colour temperature (often over 10,000 K) and “warm” reddish light is assigned a lower temperature (say 3,000 K)!

3.2.5 External Quantum Efficiency and Luminous Efficiency

For research applications another companion to power efficiency is external quantum efficiency, which is the number of photons that are emitted from the device per electron passed through it. As is noted later in Section 3.4.4 not all photons escape from the device and so if a calculation is performed to find how many photons were created within the device we can find the internal quantum efficiency.

External quantum efficiency is a parameter that is useful in a research context but is not directly valuable in a finished device. While power efficiency can be improved by reducing drive voltage by optimising device thicknesses, cathode and anode materials and by choosing high mobility host materials (all of which are discussed further on in this chapter) external quantum efficiency provides a measure of how efficient a material can be in a device context before this optimisation has been done and so it is a measure of the material’s promise. Luminous efficiency per unit current (measured in cd/A) is a closely related parameter. For a given emission spectrum or colour of device these numbers are related by a simple ratio determined by the human eye’s sensitivity to that colour. This means that luminous efficiency values are highest for green devices and lower for red and blue devices for a given external quantum efficiency.

3.2.6 Lifetime

Another important parameter for practical devices is the lifetime. The time that a device can function at a given initial brightness before its brightness has dropped to 80% or 50% without changing the drive conditions is the T80 or T50 lifetime. The lifetime of OLEDs is affected by the choice of materials used but as these are degraded by the leakage of oxygen or water into the device the technology used to encapsulate the devices is very important. In addition longer lifetimes can be achieved by avoiding the use of reactive metals in the devices as the cathodes. Currently lifetimes for OLED displays and lighting panels used commercially are rated to

exceed 10,000 hours of continuous use and some exceed 100,000 hours. In practice these tests are done using accelerated aging techniques to model performance.

3.3 Light Emission In OLEDs

In order to be a suitable choice of material for use in the emissive layer of an OLED a material must first be an efficient light emitter. This is measured by seeing what fraction of excitations of a molecule result in the emission of a photon and what fraction decay non-radiatively. If an optical excitation is used this number is called the photoluminescence quantum yield or PLQY (Φ) [10, 11].

Provided the electron and hole recombine to form a singlet exciton there is no difference between optically excited molecules and electrically excited molecules and so the PLQY is a relevant parameter for choosing which materials are suitable for use in OLEDs. Unfortunately ~75% of electrons and holes will instead recombine to form a triplet exciton, which is non-emissive in ordinary fluorescent emitters. Some materials, known as phosphorescent emitters, also allow emission from the triplet excitons. This effect is discussed in detail in Chapter 6, which concerns phosphorescent polymers. In this chapter the ratio of singlet to total excitons formed is expressed as η_{spin}.

For electrical current through an OLED to produce light, electrons and holes must recombine rather than simply passing all the way through the device from one side to the other. In the best organic devices careful device design means that close to 100% of charge carriers recombine effectively. This recombination or capture fraction is $\eta_{capture}$.

Finally any light emitted by the emissive material must find a way to leave the device. Unfortunately solids have higher refractive indexes than air and this leads to a situation where emitted light can be trapped in waveguided modes inside the device. Organic semiconductors typically have a refractive index of about 1.6-1.8 [12-14]

which is lower than most inorganic semiconductors but still poses problems for light extraction if no special steps are taken.

In simple planar devices with no out-coupling enhancement the light is trapped in the device if it is totally internally reflected at the air interface. Using a ray optical model this will happen if the light is emitted outside the escape cone i.e. an angle to the normal greater than the critical angle θ_c. The condition for internal reflection is shown in Equation 3.6. The lower refractive index of the intermediate layers (such as the glass substrate) does not allow more light to be extracted as any light passing out of the organic layer into the lower index layer will be refracted following Snell's law which keeps the critical angle for light emission in the organic layer exactly the same even though the critical angle in the lower index layer θ_{gc} is higher. Thus the formula for the critical angle θ_c is given by Equation 3.7 below.

$$n_{organic} \sin\theta_c = n_{glass} \sin\theta_{cg} = 1 \qquad [3.6]$$

$$\theta_c = \sin^{-1}\left(\frac{1}{n_{organic}}\right) \qquad [3.7]$$

As the cathode is generally reflective in OLEDs any light emitted in this direction at less than the critical angle will also be reflected out of the device. This escape cone model is illustrated in Figure 3.12 and by integrating over all solid angles it leads to a fraction of light being coupled out of the device given by η_{out} in Equation 3.8.

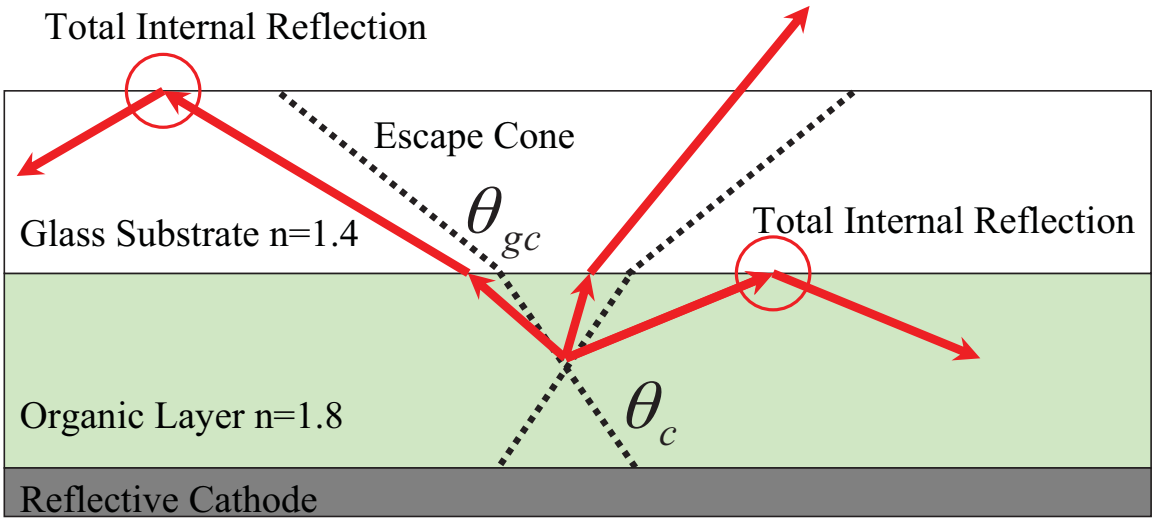

Figure 3.5 The escape cone model of light extraction from an OLED.

$$\eta_{out} = 1 - \cos\theta_c = 1 - \sqrt{1 - \frac{1}{n_{organic}^2}} \qquad [3.8]$$

Using a refractive index of 1.6-1.8 this gives a light extraction efficiency η_{out} of 22-17%. Thus ~20 % can be used as a rule of thumb to estimated the extraction efficiency of an OLED device. Of course this model uses ray optics in a wavelength scale structure and neglects micro-cavity effects arising from reflection and absorption at the metal electrode and transparent electrode interfaces [15]. Together with refractive index changes with wavelength these effects can lead to significant changes in the emission spectrum of devices compared to the emission of isolated chromophores [9]. Finally this model has assumed that the emission from the molecules in the device is isotropic where-as polymers can be expected to lie in the plane of the device and so their emission dipoles cannot be assumed to give isotropic emission.

Taking the fraction of charges that recombine $\eta_{capture}$, the fraction singlet excitons formed (if the material is fluorescent) η_{spin}, the PLQY Φ and the light extraction efficiency η_{out} the external quantum efficiency of a device is given by Equation 3.9. Thus by maximising each of these parameters efficient OLEDs can be produced.

$$\Phi_{EQE} = \eta_{capture} \times \eta_{spin} \times \Phi \times \eta_{out} \qquad [3.9]$$

3.4 Materials for OLED devices

The very earliest work on organic electroluminescent devices was in 1953 in thin crystalline films of acridine orange [16] which was dissolved in cellulose. The first reported thermally evaporated organic light emitting diode or OLED was made in 1987 using 8-hydroxyquinoline aluminium (Alq_3) [17]. The first work on solution processable organic molecules came in the form of conjugated polymers, initially poly(vinylcarbazole) (PVCz, also known as PVK) which was patented in 1976 [18] and later published on in 1983 [19, 20] and later poly(p-phenylene vinylene) (PPV) in 1990 [21]. The chemical structures of acridine orange, Alq_3, PVK and PPV are shown below in Figure 3.6.

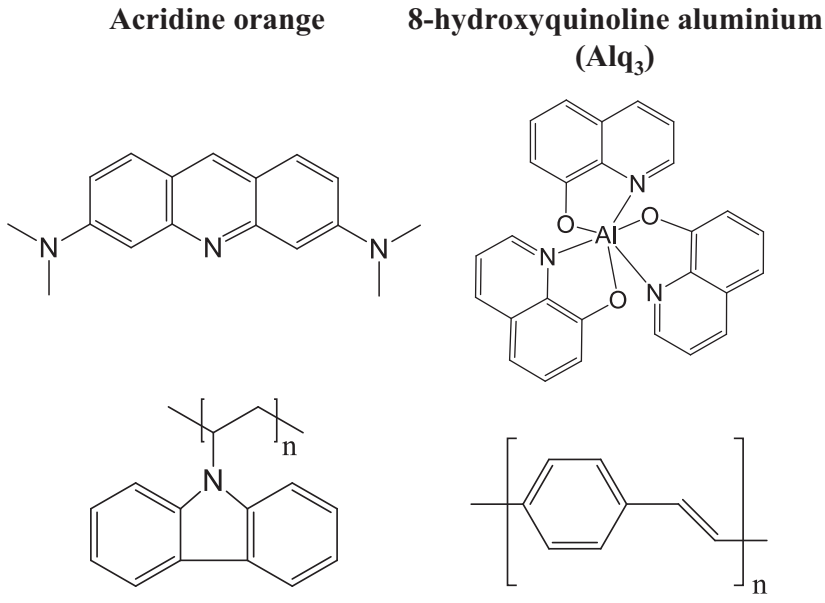

Figure 3.6 The structures of materials used in the development of early OLEDs.

As was discussed in Chapter 2, solution processing of OLEDs offers significant advantages over thermal evaporation as it is a lower cost fabrication method. Unfortunately the complexity of device structures that can be used with solution processed materials is limited by the fact that previously deposited layers can be washed away during the formation of other layers [22]. This problem can be avoided

by using orthogonal solvents for the next layer that will not dissolve the previous one. A good example of this is the adding a layer of the water soluble conducting polymer poly(3,4-ethylenedioxythiophene) poly(styrenesulfonate) or PEDOT:PSS [23]. This polymer is often used to improve electrical contact and hole injection at the anode and is insoluble in most organic solvents. Alternatively thermal [24, 25] or ultraviolet [26] cross-linking can be used to make previous layers insoluble but these add processing steps and put extra requirements on the materials used. As solution processing is lower cost but multilayer evaporated small molecule devices can have higher performance both approaches have been developed over the last two decades.

3.4.1 Host-Guest Blending

In a single material OLED the emissive material must also be optimised for its charge transport properties and it can be difficult to optimise both emissive and charge transport properties at the same time. An alternative is to use a second material to transport the charge carriers and doping this material with the emissive material. This strategy is called host-guest blending. The host can have a higher LUMO and lower HOMO energy than the emissive material so that both charges hop off the host and onto the emissive guest. This does not necessarily need to be the case however as provided the energy gap of the guest is narrower than that of the host the excitations will form on the host and lose energy transferring to the guest [27]. This can also work with larger energy gaps provided the energy gap difference is lower than the Boltzmann thermal energy [28]. If, however, the host has a lower energy gap than the emissive material excitations can transfer back and be lost [29]. This can be problematic for high energy blue emitters [30]. Preferably the host will also have a long lifetime for excited states so that excitations will have a long time to transfer from the host to the emissive guest.

3.4.2 Phosphorescent Emitters

In OLEDs most electrons and holes combine to form triplet excitons while only a minority form singlet excitons in which can emit light in fluorescent materials. This puts a significant limit on the efficiency of these materials. By incorporating heavy

metal complexes it is possible to make materials that can emit from the triplet state and thus dramatically improve the maximum efficiency of devices. These materials are said to be phosphorescent.

Only phosphorescent materials allow emission from both singlet and triplet excitons [31, 32] that are formed within an electroluminescent device and thus allow 100% internal quantum efficiency [4, 33-35]. Recently phosphorescent emitters have allowed power efficiencies of 90 lm/W at 1,000 cd/m^2 in white OLEDs that exceed the 60-70 lm/W typical for fluorescent tubes [4].

Small molecules used to have the advantage over conjugated polymers in that they could be heavy metal complexes, which allow phosphorescent emission where as solution processable conjugated polymers were typically only capable of fluorescent emission at room temperature. However, more recently phosphorescent polymers have been develop like those discussed in Chapters 6 and 7.

An alternative approach is to make small molecules into solution processable dendrimers by surrounding small molecule cores with branched dendrons which make the cores soluble [36].

Singlet excitons form when a material is excited by an electric dipole transition when absorbing a photon or under electrical excitation when an electron hole pair recombines in such a way that their net spin is zero. In fluorescent materials these can quickly relax to the ground state and emit light via a dipole transition without difficulty. For the triplet exciton the electron hole pair forms in such a way as to have a net spin of 1. These two types of excitons are illustrated in Figure 3.7.

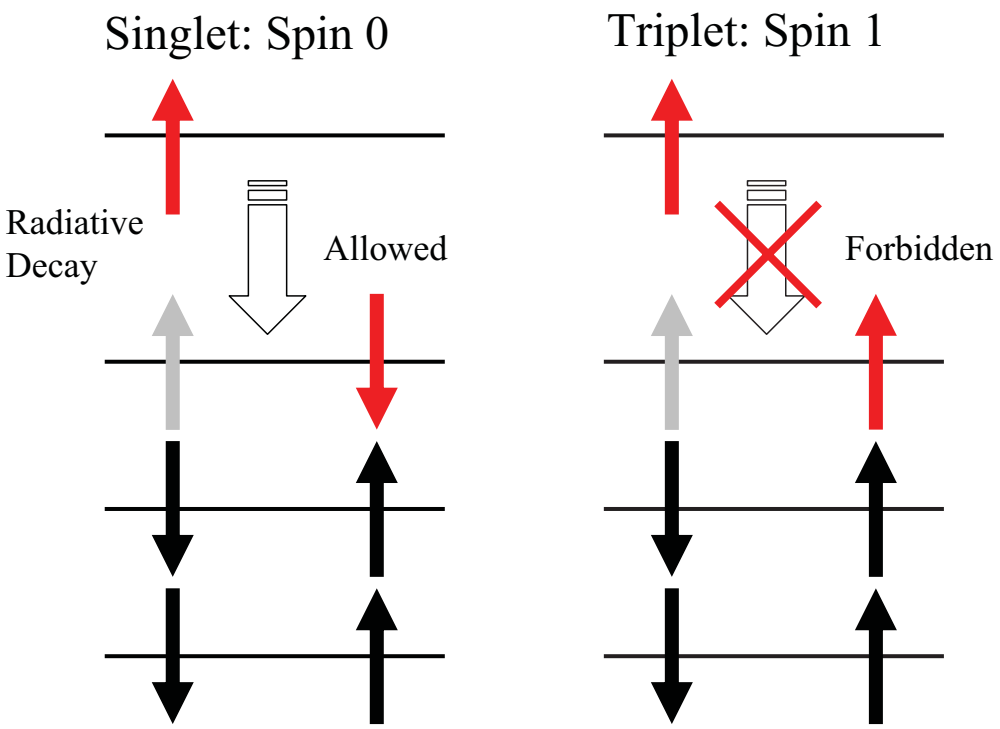

Figure 3.7 Spin configurations in singlet and triplet excitons (shown by solid arrows). The highest energy electrons which make up the excitions are shown in red and the vacant state left by the hole is shown in grey. Triplet excitons cannot decay by the electric dipole transition as this cannot flip the electron spin and the Pauli Exclusion Principle means that two electrons in the same energy level cannot have the same spin.

As electron spin is not coupled via the electric dipole transition the triplet cannot radiatively decay back to the ground state (which has zero spin). Even if this was not the case the symmetry of the triplet and singlet orbital wavefunctions means that the dipole transition between them is zero. This problem is overcome in organic phosphorescent materials by including a heavy metal atom that can couple the spin and angular momentum of the orbiting electrons. This allows triplet excitons to decay radiatively but at the cost that the dipole transition is much weaker than in fluorescent materials, this means that the radiative lifetime is longer. In phosphorescent materials this can take seconds or minutes and it means these materials are often used for "glow in the dark" applications instead of nanoseconds which are typical of fluorescent materials like those seen in Chapter 5. As a result of the longer lifetimes in phosphorescent materials triplet-triplet annihilation can become a significant loss mechanism at high excitation densities and OLED brightnesses [37]. As a result the

phosphorescent materials used in OLEDs have lifetimes order of 1 or 2 microseconds in order to reduce triplet-triplet annihilation.

The ratio of singlets to triplets in electroluminescent devices might be expected to be 1 to 3 from the argument that there are 3 possible states making up the triplet (spin in the z direction of 1, 0 or -1) and only one possible singlet state. This is referred to as the spin – statistics argument. The exact ratio of singlets to triplets is difficult to measure but this 1 to 3 ratio has been disputed [15, 38, 39]. For example careful optical modelling could not explain the high efficiency of a poly(p-phenylene vinylene) based OLEDs without invoking a higher ratio of singlets to triplets [15]. In one case a phosphorescent polymer capable of giving emission from both singlets and triplets, and doing so at different wavelengths, was used to probe the singlet to triplet ratio [39]. In this case it was found that the individual monomers did indeed result in a 22 ± 1 % singlet states however in the case of the platinum based polymer the fraction of triplet states was found to rise to 57 ± 4%. This result suggests that the ratio of singlets to triplets can vary. This is believed to be based on different capture cross sections for electron hole pairs dependent on their spin ratios. This effect seems to cause divergence from the 1:3 ratio in some materials. Nevertheless phosphorescence would still offer at least at least a factor 2 increase in the maximum quantum efficiency of devices made with these materials.

Triplets have a lower energy than singlets in the same material because of the exchange interaction. This results from the fact that electrons are fermions and thus that they must have anti-symmetric wavefunctions under exchange (bosons are symmetric under exchange). Anti-symmetric under exchange means that if any two electrons are relabelled in the wavefunction for all the electrons in a system the sign of the overall wavefunction must change. If the spin parts of the wavefunction are symmetric under exchange (which is the case for a triplet) then the orbital parts of the wavefunction are anti-symmetric which puts a greater distance between the electrons minimising electrostatic repulsion. In the singlet, the spin parts of the wavefunction are anti-symmetric and thus the orbital parts of the wavefunction must be symmetric and so the electrostatic repulsion is higher. This can be seen most easily in a two particle system. The two particle wavefunctions for the singlet and the three triplet states are given below in Equation 3.10 and Equation 3.11-3.13 respectively. The

multielectron wavefunctions, Ψ, are shown as a function of the special wavefunctions ψ of the positions x of electrons 1 and 2 (denoted by subscripts) and their spin wavefuctions s. The spin up and down states are shown by $\uparrow$ and $\downarrow$.

$$\Psi_{Singlet} \propto \left(\psi_1(x_1)\psi_2(x_2)+\psi_2(x_1)\psi_1(x_2)\right)\left(s_1(\uparrow)s_2(\downarrow)-s_2(\uparrow)s_1(\downarrow)\right) \quad [3.10]$$

$$\Psi_{Triple+1} \propto \left(\psi_1(x_1)\psi_2(x_2)-\psi_2(x_1)\psi_1(x_2)\right)\left(s_1(\uparrow)s_2(\uparrow)\right) \quad [3.11]$$

$$\Psi_{Triplet0} \propto \left(\psi_1(x_1)\psi_2(x_2)-\psi_2(x_1)\psi_1(x_2)\right)\left(s_1(\uparrow)s_2(\downarrow)+s_2(\uparrow)s_1(\downarrow)\right) \quad [3.12]$$

$$\Psi_{Triplet-1} \propto \left(\psi_1(x_1)\psi_2(x_2)-\psi_2(x_1)\psi_1(x_2)\right)\left(s_1(\downarrow)s_2(\downarrow)\right) \quad [3.13]$$

In can be shown that it is a change in the inter-particle spacing that gives rise to these exchange forces in an infinite one dimensional potential well, illustrated below. To simplify the calculation I have used particles with no charge so that inter-particle interactions do not affect the wavefunctions. Here one particle is in the ground state and the other one is in the first excited state, as shown in Figure 3.8. Although, because in quantum mechanics these particles are indistinguishable, we cannot say which is in which energy level. The distance between the two particles in a single state and a triplet states for two electrons in an infinite potential well is shown below in Figure 3.9. As can the seen from the diagrams the particles have a higher probability of being further apart in the anti-symmetric triplet state and so electrostatic repulsion would be reduced if these particles were electrons, reducing the energy of the triplet state compared to the singlet.

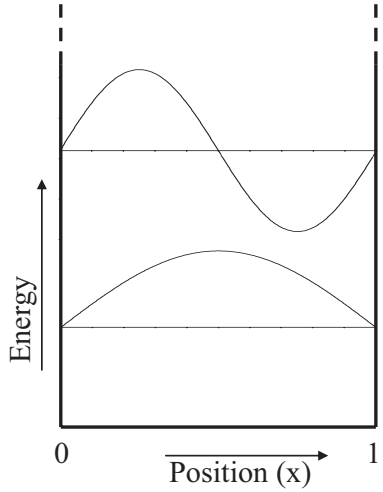

Figure 3.8 Ground state and first excited state for particles in an infinite one dimensional potential well. These are used for the calculation of the probability densities of the positions of the particles below.

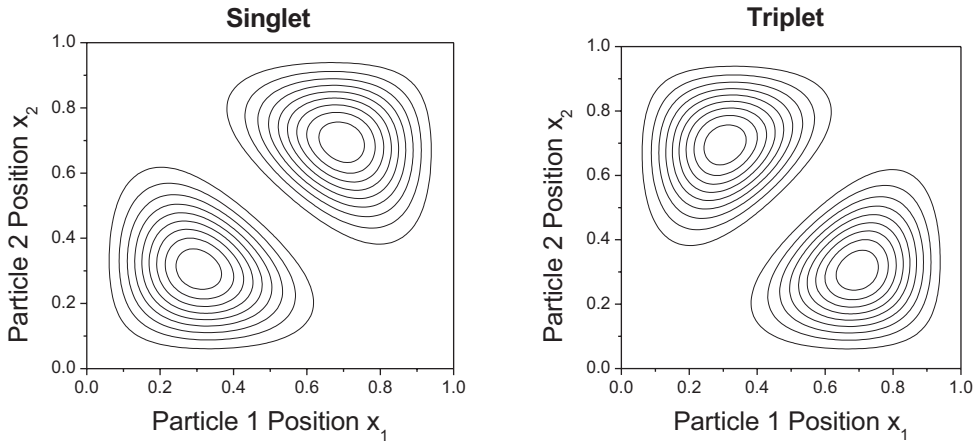

Figure 3.9 The probability density of one particle given the position of the other. For the case of the infinite potential well shown above. Shown for the spatially symmetric singlet and the spatially anti-symmetric triplet state.

This difference in energy means that in photoluminescence light is normally absorbed into the stronger dipole moment singlet states and is then converted to the lower energy triplet state via intersystem crossing before being re-emitted. This is illustrated in the Jablonski diagram in Figure 3.10. In electroluminescence, singlet or triplet excitons can form directly on emissive material or that of fluorescent host molecules before transferring into the emissive material's triplet state. This means that shorter excitation wavelengths or higher drive voltages are required in phosphorescent

materials than fluorescent materials and this has created problems with finding suitable deep blue emitters.

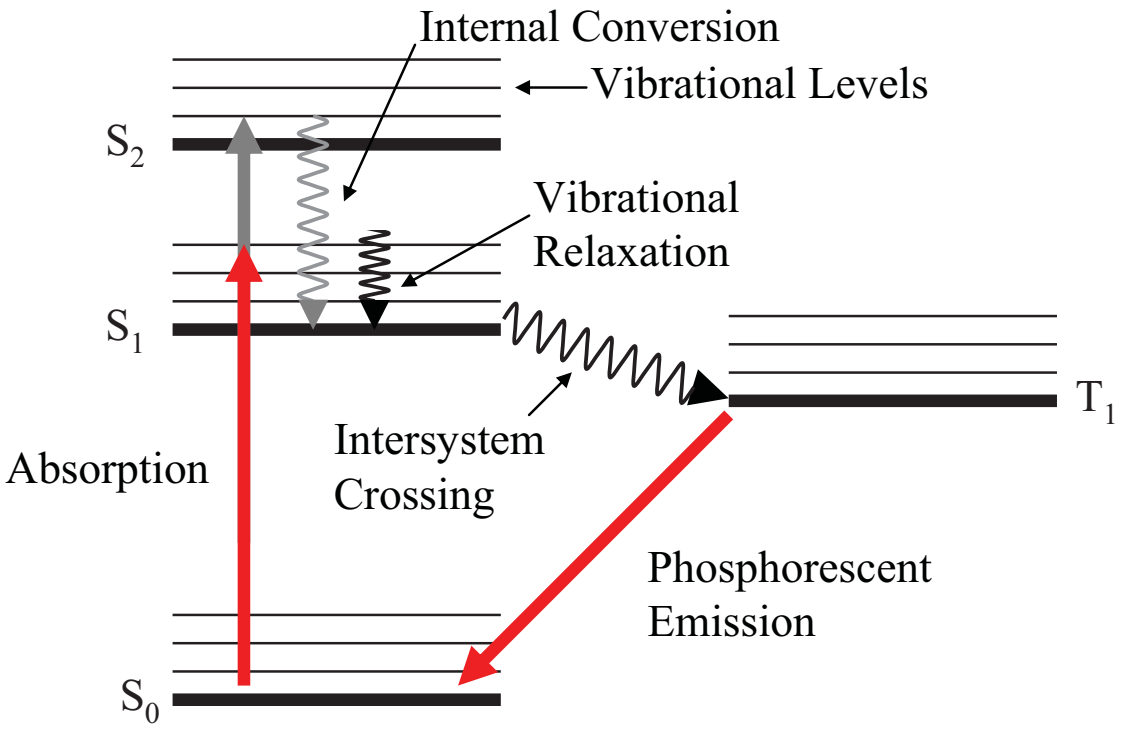

Figure 3.10 Jablonski diagram of the energy levels in a typical phosphorescent system. Arrows indicate the transitions undergone during absorption into the singlet state and subsequent emission from the triplet in photoluminescence.

Many heavy metals have been used in phosphorescent materials for OLEDs, including platinum [40], terbium [41, 42] and europium [40]. However the most successful OLEDs materials are based on iridium complexes which have short radative lifetimes of only 1-2 microseconds. A good example is *fac*-tris(2-phenylpyridine) iridium(III) or $Ir(ppy)_3$ which emits in the green [43, 44]. $Ir(ppy)_3$ has also been used as the basis of highly efficient solution processed dendrimers for OLEDs [45]. The structures of both $Ir(ppy)_3$ and the first generation $Ir(ppy)_3$ based dendrimer are shown in Figure 3.11.

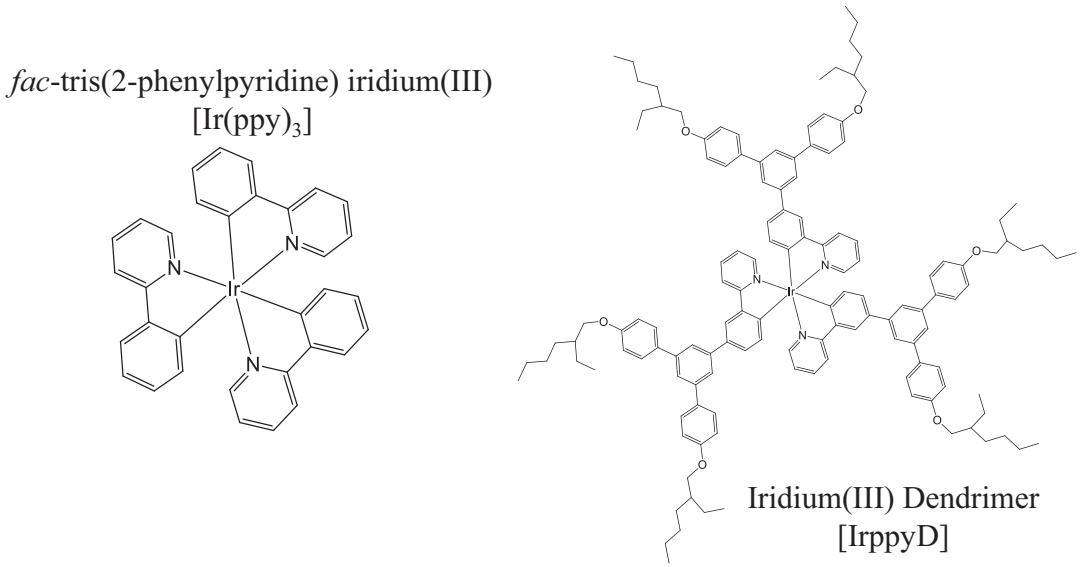

Figure 3.11 The molecular structures of green emitting Ir(ppy)$_3$ and a first generation single dendron iridium dendrimer.

Many other colours have been demonstrated by changing the iridium's ligands, including blue [8] and red [46]. These colour changes can be made because the HOMO in iridium complexes is a metal to ligand charge transfer (MLCT) state, which provides the spin orbit coupling, mixed with a π-π* transition on the ligand, while the LUMO is entirely a π* orbital that sits entirely on the ligands [47]. The fact the HOMO and LUMO have ligand character means both can be altered by changing the ligand chemistry.

3.4.3 Aggregated States: Dimers and Excimers

In organic systems there can be significant problems with concentration quenching [48-50], that is to say placing the emissive molecules close to one another can result in reduced luminescence. This is a problem in solution [48, 49] but it poses a much more significant problem in the solid state [49-51] and so creates many problems for devices.

As well as improved charge transfer another advantage of host-guest blending is that it separates the chromophores spatially which means that they do not interact with one another, thereby avoiding quenching or modification of their emission. Small

molecules are typically prone to π-stacking with one another and often quench each other's emission without a host. This means that if they were deposited from solution they may phase separate and quench their luminescence, if used in high concentrations. In polymers long, sterically bulky side groups are often added to provide some protection against these concentration quenching effects [51, 52]. In dendrimers the highly branched dendrons separate their cores, reducing inter-chormophore interactions [36, 45, 53].

If two molecules are close enough to each other that their wavefunctions overlap then they can form a system of coupled oscillators. This means the interaction potential between the two molecules leads to splitting of molecular energy levels into higher and lower states with oscillations on each molecule that are either in or out of phase. If there is a superposition of these two stationary states the exciton can be thought of as coherently moving back and forth between the two molecules. The dependence on the splitting for the energy levels on the phase difference is illustrated in Figure 3.12. Here the analogy of a pair of classical balls on springs interacting via a repulsive electrostatic interaction is used. If the repulsion acts in the same direction as the resulting force on the springs, the frequency of the oscillations is increased giving a higher energy state. If the electrostatic repulsion acts against the springs the balls will oscillate slower with lower energy. This means that for the head to tail configuration the energy is lower when the balls are in phase and for the parallel configuration the lower energy state has the balls oscillating out of phase. This is exactly what is found in quantum mechanical dipole oscillations in molecules [54]. The head to tail configuration where the lower energy state gives constructive inference is known as a J aggregate while the parallel dipole case where the lower energy state is out of phase is known as an H aggregate [55, 56].

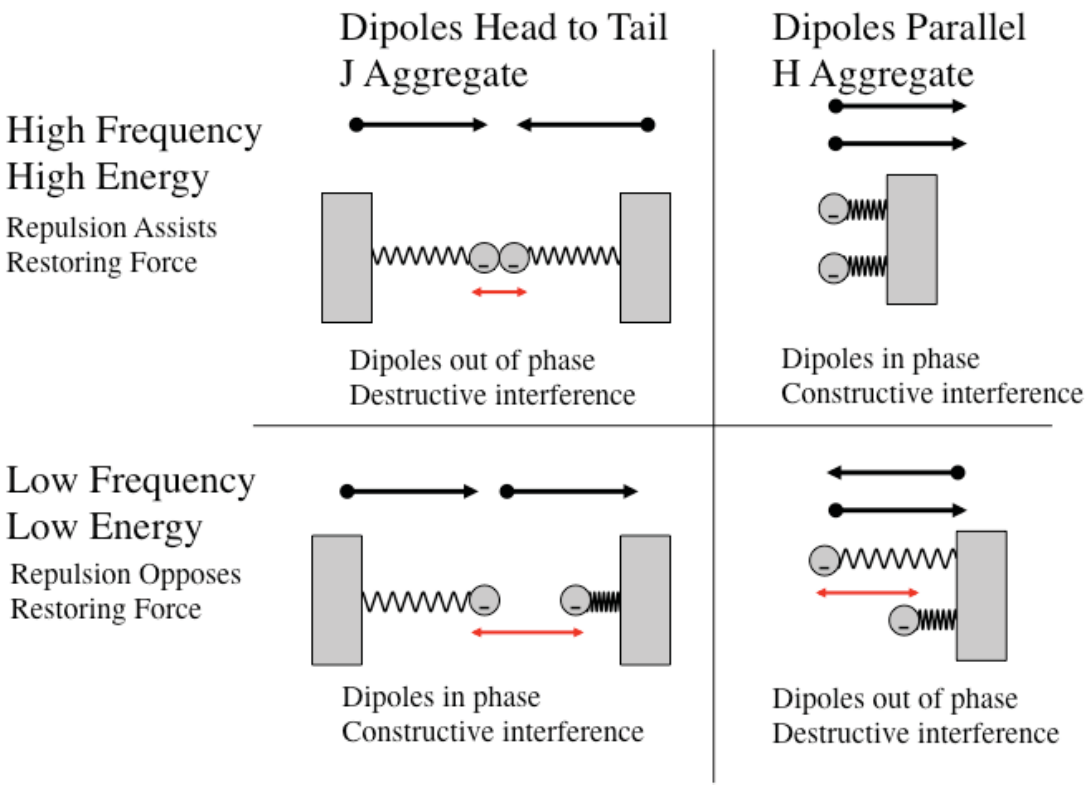

Figure 3.12 Diagram illustrating how the energy levels and overall dipole moments of dimers depend on the orientation of the dipoles of individual molecules. An analogous system of charged particles oscillating on springs is also shown to explain the relationship between dipole orientation and phase, and energy of the dimer states.

Depending on the orientation of the two molecules in the dimer and the phase relationship between the molecular dipole moments can add constructively or destructively. The dipole moments in π-π* transitions lie in the plane of the conjugated system [57] and these systems tend to dimerise by π stacking with the molecules lying flat on top of one another. This means that for conjugated organic molecules dipole moments will tend to be parallel and not head to tail. As a result the net dipole moment will tend to be reduced as the individual dipoles interfere destructively in the lower energy state (this is the bottom right case in Figure 3.12).

In general, in a dimer, the exciton will lose energy and end up in the lower of these two energy states. As the molecules used in OLEDs are chosen for their highly emissive properties as isolated choromphores the dimer state is in general a much less efficient emitter than the monomer, with a lower radiative rate. As the two molecule system has no covalent bonds between the molecules the system is less rigid and it is

likely to have a higher non-radiative de-excitation rate. As the properties of a dimer system depend on the position and orientation of the molecules involved this means that in a system containing dimers there is a collection of many different emissive species. This means aggregated systems tend to have broad, featureless, red-shifted and less efficient emission than the systems of isolated molecules. However in some unusual cases emission from organic molecules can be enhanced by dimerisation [49].

Like dimers, excimers are formed when two molecules or atoms come together to form an aggregate. However unlike dimers, excimers are atoms or molecules which only come together when one is in the excited state. Excimer lasers use gas atoms which bond together after one has been excited to form a single emissive species by collision with another atom. They are commonly used to produce high power ultra-violet light for applications such as lithography for making semiconductor chips. Excimer emission has also been used to make highly efficient broad spectrum phosphorescent organic light emitting diodes [58-60]. This broad featureless spectrum has made them good candidate for white OLED devices using only a single emissive material [58]. Like normal dimers, excimers typically lead to a red-shifting of the emission spectrum compared to the monomer and (despite the above examples) are often less emissive than the isolated monomers and so usually undesirable.

3.4 Design of OLEDs

3.4.1 Charge Injection

Before electroluminescence can happen charges must be injected into the device. With inorganic materials this means electrons must be injected into the conduction band and holes into the valance band. In organic materials this means electrons must move to occupy the lowest unoccupied molecular orbital (LUMO) and holes are injected by removing a charge from the highest occupied molecular orbital (HOMO). This is shown in Figure 3.13. In both cases if there is an energy gap between the work function of the contact and the energy level being injected into then there can be a barrier to charge injection [61]. The work function is the energy required to remove an electron from the material and allow it to escape into vacuum, such as via the photoelectric effect.

The two main mechanisms for injection are thermionic emission [62] and Fowler-Nordheim tunnelling [63]. The former involves the carriers having enough thermal energy to overcome the injection batter, with a field dependant factor due to image-force barrier lowering. The latter involves quantum mechanical tunnelling into the semiconductor transport states pulled downwards in energy by the applied field. In addition, due to the low mobility of disordered organic semiconductors, injected carriers build up at the interface resulting in a strong backflow recombination current. This reduces the injected current from that predicted by the original thermionic emission and Fowler-Nordheim tunnelling theories by many orders of magnitude [63]. In the negligible barrier regime it is also possible to achieve an ohmic contact, where the current becomes space-charge limited [62] and is no longer dependent on injection processes but is controlled by the charge transport properties.

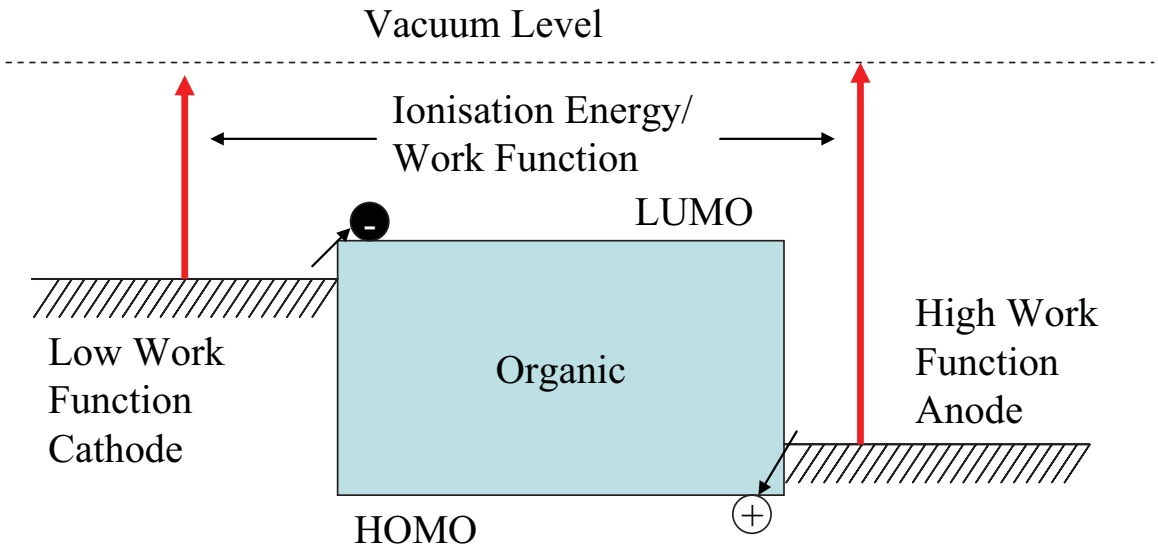

Figure 3.13 Charge injection in OLEDs. Electrons are injected via the cathode and holes are injected via the anode.

As charge injection occurs by applying a bias to the device that overcomes the energy barriers. The higher these barriers the higher the required drive voltage and so the less power efficient the device will be. In addition if the energy barriers are significantly different only one charge carrier will flow through the device at low voltages, giving no light emission. When the voltage is increased one charge carrier may still dominate over the other once the light emission switches on. This will result in low quantum

efficiency as a current is flowing but not all the charges will recombine, reducing $\eta_{capture}$ in Equation 3.4. In OLEDs it is often harder to inject electrons than holes and this means that low workfunction, and thus reactive metals, such as calcium, magnesium or barium are often needed as the cathode material

3.4.2 Electrode Quenching

Once the charges have been injected they must move through the device to recombine and form excitons which can emit light. This charge transport typically has a field and temperature dependent mobility due to the disordered energy levels in amorphous organic materials (as discussed in Chapter 2). Significantly for OLEDs the electron mobility in organic materials is often orders of magnitude lower than the hole mobility [64]. This means that in situations where the charge injection is perfectly balanced the charge carriers often recombine very close to the cathode.

As the cathode is very often a metal, or is at the very least conductive, it produces image charges and dipoles in response to the charges and excitons in the organic layer. If a molecule is trying to emit too close to the contact (say one tenth of a wavelength in the medium) then the dipole and the image dipole will interfere out of phase with one another and luminescence will be significantly reduced [15]. In addition the metal dielectric interface can support surface plasmon modes which can be excited by nearby emissive molecules [65]. These modes are trapped within the device and so do not contribute to light emission.

3.4.3 Charge Transport Layers

In order to improve charge injection, achieve charge balance and keep recombining charges away from the electrodes hole-transport and electron-transport layers can be used [66]. These materials can perform these roles by having suitable HOMO and LUMO levels as shown in Figure 3.14. Charge injection at the electrodes can be improved by having a lower energy barrier at the electrodes. This necessitates another small energy step inside the device when the charge carriers reach the emissive layer but these small energy barriers are easier to overcome by mechanisms such as

thermionic emission. Charge balance can be enforced by choosing a large HOMO barrier that prevents holes entering the electron-transport layer or a LUMO barrier that prevents electrons entering the hole-transport layer. The blocked charges build up at these internal interfaces creating a strong attraction for the opposite sign of charge carrier increasing their flow into the emissive layer.

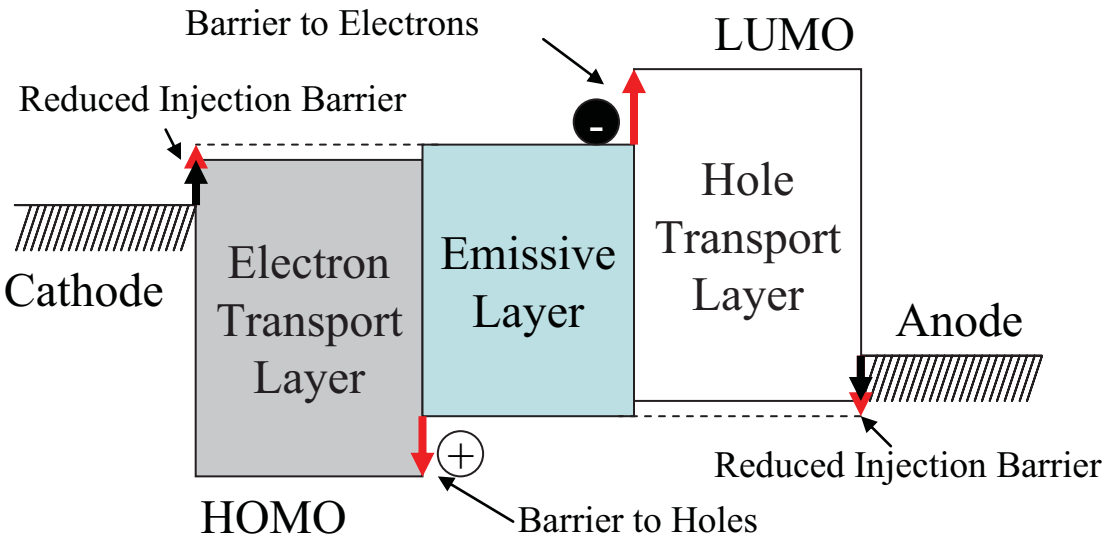

Figure 3.14 The energy levels in a multilayer OLED structure showing the use of hole transport and electron transport layers. In this diagram these layers reduce the charge injection barriers at the electrode and block charge carriers moving all the way through a device using energy barriers.

Additionally the hole and electron transport layer materials can be chosen so that the mobility of the particular charge carrier is much higher. This slows charge carriers of the wrong type and moves the recombination zone and light emission away from the electrodes. However, when using mobilities without internal energy barriers to block charges the transport layer(s) could contain excitons and may have to be doped with the emissive material to allow light emission.

Not all electron and hole transport layers have all of these properties at once depending on the needs of the device. In addition the favourable injection properties and the transport/blocking properties can be separated into two materials using an injection layer and a separate transport layer. Charge injection layers can also be doped to include extrinsic charges to lower the injection barrier by producing a thin

depletion region, which helps align the electrodes workfunction with the organic semiconductor's HOMO or LUMO [67, 68]. This can lead to devices with 5 or more layers. This can be achieved using thermal evaporation but it is increasingly difficult to add multiple layers to solution processed devices. Therefore in solution processed devices it is better if materials properties allow efficient devices with only one or two layers [22].

3.4.4 Light Extraction

As only ~20% of light leaves conventional OLED structures, improved light extraction efficiency offers a way to make large gains in performance. Unfortunately the cost is often increased device complexity if the light extraction enhancement is within the device or blurring of pixels with their neighbours if the enhancement is applied to the substrate.

Strategies that have been tried for enhancing emission from the layer itself include incorporating photonic crystals [69-72], inserting a low refractive index grid to scatter light [73], patterning the organic layer into a Bragg grating by imprinting [74], buckling the reflective electrode [75] or using a semi-transparent electrode to create a micro-cavity [76]. These approaches can give ~100% improvement in quantum efficiency [75]. Unfortunately the strategies that use periodic gratings or microcavities also lead to angle dependent emission and colour, which is not ideal unless another layer is added to scatter the light and restore even lambertian emission [9].

Adding a diffuser [9], microlens array [73] or luminaire [77] to the top of the device is generally an easier way to enhance emission but is only suitable for large area single colour lighting or signage applications. Again the outcoupling efficiency can be approximately doubled using these approaches [77]. Since it offers such large improvements in device performance, it is using out-coupling enhancement in addition to the optimisation of all the other device and material parameters discussed above that has allowed the most efficient white OLEDs with over 100 lm/W power efficiency [4].

1. Friend, R.H., et al., *Electroluminescence in conjugated polymers.* Nature, 1999. **397**(6715): p. 121-128.
2. Py, C., et al., *High-contrast organic light emitting diodes with a partially absorbing anode.* Optics Letters, 2008. **33**(10): p. 1126-1128.
3. Braun, D., et al., *Nanosecond Transient Electronluminescence From Polymer Light Emitting Diodes.* Applied Physics Letters, 1992. **61**(26): p. 3092-3094.
4. Reineke, S., et al., *White organic light-emitting diodes with fluorescent tube efficiency.* Nature, 2009. **459**(7244): p. 234-U116.
5. D'Andrade, B.W. and S.R. Forrest, *White organic light-emitting devices for solid-state lighting.* Advanced Materials, 2004. **16**(18): p. 1585-1595.
6. Misra, A., et al., *White organic LEDs and their recent advancements.* Semiconductor Science and Technology, 2006. **21**(7): p. R35-R47.
7. *Commission Internationale de l'Éclairage Proceedings, 1931.*1931: Cambridge University Press.
8. Tokito, S., et al., *Confinement of triplet energy on phosphorescent molecules for highly-efficient organic blue-light-emitting devices.* Applied Physics Letters, 2003. **83**(3): p. 569-571.
9. Mulder, C.L., et al., *Saturated and efficient blue phosphorescent organic light emitting devices with Lambertian angular emission.* Applied Physics Letters, 2007. **90**(21).
10. Demas, J.N. and G.A. Crosby, *Measurement of Photoluminescence Quantum Yields - Review.* Journal of Physical Chemistry, 1971. **75**(8): p. 991.
11. Greenham, N.C., et al., *Measurement of Absolute Photoluminescence Quantum Efficiencies in Conjugated Polymers.* Chemical Physics Letters, 1995. **241**(1-2): p. 89-96.
12. Liu, Z.T., et al., *The characterization of the optical functions of BCP and CBP thin films by spectroscopic ellipsometry.* Synthetic Metals, 2005. **150**(2): p. 159-163.
13. Greenham, N.C., R.H. Friend, and D.D.C. Bradley, *Angular-Dependance of the Emission From a Conjugated Polymer Light-Emitting Diode - Implications For Efficiency Calculations.* Advanced Materials, 1994. **6**(6): p. 491-494.
14. Khalfin, V.B., et al., *Weak microcavity effects in organic light-emitting devices.* 1998. **- 58**(- 7).
15. Kim, J.-S., et al., *Electroluminescence emission pattern of organic light-emitting diodes: Implications for device efficiency calculations.* Journal of Applied Physics, 2000. **88**(2): p. 1073.
16. Bernanose, A., M. Comte, and P. Vouaux, *Sur un nouveau mode d'émission lumineuse chez certains composés organiques.* J. Chim. Phys. , 1953. **50**: p. 64.
17. Tang, C.W. and S.A. VanSlyke, *Organic electroluminescent diodes.* Applied Physics Letters, 1987. **51**(12): p. 913-915.
18. Partridge, R.H., *Radiation Sources.* U.S. Patent: 3995299, 1975.
19. Partridge, R.H., *Electro-Luminescence From Polyvinylcarbazyole Films .3. Electroluminescent Devices.* Polymer, 1983. **24**(6): p. 748-754.
20. Partridge, R.H., *Electro-Luminescence From Polyvinylcarbazyole Films .4. Electro-Luminescence Usuing Higher Work Function Cathodes.* Polymer, 1983. **24**(6): p. 755-762.
21. Burroughes, J.H., et al., *Light-emitting diodes based on conjugated polymers.* Nature, 1990. **347**: p. 539 - 541.

22. Forrest, S.R., *The path to ubiquitous and low-cost organic electronic appliances on plastic.* Nature, 2004. **428**: p. 911.
23. Brown, T.M., et al., *Built-in field electroabsorption spectroscopy of polymer light-emitting diodes incorporating a doped poly(3,4-ethylene dioxythiophene) hole injection layer.* Applied Physics Letters, 1999. **75**(12): p. 1679-1681.
24. Yan, H., et al., *High-performance hole-transport layers for polymer light-emitting diodes. Implementation of organosiloxane cross-linking chemistry in polymeric electroluminescent devices.* Journal of the American Chemical Society, 2005. **127**(9): p. 3172-3183.
25. Klarner, G., et al., *Cross-linkable polymers based on dialkylfluorenes.* Chemistry of Materials, 1999. **11**(7): p. 1800-1805.
26. Contoret, A.E.A., et al., *The photopolymerization and cross-linking of electroluminescent liquid crystals containing methacrylate and diene photopolymerizable end groups for multilayer organic light-emitting diodes.* Chemistry of Materials, 2002. **14**(4): p. 1477-1487.
27. Jeon, W.S., et al., *Ideal host and guest system in phosphorescent OLEDs.* Organic Electronics, 2009. **10**(2): p. 240-246.
28. Holmes, R.J., et al., *Blue organic electrophosphorescence using exothermic host-guest energy transfer.* Applied Physics Letters, 2003. **82**(15): p. 2422-2424.
29. Sudhakar, M., et al., *Phosphorescence quenching by conjugated polymers.* Journal of the American Chemical Society, 2003. **125**(26): p. 7796-7797.
30. Yeh, S.J., et al., *New dopant and host materials for blue-light-emitting phosphorescent organic electroluminescent devices.* Advanced Materials, 2005. **17**(3): p. 285-+.
31. Malliaras, G. and R. Friend, *An organic electronics primer.* Physics Today, 2005. **58**(5): p. 53-58.
32. Baldo, M.A., et al., *Highly efficient phosphorescent emission from organic electroluminescent devices.* Nature, 1998. **395**(6698): p. 151-154.
33. Adachi, C., et al., *Nearly 100% internal phosphorescence efficiency in an organic light-emitting device.* Journal of Applied Physics, 2001. **90**(10): p. 5048-5051.
34. Wang, Q., et al., *Harvesting Excitons Via Two Parallel Channels for Efficient White Organic LEDs with Nearly 100% Internal Quantum Efficiency: Fabrication and Emission-Mechanism Analysis.* Advanced Functional Materials, 2009. **19**(1): p. 84-95.
35. Williams, E.L., et al., *Excimer-based white phosphorescent organic light emitting diodes with nearly 100 % internal quantum efficiency.* Advanced Materials, 2007. **19**(2): p. 197.
36. Burn, P.L., S.C. Lo, and I.D.W. Samuel, *The development of light-emitting dendrimers for displays.* Advanced Materials, 2007. **19**(13): p. 1675-1688.
37. Baldo, M.A., C. Adachi, and S.R. Forrest, *Transient analysis of organic electrophosphorescence. II. Transient analysis of triplet-triplet annihilation.* Physical Review B, 2000. **62**(16): p. 10967-10977.
38. Cao, Y., et al., *Improved quantum efficiency for electroluminescence in semiconducting polymers.* Nature, 1999. **397**(6718): p. 414-417.
39. Wilson, J.S., et al., *Spin-dependent exciton formation in pi-conjugated compounds.* Nature, 2001. **413**(6858): p. 828-831.
40. !!! INVALID CITATION !!!

41. Capecchi, S., et al., *High-efficiency organic electroluminescent devices using an organoterbium emitter.* Advanced Materials, 2000. **12**(21): p. 1591-+.
42. Kido, J. and Y. Okamoto, *Organo lanthanide metal complexes for electroluminescent materials.* Chemical Reviews, 2002. **102**(6): p. 2357-2368.
43. King, K.A., P.J. Spellane, and R.J. Watts, *Excited-State Properties of a Triply Ortho-Metalated Iridium(III) Complex.* Journal of the American Chemical Society, 1985. **107**(5): p. 1431-1432.
44. Baldo, M.A., et al., *Very high-efficiency green organic light-emitting devices based on electrophosphorescence.* Applied Physics Letters, 1999. **75**(1): p. 4-6.
45. Lo, S.C., et al., *Green phosphorescent dendrimer for light-emitting diodes.* Advanced Materials, 2002. **14**(13-14): p. 975.
46. Tsuboyama, A., et al., *Homoleptic cyclometalated iridium complexes with highly efficient red phosphorescence and application to organic light-emitting diode.* Journal of the American Chemical Society, 2003. **125**(42): p. 12971-12979.
47. Hay, P.J., *Theoretical studies of the ground and excited electronic states in cyclometalated phenylpyridine Ir(III) complexes using density functional theory.* Journal of Physical Chemistry A, 2002. **106**(8): p. 1634-1641.
48. Melhuish, W.H., *Quantum Efficiencies of Fluorescence of Organic Substances: Effect of Solvent and Concentration on the Fluorescent Solute.* Journal of Physical Chemistry, 1961. **65**: p. 229.
49. Hong, Y.N., J.W.Y. Lam, and B.Z. Tang, *Aggregation-induced emission: phenomenon, mechanism and applications.* Chemical Communications, 2009(29): p. 4332-4353.
50. Schouwink, P., et al., *The influence of molecular aggregation on the device properties of organic light emitting diodes.* Thin Solid Films, 2000. **372**(1-2): p. 163-168.
51. Setayesh, S., et al., *Polyfluorenes with polyphenylene dendron side chains: Toward non-aggregating, light-emitting polymers.* Journal of the American Chemical Society, 2001. **123**(5): p. 946-953.
52. Gambino, S., A.K. Bansal, and I.D.W. Samuel, *Comparison of hole mobility in thick and thin films of a conjugated polymer.* Organic Electronics, 2010. **11**(3): p. 467-471.
53. Lo, S.C., et al., *Encapsulated cores: Host-free organic light-emitting diodes based on solution-processible electrophosphorescent dendrimers.* Advanced Materials, 2005. **17**(16): p. 1945-+.
54. Pope, M. and C.S. Swenberg, *Electronic Processes in Organic Crystals and Polymers (2nd Edition)*. 2 ed1982: Oxford University Press.
55. Gadde, S., et al., *Control of H- and J-Aggregate Formation via Host-Guest Complexation using Cucurbituril Hosts.* Journal of the American Chemical Society, 2008. **130**(50): p. 17114-17119.
56. Ghosh, S., et al., *Control of H- and J-Type pi Stacking by Peripheral Alkyl Chains and Self-Sorting Phenomena in Perylene Bisimide Homo- and Heteroaggregates.* Chemistry-a European Journal, 2008. **14**(36): p. 11343-11357.
57. Birge, R.R., et al., *Transition dipole orientation of linear polyenes: Semiempirical models and extrapolation to the infinite chain limit.* Journal of Physical Chemistry A, 1999. **103**(14): p. 2251-2255.

58. Kalinowski, J., et al., *Mixing of excimer and exciplex emission: A new way to improve white light emitting organic electrophosphorescent diodes.* Advanced Materials, 2007. **19**(22): p. 4000-+.
59. Cocchi, M., et al., *Highly efficient near-infrared organic excimer electrophosphorescent diodes.* Applied Physics Letters, 2007. **90**(2).
60. Kalinowski, J., et al., *Bi-molecular emissive excited states in platinum (II) complexes for high-performance organic light-emitting diodes.* Chemical Physics, 2010. **378**(1-3): p. 47-57.
61. Brown, T.M., et al., *Electronic line-up in light-emitting diodes with alkali-halide/metal cathodes.* Journal of Applied Physics, 2003. **93**(10): p. 6159-6172.
62. Davids, P.S., I.H. Campbell, and D.L. Smith, *Device model for single carrier organic diodes.* Journal of Applied Physics, 1997. **82**(12): p. 6319-6325.
63. Davids, P.S., et al., *Charge injection in organic light-emitting diodes: Tunneling into low mobility materials.* Applied Physics Letters, 1996. **69**(15): p. 2270-2272.
64. So, F., et al., *Recent progress in solution processable organic light emitting devices.* Journal of Applied Physics, 2007. **102**(9).
65. Hobson, P.A., et al., *The role of surface plasmons in organic light-emitting diodes.* Ieee Journal of Selected Topics in Quantum Electronics, 2002. **8**(2): p. 378-386.
66. Kulkarni, A.P., et al., *Electron transport materials for organic light-emitting diodes.* Chemistry of Materials, 2004. **16**(23): p. 4556-4573.
67. Pfeiffer, M., et al., *Doped organic semiconductors: Physics and application in light emitting diodes.* Organic Electronics, 2003. **4**(2-3): p. 89-103.
68. Walzer, K., et al., *Highly efficient organic devices based on electrically doped transport layers.* Chemical Reviews, 2007. **107**(4): p. 1233-1271.
69. Ziebarth, J.M. and M.D. McGehee, *A theoretical and experimental investigation of light extraction from polymer light-emitting diodes.* Journal of Applied Physics, 2005. **97**(6).
70. Do, Y.R., et al., *Enhanced light extraction efficiency from organic light emitting diodes by insertion of a two-dimensional photonic crystal structure.* Journal of Applied Physics, 2004. **96**(12): p. 7629-7636.
71. Matterson, B.J., et al., *Increased efficiency and controlled light output from a microstructured light-emitting diode.* Advanced Materials, 2001. **13**(2): p. 123-127.
72. Lupton, J.M., et al., *Bragg scattering from periodically microstructured light emitting diodes.* Applied Physics Letters, 2000. **77**(21): p. 3340-3342.
73. Sun, Y. and S.R. Forrest, *Enhanced light out-coupling of organic light-emitting devices using embedded low-index grids.* Nature Photonics, 2008. **2**(8): p. 483-487.
74. Yates, C.J., et al., *Surface plasmon-polariton mediated emission from phosphorescent dendrimer light-emitting diodes.* Applied Physics Letters, 2006. **88**(16).
75. Koo, W.H., et al., *Light extraction from organic light-emitting diodes enhanced by spontaneously formed buckles.* Nature Photonics, 2010. **4**(4): p. 222-226.
76. Meerheim, R., R. Nitsche, and K. Leo, *High-efficiency monochrome organic light emitting diodes employing enhanced microcavities.* Applied Physics Letters, 2008. **93**(4).

77. D'Andrade, B.W. and J.J. Brown, *Organic light-emitting device luminaire for illumination applications.* Applied Physics Letters, 2006. **88**(19).

4. Experimental Methods

4.1 Overview

This chapter contains an overview of many of the experimental methods used throughout this work. The importance of and methods for keeping samples oxygen free is discussed in Section 4.2. Absorption and photoluminescence spectroscopy is essential to most of the methods and is described in Section 4.3. Section 4.4 is concerned with the measurement of the photoluminescence quantum yield (PLQY) of materials. Section 4.5 covers the Time-Correlated Single Photon Counting (TCSPC) method for determining the luminescence lifetime of materials. Section 4.6 contains a description of the methods for making OLED devices and Section 4.7 cover OLED characterisation.

The PLQY of a material is the efficiency with which incident photons are re-emitted as luminescence, and as was explained in chapter 3 this is an important parameter for luminescent devices in its own right. However the PLQY also offers greater insight

into the photophysics of materials and their local environment when combined with luminescence lifetime measurements. As an excited molecule can decay either radiatively or non-radiatively, the PLQY (Φ) of the material is given by the ratio of the radiative rate (k_{rad}) to the total de-excitation rate (k_{tot}) as shown in equation 4.1 below. The total de-excitation rate (k_{tot}) is what is measured experimentally but can also be expressed as the sum of the radiated and non-radiative rates (k_{rad} and $k_{non\text{-}rad}$) [1].

$$\Phi = \frac{k_{rad}}{k_{tot}} = \frac{k_{rad}}{k_{rad} + k_{non-rad}} \qquad [4.1]$$

4.2 Phosphorescence Quenching by Oxygen

As discussed in chapter 3, phosphorescent materials have the significant advantage over fluorescent materials that in electroluminescence they can harvest both singlet and triplet excitons while fluorescent materials can harvest only singlets [2]. Phosphorescent materials convert the higher energy singlets to triplets by a process of inter system crossing and the triplet state then emits light. As the triplet state cannot radiatively decay via an allowed transition its dipole moment is small and it has a long radiative lifetime (of the order of microseconds for the iridium complexes used in this work). Unfortunately during this time triplet states can be quenched by oxygen molecules reducing the lifetime of iridium complexes to tens of nanoseconds and dramatically reducing photoluminescence quantum yield.

To avoid this problem when measuring their emissive properties film samples are measured under a nitrogen purge or in vacuum and solution samples are freeze-pump-thaw degassed to remove dissolved oxygen. In freeze-pump-thaw degassing the sample is frozen in a degassing cuvette to prevent the solvent from evaporating, the atmosphere in the cuvette is then removed by a vacuum pump and once the pressure is reduced to 6×10^{-2} mb the cuvette is sealed and the sample is allowed to thaw by placing the cuvette bulb in water. This allows the dissolved gasses to escape from the solvent. The cycle is then repeated until three pump cycles have been completed.

4.3 Absorption and Photoluminescence Spectra

Absorption measurements in either film or solution were made using a Varian Cary 300 spectrophotometer. This instrument uses a differential measurement between the monochromated light transmitted through a reference and the sample. In the case of a film measurement the reference used is a clean substrate, and for solution measurments it is a cuvette containing the same solvent. The reference allows the instrument to account for any loses due to reflections, scattering or absorption by the substrate, cuvette or solvent. The bandpass of the monochromator was set to 2 nm.

The absorbance or optical density ($\alpha(\lambda)$) of the sample at a given wavelength (λ) is calculated using formula 4.2 below where ($T(\lambda)$) is the transmitted light through the sample and ($T_0(\lambda)$) is the transmitted light through the reference.

$$\alpha(\lambda) = -\log_{10}\left(\frac{T(\lambda)}{T_0(\lambda)}\right) \qquad [4.2]$$

Photoluminescence measurements were made using a Jobin Yvon Fluoromax 2 fluorimeter. The instrument used monochromated light to excite the sample and then another monochromator was used to collect the emitted light. The excitation and emission bandpass were 1 nm. The spectral response of the instrument was corrected by multiplying the spectra by a known calibration curve and all spectra were measured in terms of number of photons detected per unit wavelength.

4.4 Photoluminescence Quantum Yield (PLQY)

4.4.1 Solution PLQY

Solution PLQY measurements were made using the method from Demas and Crosby [3] which involves comparing the luminescence of the sample to a reference in a fixed measurement geometry and with the same excitation wavelength. Here we use the Jobin Yvon Flouromax 2 flourimeter. Unless noted otherwise a solution of quinine

sulphate in 0.5 molar sulphuric acid excited at 360 nm wavelength was used as the standard and it was taken to have a PLQY of 55% [4].

The sample and reference were made up to have an optical density in the range of 0.09-0.11 in order to ensure that the light emission in both curvettes in the same plane with respect to the collecting optics. As the absorbance is low (~16 % across the 1 cm thickness of the cuvette) the emission can be assumed to be approximately uniform and so corrections for small deviations in the absorption can be made using a first order approximation. This is done by dividing the intensity of the emitted light is by the absorption, as we would expect the amount of emitted light to be proportional to the absorption at a fixed PLQY. Sample were freeze pump thaw degassed to prevent oxygen quenching as described in section 4.2.

Another factor that is important is that the refraction of the light on leaving the cuvette affects how much light is collected into a given solid angle by the collecting optics. As the reference and the sample are often different solvents a correction needs to be made for the refractive index of the solvents. Finally a correction for the intensity of the excitation source needs to be taken into account. This is measured by an internal photodiode within the fluorimeter.

The resulting expression for determining the photoluminescence quantum yield is given below in equation 4.3 where subscript X denotes the sample and subscript R denotes the reference, D is the integrated corrected emission spectrum, $\alpha(\lambda_{ex})$ is the absorbance at the excitation wavelength, n is the refractive index and I is the excitation intensity [3].

$$\Phi_X = \Phi_R \left(\frac{D_X}{D_R} \right) \left(\frac{\alpha_R(\lambda_{ex})}{\alpha_X(\lambda_{ex})} \right) \left(\frac{n_X^2}{n_R^2} \right) \left(\frac{I_R}{I_X} \right) \qquad [4.3]$$

4.4.2 Film PLQY

For most of this work film PLQY measurements were made using the Greenham method [1] which uses a laser as an excitation source and makes use of an integrating sphere to collect the light emitted in all directions. The reason for this is that film samples often show angle-dependent emission because the films have thicknesses comparable to the wavelength of the emitted light and so a measurement at just one angle, such as in the solution PLQY method discussed above, would give misleading results. The fact polymers tend to lie in the place of the substrate, but small molecules or dendrimers might not, also means all emission angles need to be integrated over.

The intensity of the re-emitted light compared to the excitation intensity is determined by an NPL calibrated photodiode supplied by Bentham attached to a Labsphere integrating sphere. The 325 nm line of a Kimmon Electric 1K He:Cd laser was used as the excitation source. The photodiode signal from the laser beam in the sphere with no sample present (X_{laser}) is measured to determine amount of excitation light. To determine the quantity of luminescence produced by the sample a long pass filter is placed in front of the photodiode and the sample is placed in the beam and the photodiode signal is recorded (X_{sample}) while the sphere was purged with nitrogen to prevent oxygen quenching. A diagram showing these measurements is given in Figure 4.1.

As not all the excitation light is absorbed by the film corrections have to be made for secondary fluorescence generated by laser light which is reflected on the first strike and absorbed later by the sample. Firstly a measurement of the fraction of laser light reflected (R) and transmitted (T) by the sample has to be made outside the integrating sphere. Then the amount of signal produced by the secondary luminescence must be quantified. This is done by placing the sample in the sphere but out of the path of the laser beam and measuring the photodiode signal through the long pass filter (X_{sphere}). This is shown in Figure 4.1. The secondary fluorescence because of the reflected and transmitted light is then subtracted from signal on the photodiode when the sample is in the beam.

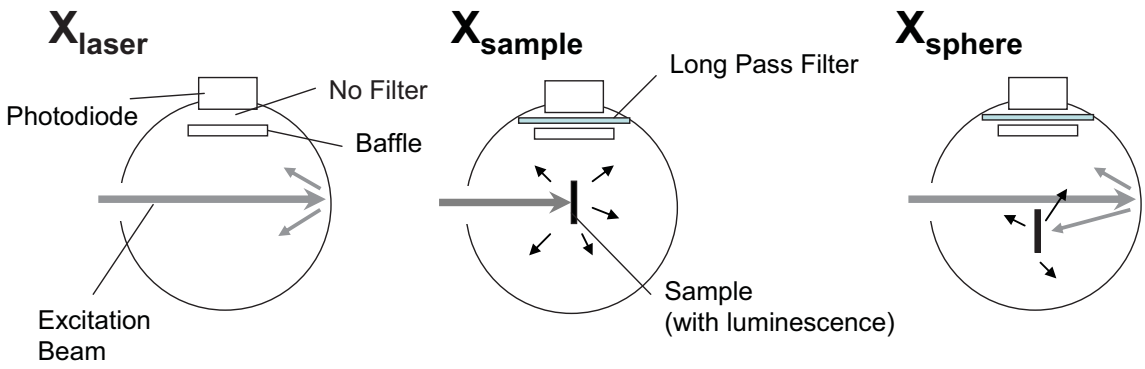

Figure 4.1 Illustration of the integrating sphere during X_{laser}, X_{sample} and X_{sphere} measurements.

Taking this value of the luminescence due to the first pass of the laser through the sample and dividing it by the fraction of excitation light absorbed in the first pass allows us to recover the signal we would expect if all the excitation light was absorbed. Dividing this value by X_{laser} gives us the Greenham *x* value (equation 4.4), which is a measure of the PLQY neglecting the spectral response of the system.

$$x = \frac{X_{sample} - (R+T)X_{sphere}}{(1-R-T)X_{laser}} \qquad [4.4]$$

The x value must be corrected for the different spectral response of the sphere $S(\lambda)$, filter $F(\lambda)$ and photodiode $G(\lambda)$ at the excitation wavelength compared to the emission spectrum $D(\lambda)$. This is done using the Greenham y value (equation 4.5) given below. The spectral response of the sphere is calculated by measuring the light out of the photodiode port when collimated light of a given wavelength is shined in through the excitation laser port and taking the ratio of output/input.

$$y = \frac{\int S(\lambda)F(\lambda)G(\lambda)D(\lambda)d\lambda}{S(\lambda_{ex})G(\lambda_{ex})\int D(\lambda)d\lambda} \qquad [4.5]$$

The PLQY (Φ) can then be found using Equation 4.6.

$$\Phi = \frac{x}{y} \qquad [4.6]$$

4.4.3 Powder PLQY

PLQY measurements from powders were performed using a method similar to the Greenham [1] method, however an Andor Model DV420-BV CCD spectrometer was used to determine the amount of scattered light from the sample as a simple measurement of transmitted and reflected does not account for all the scattered light [5].

A method for using just a CCD spectrometer to measure PLQY has been developed by de Mello [6] however it relies on the spectrometer being calibrated over a wide range of wavelengths from the excitation to the longest emission wavelengths and also requires a large dynamic range. Due to difficulties in finding a suitable calibration light source over this wide wavelength range a method based on adapting the Greenham and de Mello approaches so that an uncalibrated CCD spectrometer could be used to measure the scattered light [5].

The CCD spectrometer was attached to the integrating sphere for the measurements along with the photodiode described in Section 4.5. The intensity of the scattered light was determined by integrating the laser line in the spectrum of the CCD when the sample is in the beam (C_{sample}).

In order to determine the fraction of scattered laser light it is also necessary to determine the intensity of the light exciting the sample. However a spectrometer measurement of the laser intensity with no sample in the sphere (C_{laser}) would not be sufficient as the spectral response of the sphere is significantly altered by the presence of a sample that absorbs at the excitation wavelengths.

The change in the spectral response can be determined from the ratio of the spectrometer signal with the sample in the sphere but out of the beam (C_{sphere}) to the C_{laser} measurement. This causes the C_{laser} measurement to cancel out. Thus the fraction of scattered light is given by equation 4.7.

$$S = \frac{C_{sample}}{C_{sphere}} \qquad [4.7]$$

This scattered light can then be used to correct for the secondary fluorescence using equation 4.4 using S in the place of R+T and the PLQY can be determined using equation 4.6.

4.4.4 CCD and Integrating Sphere Method

Some PLQY measurements were made using a commercial Hamamatsu C9920-02 measurement system using the method published by Suzuki [7]. Here the excitation is provided by a monochromated Xenon lamp coupled into an integrating sphere via an optical fibre. The method works by using a CCD spectrometer attached to the sphere via another fibre optic cable to measure the spectrum of the light in the integrating sphere. Two spectra are taken: one with a blank reference and then another with the sample in place. In each case the excitation and emission parts of the spectrum (in photons per wavelength) are integrated, after a spectral correction for the detectors, optics and sphere response has been applied. This yields $E(\lambda)_{reference}$ and $E(\lambda)_{sample}$ (the excitation spectra with the reference and then the sample in place) and $D(\lambda)_{reference}$ and $D(\lambda)_{sample}$ (the emission spectra). The PLQY can then be calculated using Equation [4.8].

$$\Phi = \frac{\int D(\lambda)_{sample} - D(\lambda)_{reference}\, d\lambda}{\int E(\lambda)_{reference} - E(\lambda)_{sample}\, d\lambda} \qquad [4.8]$$

This simple equation can be used because the integrating sphere used has >99% reflectivity over the entire spectral range so a change path length of the average photons before reaching the detector due to the presence of an absorbing sample is not large. Therefore the calculations involving scattered light, discussed above in Section 4.4.3, are not needed. This method can be used for films, solution and powder and is relatively fast as it requires only two measurements using the CCD spectrometer.

However it requires a high quality integrating sphere that is kept very clean to maintain its high reflectivity across all wavelengths.

4.5 Time-Correlated Single Photon Counting

Time-correlated single photon counting is a technique that determines the time delay between an excitation pulse and the detection of an emitted photon from a sample to build up statistics about its time dependent emission. The time between the excitation pulse and the arrival of the first photon at the detector is determined using a time to amplitude converter (TAC) which converts it to an electrical signal that can be recorded by a computer. The detected signal intensity is kept low enough so that the count rate of photons is less than 5% of the excitation repetition frequency so that the probability of multiple photons arriving at the detector as the result of a single pulse is low. This is important because the TAC cannot detect multiple photons from a single pulse and thus multiple photons would lead to skewed statistics.

In these experiments a Picoquant LDH C400 393 nm GaN laser diode and a twice frequency doubled Alphalas Pulselas-532-30-P Nd:YAG microchip laser at 266 nm were used as excitation sources. The GaN laser diode resulted in an instrument response function of <300 ps full width half maximum and the Nd:YAG laser gave a response of ~500 ps full width half maximum. The detector used was a Hamamatsu RU-3809 U-50 micro-channel plate photomultiplier tube behind a monochromator to select the emission wavelength and a filter for the excitation light. Solution samples were freeze pump thaw degassed as described in Section 4.2 and film samples were measured in vacuum to prevent oxygen quenching or sample degradation.

For short lifetime fluorescent the data was analysed using an iterative reconvolution method to take account of the response function. The goodness of fit was calculated using a chi-squared parameter using Poissonian errors and this value was minimised over multiple iterations.

4.6 OLED Device Fabrication

Organic light emitting diodes (OLEDs) were made by sandwiching a spin-coated layer of organic semiconductor material between a transparent indium tin oxide (ITO) anode on a glass substrate and an evaporated cathode topped with a reflective aluminium layer. The ITO was 120 nm thick with a conductivity of 15ohm/Sq supplied on a 12x12x0.7 mm glass substrate by Merck Germany, Liquid Crystals Division. The area of the anode is controlled by etching the ITO to remove it from the glass and the cathode is deposited though a shadow mask to control the evaporation area. The active area is described by the region in which the anode and cathode overlap, as shown in Figure 4.2. The light is emitted through the ITO and the glass substrate and so the device is said to be bottom emitting.

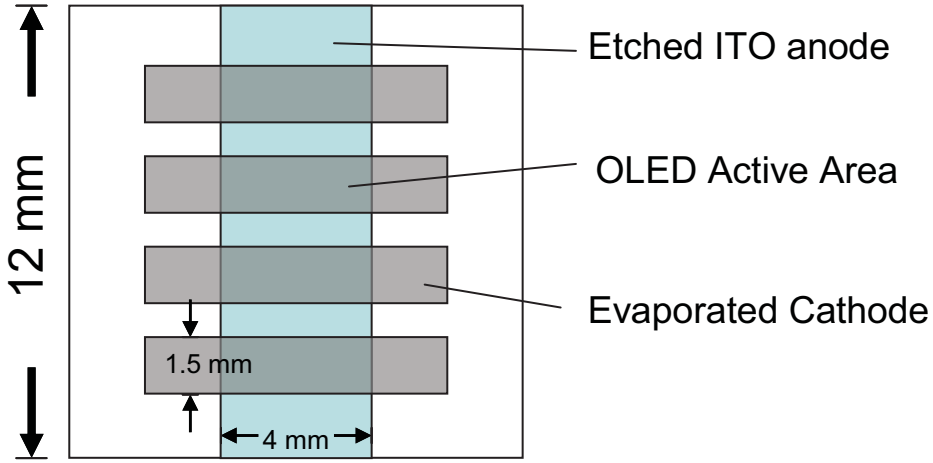

Figure 4.2 Diagram showing a top down view of an OLED device.

The ITO was etched by masking the anode area with a strip of electrical tape 4 mm wide. The substrate is then dusted with zinc powder catalyst and then etched with drops of 37% HCl from a pipette. The substrate was rinsed with isopropyl alcohol (IPA) within a few seconds to remove excess acid and then dried with dry nitrogen. The tape mask is then removed and the substrate was rinsed in IPA and dried once more.

The properties of the interface of the anode with the organic layer are very important to achieve efficient devices. First the interfaces must be clean as dust particles can

puncture the emissive layer causing short circuits and holes through which contaminants can enter the device. Grease and other residue can act as an insulator and increase the operating voltages and reduce the active area. Secondly the organic layer must properly wet the sample which is dependent on the surface energy. Finally the work function of the anode must be high enough that holes can be injected into the HOMO of the organic layer. It has been found that cleaning by oxygen plasma ashing following degreasing in organic solvents can increase the work function of ITO [8-10], as well as producing an easily wet high energy surface and removing contaminants. Therefore the substrates where cleaned by sonication in dichloromethane (DCM), then acetone and finally in IPA for 15 minutes each. The substrates where then dried with dry nitrogen and oxygen plasma ashed in an Emitech K-1050X for 5 minutes at 100 W.

Many workers employ the conducting polymer poly(3,4-ethylenedioxythiophene) poly(styrenesulfonate) (PEDOT:PSS) [11] on top of the ITO layer as the anode because of its ability to smooth roughness of the ITO, its lower work function for better hole injection and to improve electrical contact with the organic layers. These factors can reduce drive voltage, improve device reliability and improve charge balance in devices that are lacking in hole injection. In this work PEDOT was not used as in the phosphorescent polymers reported in Chapters 6 & 7 it was not observed to give any improvement and in some cases it actually reduced performance. This may be because these materials already allowed good hole injection.

The emissive layer was then spin coated from solution on the substrate as soon as the samples had been removed from the asher. Typically dichloromethane (DCM) was used as the solvent. The material was often blended with 4,4'-N,N'-dicarbazolyl-biphenyl (CBP) (Figure 4.3) as an ambipolar charge transport host typically with 20 wt% of the emissive material in 80 wt% host as this ratio has given good results in solution processable iridium dendrimers before [12]. This fraction was chosen originally to correspond to the same molar ratio as the best values for $Ir(ppy)_3$ doping in evaporated devices (~6 wt%) [13]. The advantages of host guest blending are discussed in Chapter 3.

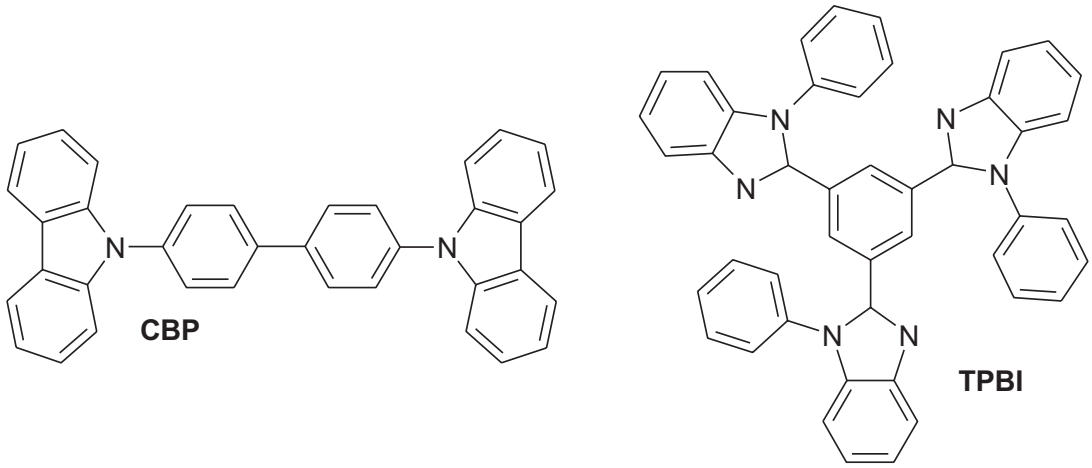

Figure 4.3 The chemical structures of charge transport host 4,4'-N,N'-dicarbazolyl-biphenyl (CBP) and electron transport/hole blocking material 1,3,5,-tris(2-N-phenylbenzimidazolyl)benzene (TPBI).

After spin-coating the samples were placed on a shadow mask for the deposition of 1.5 mm stripes of the subsequent layers shown in Figure 4.2 and placed in an Edwards FL 400 evaporator operating at a pressure of 10^{-6} mb. The area of shadow mask and ITO overlap defines the active area of the OLED devices. This transfer was made as quickly as possible to avoid sample contamination or degradation.

The evaporated layers deposited were different for single layer and bi-layer devices. A diagram showing both structures can be found in Figure 4.4. Single layer devices used a 20 nm low work function calcium layer for electron injection and were then topped with >100 nm of aluminium to protect the calcium from oxygen and to increase the cathode conductivity. Bi-layer devices used a second evaporated organic layer of 60 nm of 1,3,5,-tris(2-N-phenylbenzimidazolyl)benzene (TPBI) as an electron transport / hole blocking layer (structure in Figure 4.3). This ensures that the electron and hole currents in the device are well balanced as discussed in chapter 3.

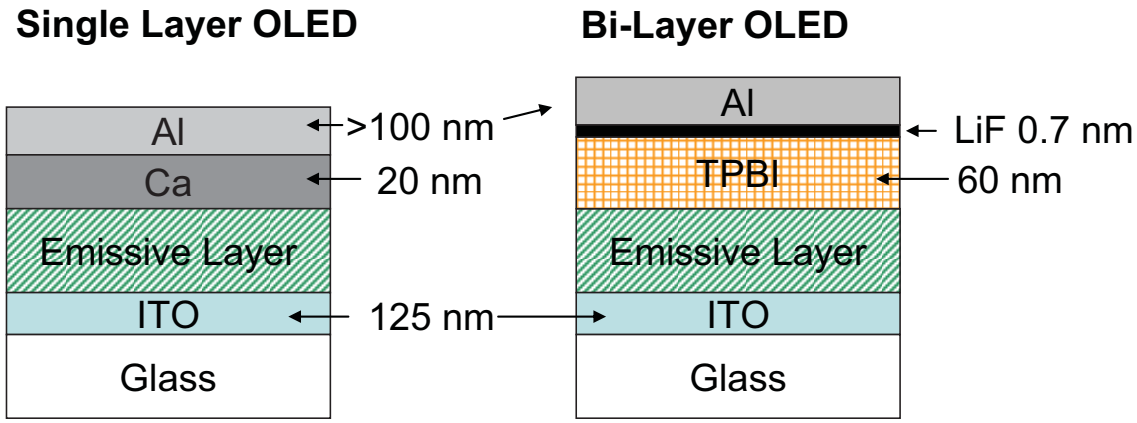

Figure 4.4 Single layer and bi-layer OLED structures.

The cathode is then evaporated on top of the TPBI layer. This consisted of a thin 0.7 nm layer of LiF and topped with >100 nm of aluminium. LiF has been shown to improve electron injection into some organic materials when used with aluminium [14] or calcium [15] cathodes. An advantage of Al/LiF cathodes over low work function metals is that it has increased chemical stability as an electrode. Unfortunately LiF's effectiveness seems to depend on the organic material deposited beneath it and so it cannot be used in all cases. Here we use it because of its known effectiveness on TPBI with an aluminium capping layer.

LiF must be deposited as a thin layer as bulk LiF is an insulator and so it can only be effective by modifying the properties at the interface. Proposed mechanisms have been the formation of a LiF dipole monolayer that reduces the work function of the aluminium, liberation of lithium metal to function as a low work function contact or doping of the organic layer with Li^+ ions [15]. Similar effects could be the reason that thin layers of MgO, CsF and Li_3PO_4 are also found to be effective [14-16].

More generally it is thought possible that any hot evaporated material can react chemically with the organic layer, the metal deposited above it or both to induce inter-band defect states into the organic which permit easier charge injection. These inter-band states are believed to exist and make electron injection easier even when less reactive materials like ITO are evaporated onto organic layers [17]. In this case ITO was used as the substrate and was also evaporated onto the top of the organic layer meaning that both cathode and anode should have similar work functions and thus

charge injection properties. However it was found that only the evaporated ITO contact could inject electrons and function as the cathode. This shows that the evaporation of the ITO caused an improvement in electron injection.

4.7 OLED Characterisation

The OLEDs were characterised in vacuum to avoid oxygen quenching or sample degradation during the measurement. The current / voltage characteristics were recorded using a Keithley 2400 Sourcemeter and the emission intensity was measured using a calibrated photodiode with a surface area of 1 cm^2 at a distance of 4 cm from the sample. The photodiode current was put through a transimpedance amplifier and the resulting voltage measured by a Keithley 2000 Multimeter. The emission spectrum of the OLED was measured using an Andor DV420-BV CCD spectrometer. This emission spectrum was also used to correct for the spectral response of the photodiode in order to determine the external quantum efficiency and match it to the eye's brightness response to allow measurement in photometric units.

In order to calculate the fraction of emitted light collected by the photodiode the emission of the OLED is assumed to be Lambertian meaning that the intensity of the emitted light goes as the cosine of the viewing angle from the normal. To simplify the calculation the square photodiode is taken to be a circle with the same active area (1 cm^2). The OLED is 4 cm from the detector and this is assumed to be sufficiently distant from the detector compared to the OLED's size (1.5 mm × 4 mm) that it can be taken as a point source and it is assumed to be aligned with the centre of the detector. The photodiode is taken to be the base of a cone of angle α with the point at the OLED as shown in Figure 4.5.

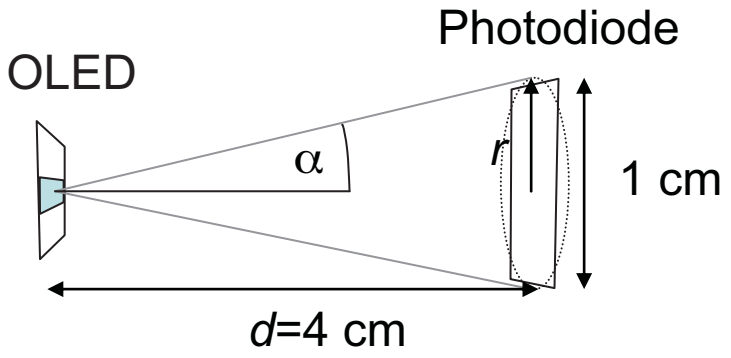

Figure 4.5 The geometry of the OLED and photodiode in the OLED characterisation setup.

The fraction of light emitted into the cone described by the angle α compared to the forward hemisphere by a Lambertian emitter (emission $\propto \cos(\theta)$) is given by Equation 4.9.

$$\eta_{\text{det}} = \frac{2\pi\int_0^{\alpha}\cos(\theta)\bullet\sin(\theta)d\theta}{2\pi\int_0^{\pi/2}\cos(\theta)\bullet\sin(\theta)d\theta} = \sin^2(\alpha) = \frac{r^2}{r^2+d^2} \qquad [4.9]$$

4.7.1 External Quantum Efficiency Calculation

The external quantum efficiency of an OLED is a measure of the number of photons emitted by the device for each electron worth of charge that crosses the device. As discussed in chapter 3, this parameter gives insight into how close to the theoretical maximum efficiency can be achieved by a given material but is not in itself an important parameter in a useful device.

As this quantity depends on the number of photons emitted if the spectral responsivity of the photodetector $R(\lambda)$ expressed in current per unit incident power then this number needs to be converted into a quantum efficiency $E(\lambda)$ in order to determine the number of photons N collected from the detected current I. For a single wavelength λ this is done by multiplying $R(\lambda)$ by the photon energy and dividing by

the charge on an electron *e*. This is shown in Equation 4.10 where *h* is plank's constant and *c* is the speed of light in vacuum.

$$E(\lambda) = R(\lambda)\frac{hc}{e\lambda} \qquad [4.10]$$

The average quantum efficiency of the detector for the emission spectrum of the sample $B(\lambda)$ should thus be calculated by Equation 4.11.

$$E_{avg} = \frac{hc}{e}\left\langle \frac{R(\lambda)}{\lambda} \right\rangle = \frac{hc\int B(\lambda)\frac{R(\lambda)}{\lambda}d\lambda}{e\int B(\lambda)d\lambda} \qquad [4.11]$$

The voltage measured by the Keithley 2000 Multimeter (V_{det}) as a result of the photocurrent (I_{det}) depends on the value of the transimpedance amplifier (Z_{det}) as shown in Equation 4.12.

$$V_{\mathrm{det}} = I_{\mathrm{det}} Z_{\mathrm{det}} \qquad [4.12]$$

Taking both the fraction of light collected by the photodiode (Equation 4.9) and the photodiode's quantum efficiency (Equation 4.11) it is possible to calculate the number of emitted photons. By dividing this by the OLED current I_{OLED} the external quantum efficiency (η_{ex}) can be calculated using Equation 4.13.

$$\eta_{ex} = \left[\frac{r^2 + d^2}{r^2}\right]\left[\frac{e\int B(\lambda)d\lambda}{hc\int B(\lambda)\frac{R(\lambda)}{\lambda}d\lambda}\right]\left[\frac{V_{\mathrm{det}}}{Z_{\mathrm{det}}}\right]\left[\frac{1}{I_{OLED}}\right] \qquad [4.13]$$

4.7.2 Luminous Efficiency Calculation

The brightness of a device as observed by the human eye is a useful parameter for both display and lighting applications. The human eye's relative brightness response to a given incident power given by $\bar{y}(\lambda)$ is not the same over all wavelengths and peaks in the green as shown in Figure 4.6 [18]. This means that blue and red light sources of a given power appear dimmer than the equivalent green light. In order to account for this the emission spectrum of the OLED needs to be taken into account to determine the perceived brightness.

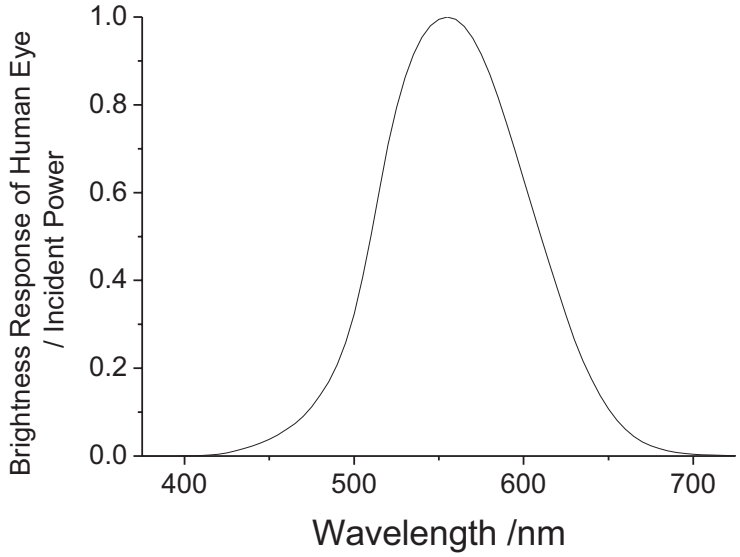

Figure 4.6 The brightness response of the human eye to incident power at a given wavelength $\bar{y}(\lambda)$.

The perceived brightness of light sources is measured in *photometric units* (as opposed to *radiometric units* for measurements of power). Photometric units are lumens (lm) which measure the total light output of a device and is most suitable for lighting applications. How bright a point light source appears at a distance is measured in candela (cd), which is a lumen per steradian. Brightness of displays or other extended light sources that are viewed directly is measured in candela per metre squared.

In order to determine the brightness of an OLED it is necessary to correct for the difference in the responsivity *R(λ)* of the photodiode to that of the human eye $\bar{y}(\lambda)$ to the emitted power spectrum of the OLED. The relative value is scaled by the peak response K_m of 683 lm/W to given an absolute response in lumens per watt. The power spectrum can be calculated by simply taking the emission spectrum, *B(λ)* in photons per unit wavelength, and dividing by the emission wavelength λ. This can be compared to the equivalent integral for the photodiode to give the measured photocurrent per lumen incident on the detector (the photopic response $R_{Photopic}$). This is given by Equation 4.14.

$$R_{Photopic} = \frac{\int_0^\infty R(\lambda)\beta(\lambda)/\lambda.d\lambda}{K_m\int_0^\infty \bar{y}(\lambda)\beta(\lambda)/\lambda.d\lambda} \qquad [4.14]$$

Using the fraction of light emitted collected by the detector from Equation 4.9 and the gain of the transimpedance amplifier the number of lumens of light emitted by the OLED, *F*, can be calculated using Equation [4.15].

$$F = \left[\frac{r^2+d^2}{r^2}\right]\frac{1}{R_{Photopic}}\frac{V_{\det}}{Z_{ref}} \qquad [4.14]$$

The assuming Lambertion emission the number of lumens per steradian or candelas in the forward direction, *L*, is calculated by determining emission in the forward direction divided by the total emission into the forward hemisphere as given in Equation [4.16].

$$f = \frac{\cos(0)}{\int_0^{2\pi}\int_0^{\pi/2}\cos(\theta)\sin(\theta)d\theta d\phi} = \frac{1}{\pi} \qquad [4.16]$$

Thus the brightness of the device in candelas, L, can be determined using Equation [4.17].

$$L = \frac{1}{\pi}\left[\frac{r^2 + d^2}{r^2}\right]\frac{1}{R_{Photopic}}\frac{V_{\det}}{Z_{ref}} \qquad [4.17]$$

1. Greenham, N.C., et al., *Measurement of Absolute Photoluminescence Quantum Efficiencies in Conjugated Polymers.* Chemical Physics Letters, 1995. **241**(1-2): p. 89-96.
2. Baldo, M.A., et al., *Highly efficient phosphorescent emission from organic electroluminescent devices.* Nature, 1998. **395**(6698): p. 151-154.
3. Demas, J.N. and G.A. Crosby, *Measurement of Photoluminescence Quantum Yields - Review.* Journal of Physical Chemistry, 1971. **75**(8): p. 991.
4. Melhuish, W.H., *Quantum Efficiencies of Fluorescence of Organic Substances: Effect of Solvent and Concentration on the Fluorescent Solute.* Journal of Physical Chemistry, 1961. **65**: p. 229.
5. Levell, J.W., et al., *Fluorescence Enhancement by Symmetry Breaking in a Twisted Triphenylene Derivative.* Journal of Physical Chemistry A, 2010. **114**(51): p. 13291.
6. de Mello, J.C., H.F. Wittmann, and R.H. Friend, *An improved experimental determination of external photoluminescence quantum efficiency.* Advanced Materials, 1997. **9**(3): p. 230-&.
7. Suzuki, K., et al., *Reevaluation of absolute luminescence quantum yields of standard solutions using a spectrometer with an integrating sphere and a back-thinned CCD detector.* Physical Chemistry Chemical Physics, 2009. **11**(42): p. 9850-9860.
8. Kim, J.S., et al., *Indium-tin oxide treatments for single- and double-layer polymeric light-emitting diodes: The relation between the anode physical, chemical, and morphological properties and the device performance.* Journal of Applied Physics, 1998. **84**(12): p. 6859-6870.
9. Wu, C.C., et al., *Surface modification of indium tin oxide by plasma treatment: An effective method to improve the efficiency, brightness, and reliability of organic light emitting devices.* Applied Physics Letters, 1997. **70**(11): p. 1348-1350.
10. Fujita, S., et al., *Surface treatment of indium-tin-oxide substrates and its effects on initial nucleation processes of diamine films.* Japanese Journal of Applied Physics Part 1-Regular Papers Short Notes & Review Papers, 1997. **36**(1A): p. 350-353.
11. Brown, T.M., et al., *Built-in field electroabsorption spectroscopy of polymer light-emitting diodes incorporating a doped poly(3,4-ethylene dioxythiophene) hole injection layer.* Applied Physics Letters, 1999. **75**(12): p. 1679-1681.
12. Lo, S.C., et al., *Green phosphorescent dendrimer for light-emitting diodes.* Advanced Materials, 2002. **14**(13-14): p. 975.
13. Baldo, M.A., et al., *Very high-efficiency green organic light-emitting devices based on electrophosphorescence.* Applied Physics Letters, 1999. **75**(1): p. 4-6.

14. Hung, L.S., C.W. Tang, and M.G. Mason, *Enhanced electron injection in organic electroluminescence devices using an Al/LiF electrode.* Applied Physics Letters, 1997. **70**(2): p. 152-154.
15. Brown, T.M., et al., *Electronic line-up in light-emitting diodes with alkali-halide/metal cathodes.* Journal of Applied Physics, 2003. **93**(10): p. 6159-6172.
16. Gassmann, A., et al., *Interface properties of a Li3PO4 /Al cathode in organic light emitting diodes.* Journal of Applied Physics, 2009. **105**: p. 124517.
17. Parthasarathy, G., et al., *High-efficiency transparent organic light-emitting devices.* Applied Physics Letters, 2000. **76**(15): p. 2128-2130.
18. *Commission Internationale de l'Éclairage Proceedings, 1931*.1931: Cambridge University Press.

5. Fluorescent Enhancement Using a Twisted Tripheneylene Derivative

5.1 Introduction

Aggregation effects, described in Chapter 3, often result in quenching of luminescence in organic light emitting materials. This problem is also referred to as concentration quenching as the light emission is quenched by two or more of the emissive chromophores interfering with one another [1, 2]. These interactions appear in solution but result in greater problems in the solid state as the molecules are much closer together so excitations can diffuse to lower energy quenching sites [3, 4].

Various strategies are used to control aggregation in light emitting materials. Bulky side groups can be attached to conjugated polymers [4, 5], branching dendrimer arms can be attached to emissive cores [6-8] or higher energy host molecules can be used to physically separate the cores. Another approach is to twist the geometry of the molecules out of a single plane so that stacking is not possible, for example in the case of spiro-fluorenes [9]. In this chapter I explore an exampole of this last type of aggregation.

Triphenylene is an example of a planar molecule which is prone to aggregation by π stacking. In fact it is commonly used to make columnar structures for liquid crystals [10-13]. In this work, I have investigated the improvement in the fluorescence efficiency of triphenylene when additional methyl groups are added to the 1,4,5,8,9 and 12 positions which forces the molecule out of the plane [14]. This modified

material was synthesised and characterised chemically by Yi Wang and Trent Galow at the University of Edinburgh. The structure of these materials is shown in Figure 5.1 and an illustration of the 3D structure of both these molecules is shown in Figure 5.2. While 1,4,5,8,9,12-hexamethyltriphenylene (HMTP) could be expected to form a propeller shaped molecule that is identical if rotated by 120 degrees on an axis vertically through the central ring (said to have D_3 symmetry). However, data from NMR and X-ray crystallography shows that the molecule prefers instead to adopt a C_2 symmetry arrangement [14]. In this conformation it has 2 fold rotational symmetry along an axis lying in the plane of diagram below. Minor distortions with this C_2 symmetry are actually observed in triphenylene using X-ray diffraction but these deviations from planarity are very small, being of the order 0.1 Å [15].

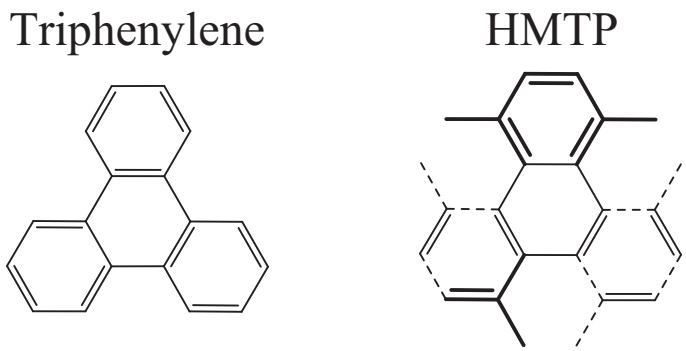

Figure 5.1 The materials structures of tripheneylene and 1,4,5,8,9,12-hexamethyltriphenylene (HMTP).

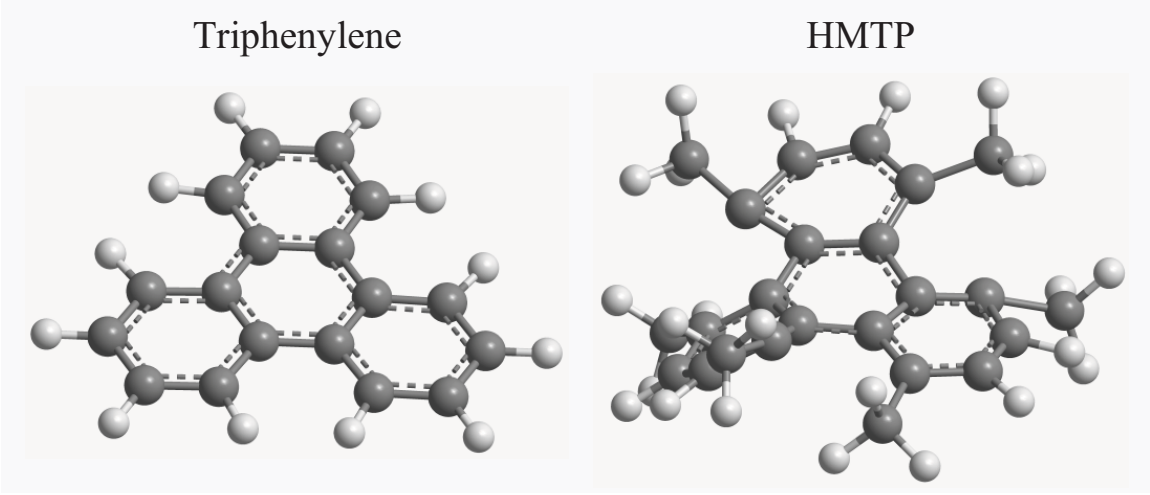

Figure 5.2 An illustration of the 3 dimensional structures of triphenylene and HMTP.

Triphenylene has an unusually low radiative rate for a fluorescent material (27 μs^{-1}), because its symmetry forbids transitions between the first excited singlet (S1) and ground state (S0) [10, 16, 17]. As a result of the twisting HMTP should break this symmetry which should result in a change in the emissive properties.

5.2 Measuring Oscillator Strength

In this work I have used the absorption strength and the radiative lifetime of the triphenylene and HMTP to calculate and compare the transition dipole moments of these two molecules. This dipole moment determines the efficiency of light emission from the molecules and thus crucial to light emitting applications. This measurement was done following the work of Strickler-Berg [18] and Förster [19] by looking at the molecules' radiative lifetime and molar extinction coefficient.

In 1917 Einstein argued using the thermodynamics of the black body spectrum that, for a two level system, the rates of spontaneous emission (A coefficient) and absorption and stimulated emission (B coefficient) must be related [20]. This situation is shown in Figure 5.3. The black body photons with an energy equal to the energy difference (ΔE) between the two states can be absorbed (Equation 5.1) or induce stimulated emission (Equation 5.2). However, spontaneous emission is only determined by the population of the upper state (Equation 5.3).

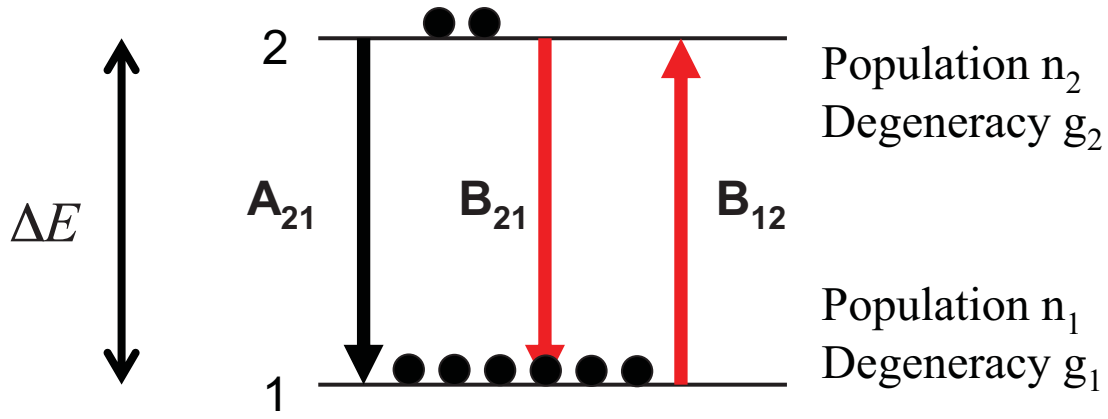

Figure 5.3 A two level system showing Einstein's A and B coefficients for spontaneous emission, absorption and stimulated emission.

$$\Gamma_{Absorption} = n_1 B_{12} I(\Delta E) \quad [5.1]$$

$$\Gamma_{Stimulated} = n_2 B_{21} I(\Delta E) \quad [5.2]$$

$$\Gamma_{Spontainious} = n_2 A_{21} \quad [5.3]$$

Where the rate of absorption is $\Gamma_{Absorption}$, $\Gamma_{Stimulated}$ is the rate of stimulated emission, $\Gamma_{Spontainious}$ is the rate of spontaneous emission and $I(\Delta E)$ is the spectral radiance of the black body radiation at the transition energy. At equilibrium the population of states in the two levels must be described by a Boltzmann distribution (Equation 5.4) which must have the same temperature as the black body radiation field it is bathed in.

$$\frac{n_1}{n_2} = \frac{g_1}{g_2} e^{\Delta E / k_B T} \qquad [5.4]$$

The black body spectrum is given by Plank's law in Equation 5.5. Here k_B is Boltzmann's constant, T is the temperature, c is the speed of light in vacuum and h is Plank's constant.

$$I(\Delta E) = \frac{2\Delta E^3}{h^2 c^2} \frac{1}{e^{\Delta E / k_B T} - 1} \qquad [5.5]$$

The only way to achieve equilibrium at all possible temperatures is if the total rates of transistions up and down cancel. This is the case if Equations 5.6 and 5.7 hold, where g_1 and g_2 are the degeneracies of levels 1 and 2.

$$\frac{B_{12}}{B_{21}} = \frac{g_2}{g_1} \qquad [5.6]$$

$$\frac{A_{21}}{B_{21}} = \frac{2\Delta E^3}{h^2 c^2} \qquad [5.7]$$

This observation that absorption and spontaneous emission rates were linked was extended to molecular systems by Strickler and Berg in 1962 [18]. Molecules have multiple vibrational states in their absorption and emission bands, rather than single lines, which requires an integral over all the energy states in a band. Förster's work allows the absorption dipoles for molecules to be calculated [19], while Stickler and Berg related the rate of spontaneous emission to the emission dipole moment associated with the transition [18]. The absoption and emission dipole moments, d_a

and d_e respectively, are calculated below following Equations 5.8 and 5.9. The dipole moments are expressed in units of Debye (D). One Debye is 3.33564×10^{-30} Cm. The absorption dipole moment is calculated using the integrated molar extinction coefficient spectrum $\varepsilon(\tilde{\nu})$ in $M^{-1}cm^{-1}$ integrated over photon energy in units of wavenumber in cm^{-1} ($\tilde{\nu}$) and the local refractive index *n*.

$$\left|d_a\right|^2 = 9.186\times10^{-3} n \int \frac{\varepsilon(\tilde{\nu})}{\tilde{\nu}} d\tilde{\nu} \qquad [5.8]$$

The emission dipole moment d_e is calculated using the radiative lifetime τ_R in seconds and the emission spectrum versus energy in photons per joule $I(E)$. Here ε_0 is the electric permittivity of free space in Fm^{-1}, c is the speed of light in ms^{-1} and $\hbar$ is the reduced Planck's constant in J s.

$$\left|d_e\right|^2 = \frac{3\pi\varepsilon_0\hbar^4c^3\left(\int E^{-3}I(E)dE \,/\, \int I(E)dE\right)}{3.33564\times10^{-30} n\tau_R} \qquad [5.9]$$

Stickler and Berg note that their formula can only be expected to provide the same dipole moment in absorption and emission in cases where the molecule does not significantly change shape in the excited state, as this would obviously affect the dipole moments. They also note that their calculations make use of an assumption that the transitions are strongly allowed, unlike those in triphenylene. However as I am only aiming to compare the relative strengths of dipole moments of HMTP and triphenylene rather than provide exact values, these equations should be sufficient. The measured photoluminescence quantum yield and transient luminescence are direct measures of the emissive properties of the molecule and can still be used to compare molecules' emissive properties in the weakly allowed or forbidden regime.

5.3 Results and Discussion

5.3.1 Absorption Properties

The HMTP and triphenylene were dissolved in tetrahydrofuran (THF) at a known concentration of 0.01 mg/ml so that their absolute molar absorption spectra could be calculated. The resulting absorption spectra are shown in Figure 5.4.

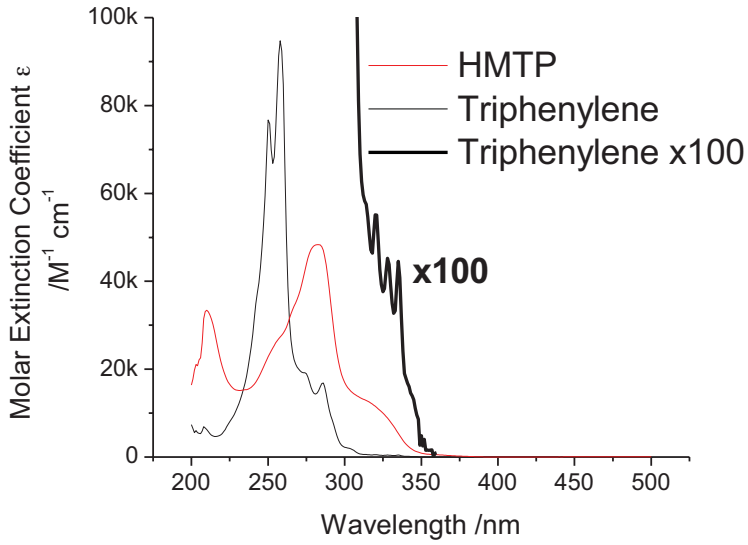

Figure 5.4 Molar extinction coefficients of triphenylene and HMTP solutions in THF at 0.01 mg/ml concentration. The thick black line shows a 100 times scale up of the longer wavelength absorption of triphenylene.

The triphenylene absorption spectrum is more structured than that of HMTP. Much of this extra structure is likely to be due to vibronic peaks that occur due to splitting of the excited and ground states into different vibrational levels. As the features of triphenylene spectrum between 300-350 nm are much smaller than the absorption at shorter wavelength I have magnified them by 100 times. The HMTP structure, by contrast, only contains 5 broader peaks and shoulders at 320 nm, 285 nm, 260 nm, 210 nm and 204 nm. The triphenylene has much weaker long wavelength absorption than the HMTP. Comparing the longer wavelength, lower energy, extinction coefficients it is clear that the triphenylene has a weaker absorption dipole moment than HMTP.

In order to calculate the absorption dipole moments the spectra need to be re-plotted in terms of energy or wavenumbers, instead of wavelength, and the absorption transistions assigned to the S0→S1 transition and its vibronic sublevels. This has been done for Triphenylene in Figure 5.5 and HMTP in Figure 5.6 below. Both graphs use the same vertical scale for clarity. From the literature we would expect to find the absorption of the triphenylene S0→S1 at around 30,500 wavenumbers (328 nm). These values were calculated using quantum chemical calculations on triphenylene [16, 17] and a hexaalkoxy-substituted triphenylene derivative [13]. There is indeed a series of peaks at this energy in the triphenylene spectrum, however it is difficult to see compared to the higher energy absorption and so in Figure 5.5 the relevant part of the curve has been magnified 100 times. The S0→S1 transition in HMTP is assigned to the lowest energy absorption peak at 31450 wavenumbers (318 nm).

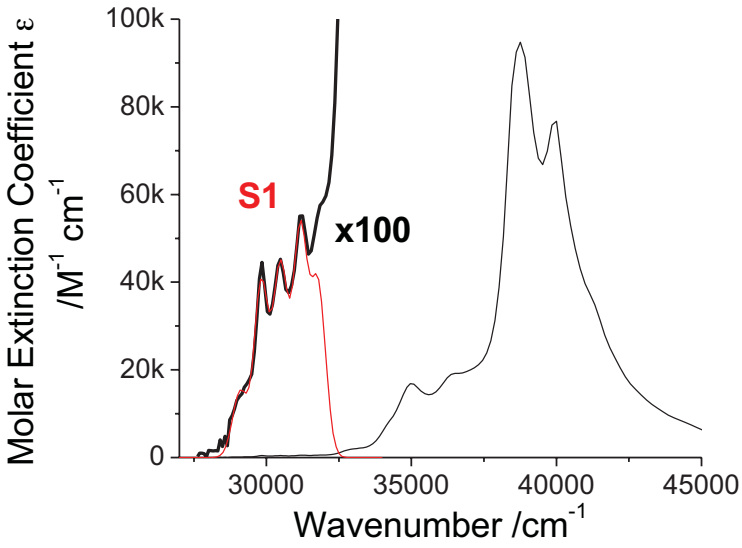

Figure 5.5 The molar extinction coefficient of triphenylene versus wavenumber. The lower energy part of the spectrum has been magnified by 100 times and is shown by the thick line. The peak corresponding to the S0→S1 transition fit is shown by the thin red line.

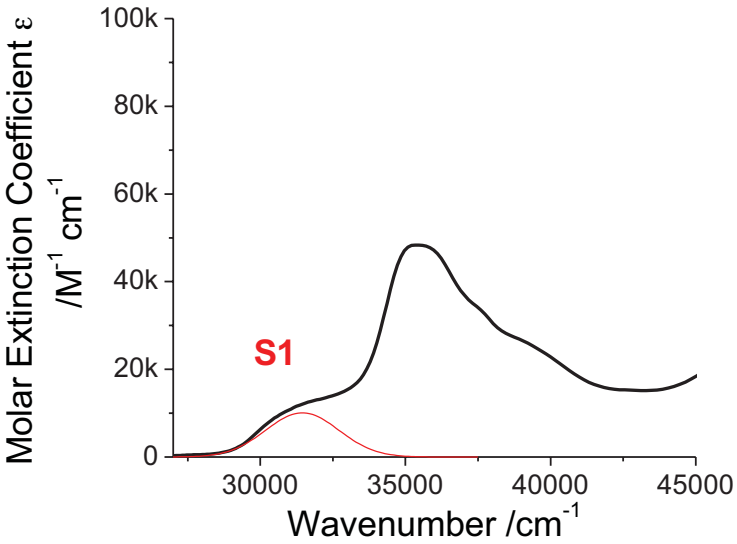

Figure 5.6 The molar extinction coefficient of HMTP versus wavenumber. The S0→S1 transition fit is shown by the thin red line.

All the transitions were fitted using Gaussian curves using SpectraSolve software. The triphenylene curve had vibronic structure and so was fitted with multiple Gaussians with approximately even energy spacing. The peak wave numbers of the curves assigned to the S0→S1 transitions are shown in Table 5.1, along with the calculated absorption dipole moments. These results confirm that the absorption dipole strength of the HMTP is much stronger than that of triphenylene.

Transition: **S0 S1**	**Absorption Peak Positions** **/cm^{-1}**	**Average Peak Spacing** **/cm^{-1}**	**Absorption Transition Dipole** **/D**
Triphenylene	29090, 29820, 30490, 31160, 31770	670	0.7
HMTP	31450	-	3.6

Table 5.1 The absorption peaks and dipole moments associated with the S0→S1 transition in triphenylene and HMTP.

5.3.2 Emission Properties

The concentration dependent emission properties of triphenylene and HMTP were investigated in THF solutions and in neat films. The films were spin coated at 2000 rpm from 20 mg/ml THF solutions onto quartz discs. The films were found have thicknesses of ~150 nm using a Vecco DekTak 3 surface profiler. Unfortunately, the absorption spectrum of triphenylene overlaps with its emission spectrum, so changes in the emission spectra may result from the inner filter effect. This effect occurs at high concentrations, where short wavelength emission can be reabsorbed by the solution itself. This is a problem in the normal fluorescence measurement geometry shown below in Figure 5.7. Instead the samples were measured using a "front face" geometry to minimise the effects of self absorption, which is also shown in Figure 5.7. The standard geometry also encounters problems at high concentration because the majority of excitation light is absorbed close to the front face of the cuvette. This means that the bulk of the emission may be outside the viewing area of the detector's optics, so the signal can be very low even though the sample contains a high concentration of efficient emitters. For triphenylene it was calculated from the absorption spectrum that at the 350 nm blue shoulder in the solution emission of the most concentrated 0.23 mg/ml solution would absorb less than 10% of the light across the entire 1 cm cuvette. As a result of these precautions the inner filter effect should be negligible.

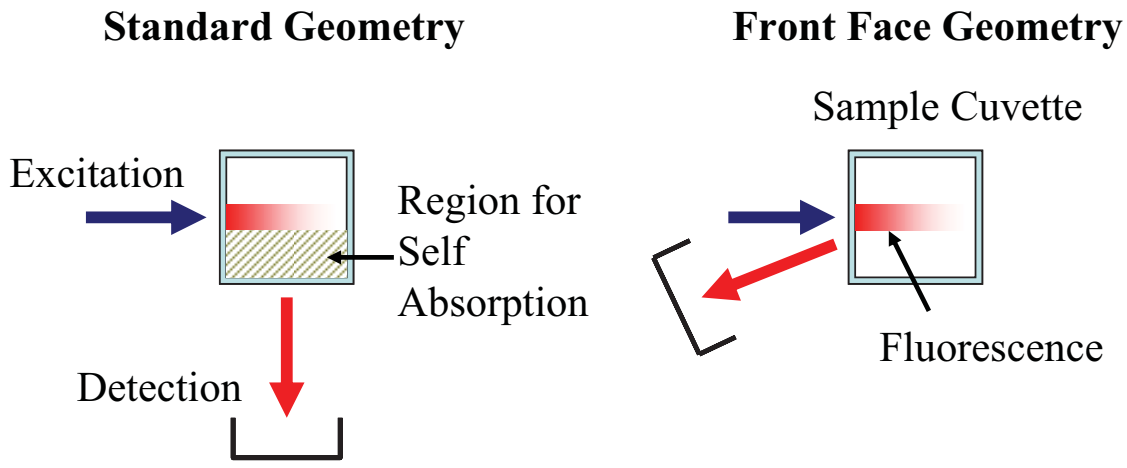

Figure 5.7 The standard right angle fluorescence measurement geometry and the front face measurement geometry.

The concentration dependent emission spectrum for triphenylene is shown in Figure 5.8 and the concentration dependent emission spectrum of HMTP is in Figure 5.9. The triphenylene spectra are structured with clearly defined peaks and shoulders. The triphenylene shows a clear red-shifting and broadening of the emission spectrum with increasing solution concentration, with the greatest change occurring between 0.04 mg/ml and 0.23 mg/ml where the emission peak moves from 369 nm to 390 nm. There is also a significant change between the solution spectra and the film which is also red-shifted and broadened with its emission peak at 404 nm. This red-shifting of the emission spectrum is consistent with aggregation effects on triphenylene based emission in organogels [12].

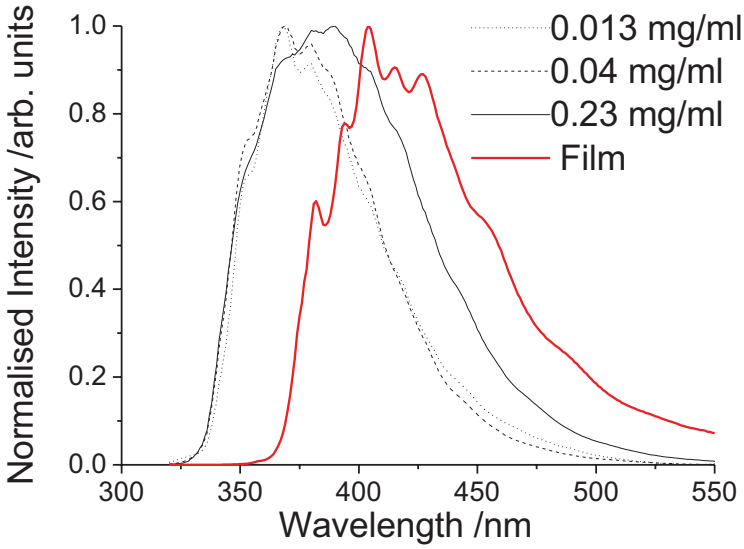

Figure 5.8 A comparison of the emission spectra of triphenylene solutions in THF at various concentrations and a thin film. All samples excited at 300 nm using front face geometry.

In contrast, the HMTP emission spectrum is relatively featureless and does not show any large change in emission peak position with concentration with the peak consistently about 423-424 nm. Using a simple model of conjugated molecules one would expect a twisted structure to shorten the conjugation length and thus blue shift the emission spectrum, however, the HMTP has longer wavelength emission than the triphenylene in dilute solution. This increase in emission wavelength is similar to the red-shifting of emission of oligo(phenylenevinylene) single molecules when they

were in a bent conformation [21]. The bent molecules were also observed to give broader and featureless emission, just like the HMTP.

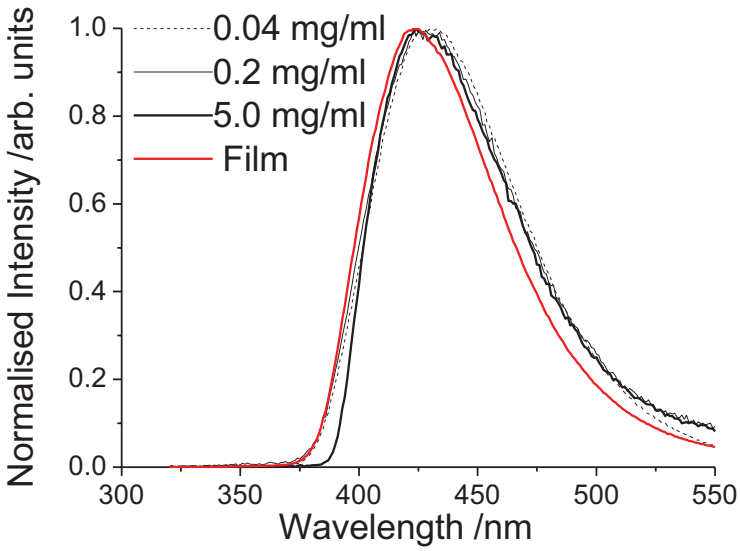

Figure 5.9 A comparison of the emission spectra of triphenylene solutions in THF at various concentrations and a thin film. All samples excited at 300 nm using front face geometry.

HMTP has longer wavelength emission but the S0→S1 absorption wavelength of both HMTP and triphenylene is at a similar wavelength of about 325 nm. This results in a larger Stoke's shift for HMTP which suggests there is more reorganisation of the excited state than for triphenylene. This might result from increased molecular flexibility because of the strained nature of HMTP's structure. Evidence from this comes from conformational inter-conversions observed at room temperature in NMR data where the methyl groups exchange positions from in to out of the page and vice versa [14].

Time-resolved luminescence measurements were made using time-correlated single photon counting (TCSPC) on 3 times freeze-pump-thaw degassed solutions in THF. These solutions were dilute as they had been chosen to have 0.1 abs at 285 nm in a 1 cm path length cuvette. This optical density was chosen so that solution photoluminescence quantum yield (PLQY) measurements could be performed on the same samples using a comparison to a 2-aminopyridine standard in 0.05 M sulphuric acid following the method described in Chapter 4. This standard has a PLQY of 60%

when excited at 285 nm [22]. Using the molar extinction coefficients this results in a concentration of 0.0014 mg/ml for triphenylene and 0.00065 mg/ml for HMTP. These concentrations are much lower than the point at which concentration dependent effects were observed in the triphenylene emission spectrum.

These samples were also compared to neat films spin coated under the same conditions as above. These samples were measured in vacuum. The samples were excited at 266 nm using twice frequency doubled Nd:YAG laser giving an instrument response function of ~500 ps full width half maximum. The results from the triphenylene solution and film are shown in Figure 5.10 and the results from the HMTP solution and film were shown in Figure 5.11.

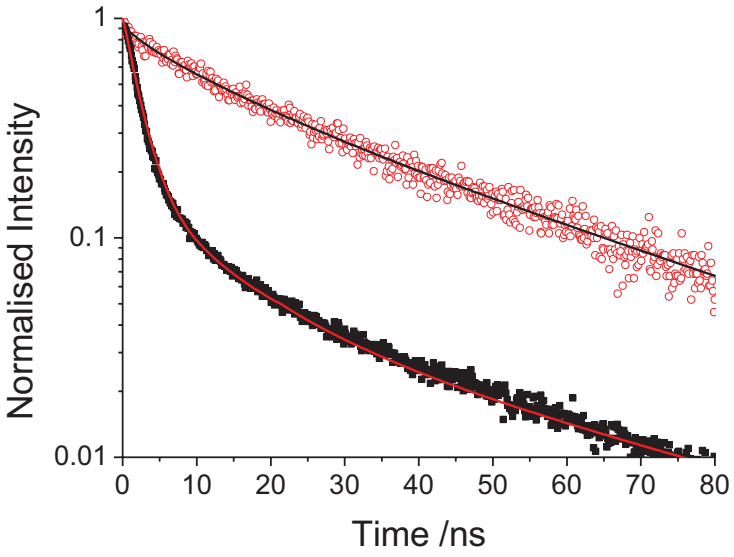

Figure 5.10 Triphenylene Time-resolved luminescence in solution (red open circles, black fit line) and film (black filled squares, red fit line). Samples were excited at 266 nm and the emission detected at 390 nm.

The triphenylene fluorescence decays are not straight lines on the log plot and so are not well fitted by a single exponential decay. This indicates that the samples contain multiple emissive environments, even in the dilute solution. By contrast HMTP shows single exponential decays in solution, film and powder indicating only one emissive state is present in both solution and solid samples.

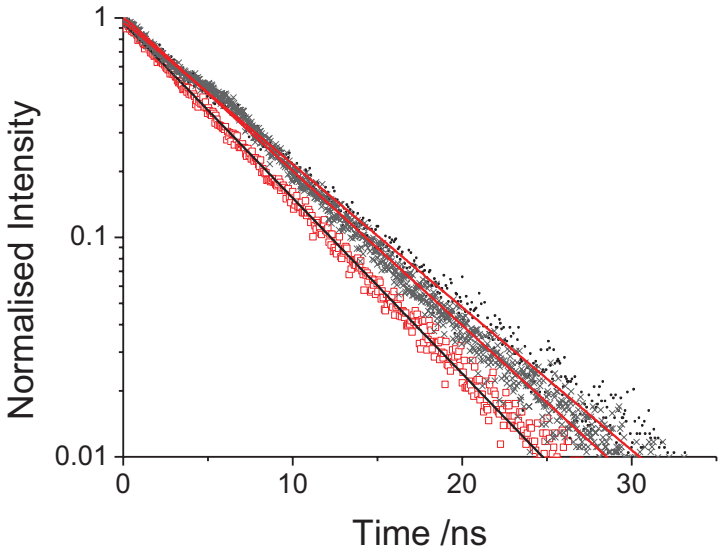

Figure 5.11 HMTP Time-resolved luminescence in solution (red open squares, black fit line) and film (black filled circles, red fit line). These samples were excited at 266 nm and the emission detected at 425 nm. HMTP powder is also shown excited at 355 nm with detection at 425 nm (black diagonal crosses, red fit line).

The PLQY values for all of the samples and the fitting parameters for the Time-resolved luminescence are shown in Table 2. These values have been used to calculate the emissive dipole moments. In the solid samples a refractive index of 1.8 has been assumed as this is a typical value for organic semiconductor films [23-25]. As the dipole moment only varies as the square root of the refractive index this should give adequate level of accuracy. For the samples with multiple lifetimes accurate dipole strength calculations cannot be made. This is because the PLQY values are an average measurement and the contribution of the individual states cannot be unpicked. In this case an estimate is calculated using a simple weighted average of all the lifetime components.

Sample	PLQY (λ Excitation)	Lifetime /ns (λ Excitation)	Radiative Rate /μs^{-1}	Emission Transition Dipole Moment / D
Triphenylene: Solution	6 % (285 nm)	10%, 2.3; 35%, 12.7; 55%, 38.6 Average = 25.8 (266 nm)	1.7*	0.5*
Triphenylene: Film	13 % (325 nm)	85%, 2.1; 11%, 11.1; 4%, 47.0 Average = 4.9 (266 nm)	27*†	1.9*†
Triphenylene: Powder	12 % (325 nm)			
HMTP: Solution	5 % (285 nm), 5 % (360 nm)	5.4 (266 nm)	9.2	1.3
HMTP: Film	31 % (325 nm)	6.7 (266 nm)	46	2.1
HMTP: Powder	31 % (325 nm)	6.2 (355 nm)	50	2.1

Table 5.2 The PLQY values, fluorescence lifetimes and emission dipole moments of triphenylene and HMTP in solution, film and powder. For multiple exponential fits the percentage figures refer to the initial amplitudes associated with each component (the pre-exponential factors).

** Calculated based on average lifetime.*

† Triphenylene film emission is dominated by aggregates and so cannot be used to calculate the molecular dipole moment.

The concentration dependence of triphenylene emission and the multiple emissive states that appear in Time-resolved luminescence both suggest that the triphenylene is π stacking, even in dilute solution, and forming aggregates. X-ray diffraction data shows that HMTP does not π stack in the solid state [14] and this is consistent with the fact that HMTP does not show concentration dependence in solution, and even in the solid state only one emissive state is present.

In dilute solution, where aggregation should not play a significant role, the PLQYs of HMTP (5%) and triphenylene (6%) are comparable but the HMTP has a much shorter lifetime (5.4 ns compared to an average lifetime of 25.8 ns). This shows that the HMTP has a higher radiative rate, and because the emission energies are not too different, this indicates a higher emission dipole moment than triphenylene. This confirms the results that the absorption dipole is higher in HMTP than triphenylene.

Both the HMTP and triphenylene films show increased PLQY compared to the solutions. This is unusual, as normally concentration quenching reduces luminescence in the solid state. In triphenylene the PLQY increases from 6% to 13% in film and this is accompanied by a decrease in the emission lifetime indicating that there is an increase in the radiative rate. As we would expect the solid state to contain π stacked aggregates this appears to be a case of aggregate enhanced emission [2]. This could be due to the fact that the isolated triphenylene molecule's symmetry is what prevents light emission. Aggregates offer a way in which this symmetry could be broken resulting in greater light emission efficiency.

When calculating the solution dipole moment for the triphenylene an average lifetime has been used, however, lifetime data from the literature gives a fluorescence lifetime of about 40 ns [17, 26]. This is a close match to the 55% 38.6 ns component present in dilute solution and so this component is likely to correspond to the monomer. If this ~40 ns lifetime is used to calculate the emission dipole moment then it decreases slightly from 0.5 D to 0.4 D. Both values are consistent with the solution absorption dipole moment of 0.7 D.

HMTP's enhancement in PLQY is more dramatic as it increases from 5% to 31% in film. In HMTP there is only one exponential component in both solution and film indicating that there is only one emissive state, and making aggregation induced changes to the emissive properties unlikely. The lifetime of the HMTP in solution is 5.4 ns, which is shorter than in film (6.7 ns) or powder (6.2 ns). This could imply that the increased PLQY in film is due to a reduced non-radiative de-excitation rate. This could happen if the HMTP molecule could de-excite through molecular vibrations which are prevented in the solid state [27]. An example of the kinds of vibrations that are possible are the conformational inter-conversion that HMTP undergoes [14]. This could offer an increased non-radiative pathway in the solution state for excitations to decay that would be blocked in the solid state by the rigid framework provided by the neighbouring molecules. Unfortunately an increased non-radiative rate does not suffice as an explanation, as the change in lifetime is too small to account for the change in PLQY by itself. This can be seen in the fact that HMTP solutions and films have significantly different calculated radiative rates in Table 5.2.

It is possible that in solution some of the HMTP molecules adopt different conformations or transition states that are capable of absorption but do not emit light. This would cause a lowering of the measured PLQY as photons would be absorbed by these conformers without emitting light, apparently increasing the number of absorbed photons for each one emitted. This hypothesis would also explain that while the absorption and emission dipole moments for triphenylene are similar (0.7 D and 0.5 D) in dilute solution they are significantly different in HMTP (3.6 D and 1.3 D). The lower emission dipole moment could be explained if I were including non-emissive conformers in my calculation. This is because the reduced PLQY reduces the radative rate, which is used in the calculation of the emission dipole. The film emission dipole moment of HMTP is 2.1 D, closer to the absorption value and so perhaps offers a better model for the isolated HMTP molecule in the C_2 conformation shown in Figure 5.1. This suggests that dark conformers are a likely explanation for the anomalously low solution PLQY in HMTP.

5.4 OLED Measurements

OLED measurements of neat HMTP films ~100 nm were attempted using a single layer structure however the material was found to be insulating. The films also crystalised within a short time after being spin cast resulting in significant film roughness that would be deleterious to device performance. OLEDs were also attempted using 20 wt% of HMTP in a host of 4,4'-N,N'-dicarbazolyl-biphenyl (CBP) to try and improve charge transport and prevent crystalisation however the performance of these devices was extremely low and the electroluminescence spectrum did not correspond to HMTP's photoluminescence spectrum. By comparing the emission spectrum of these devices to devices made with neat CBP it was determined that the HMTP was resulting in significant changes in the emission spectrum and so the emission in the blended device could not be ascribed to CBP alone.

5.5 Conclusion

By comparing the triphenylene dilute solution measurement (which contains the fewest aggregates) and the HMTP film measurement (which is not affected by non-emissive conformers) we conclude that breaking the triphenylene symmetry has meant the S1→S0 transition is no longer forbidden. This means the twisted HMTP molecule has a dipole moment by ~4 times greater and radiative rate ~20 times faster than triphenylene.

The twisted structure of HMTP also prevents π stacking and thus aggregation in the solid state. This can be seen from the fact that the concentration dependence of triphenylene's emission spectrum has been eliminated in HMTP, and single lifetime fluorescence decay from HMTP solution and films show a single emissive state. Together, with the increased oscillator strength this resulted in efficient luminescence from HMTP films with a photoluminescence quantum yield of 31%.

The PLQY of HMTP in films and powder is 6 times as high as in the solution. This difference is explained partially by an increased non-radiative rate in solution, but the main part of this difference is assigned to the presence of dark conformers within the solution, which contribute to the absorption but do not emit light.

Overall the results show that twisting molecules out of one plane is an effective strategy for eliminating intermolecular interactions, and producing efficient emissive materials.

1. Melhuish, W.H., *Quantum Efficiencies of Fluorescence of Organic Substances: Effect of Solvent and Concentration on the Fluorescent Solute.* Journal of Physical Chemistry, 1961. **65**: p. 229.
2. Hong, Y.N., J.W.Y. Lam, and B.Z. Tang, *Aggregation-induced emission: phenomenon, mechanism and applications.* Chemical Communications, 2009(29): p. 4332-4353.
3. Schouwink, P., et al., *The influence of molecular aggregation on the device properties of organic light emitting diodes.* Thin Solid Films, 2000. **372**(1-2): p. 163-168.
4. Setayesh, S., et al., *Polyfluorenes with polyphenylene dendron side chains: Toward non-aggregating, light-emitting polymers.* Journal of the American Chemical Society, 2001. **123**(5): p. 946-953.
5. Gambino, S., A.K. Bansal, and I.D.W. Samuel, *Comparison of hole mobility in thick and thin films of a conjugated polymer.* Organic Electronics, 2010. **11**(3): p. 467-471.
6. Burn, P.L., S.C. Lo, and I.D.W. Samuel, *The development of light-emitting dendrimers for displays.* Advanced Materials, 2007. **19**(13): p. 1675-1688.
7. Lo, S.C., et al., *Green phosphorescent dendrimer for light-emitting diodes.* Advanced Materials, 2002. **14**(13-14): p. 975.
8. Lo, S.C., et al., *Encapsulated cores: Host-free organic light-emitting diodes based on solution-processible electrophosphorescent dendrimers.* Advanced Materials, 2005. **17**(16): p. 1945-+.
9. Salbeck, J., et al., *Low molecular organic glasses for blue electroluminescence.* Synthetic Metals, 1997. **91**(1-3): p. 209-215.
10. Markovitsi, D., et al., *Triphenylene Columnar Liquid-Crystals - Excited States and Energy Transfer.* Journal of Physical Chemistry, 1995. **99**(3): p. 1005-1017.
11. McKenna, M.D., et al., *Discotic liquid crystalline poly(propylene imine) dendrimers based on triphenylene.* Journal of the American Chemical Society, 2005. **127**(2): p. 619-625.
12. Ikeda, M., M. Takeuchi, and S. Shinkai, *Unusual emission properties of a triphenylene-based organogel system.* Chemical Communications, 2003(12): p. 1354-1355.
13. Markovitsi, D., et al., *Triplet excitation transfer in triphenylene columnar phases.* Journal of Physical Chemistry B, 2001. **105**(7): p. 1299-1306.
14. Wang, Y., et al., *1,4,5,8,9,12-hexamethyltriphenylene. A molecule with a flipping twist.* Journal of the American Chemical Society, 2007. **129**(43): p. 13193-13200.
15. Ahmed, F.R. and J. Trotter, *The Crystal Structure of Triphenylene.* Acta Crystallographica, 1963. **16**(6): p. 503-508.
16. Di Donato, E., et al., *Tuning Fluorescence Lifetimes through Changes in Herzberg-Teller Activities: The Case of Triphenylene and Its Hexamethoxy-*

Substituted Derivative. Journal of Physical Chemistry A, 2009. **113**(23): p. 6504-6510.
17. Kokkin, D.L., et al., *Gas phase spectra of all-benzenoid polycyclic aromatic hydrocarbons: Triphenylene.* Journal of Chemical Physics, 2007. **126**(8).
18. Strickler, S.J. and R.A. Berg, *Relationship between absorption intensity and fluorescence lifetime of molecules.* Journal of Chemical Physics, 1962. **37**(4): p. 814.
19. Knox, R.S. and H. van Amerongen, *Refractive index dependence of the Forster resonance excitation transfer rate.* Journal of Physical Chemistry B, 2002. **106**(20): p. 5289-5293.
20. Einstein, A., *Zur Quantentheorie der Strahlung.* Physikalische Zeitschrift, 1917. **18**: p. 121-128.
21. Becker, K., et al., *How chromophore shape determines the spectroscopy of phenylene-vinylenes: Origin of spectral broadening in the absence of aggregation.* Journal of Physical Chemistry B, 2008. **112**(16): p. 4859-4864.
22. Rusakowicz, R. and A.C. Testa, *2-Aminopyridine as a Standard for Low-Wavelength Spectrofluorimetry.* Journal of Physical Chemistry, 1968. **72**(7): p. 2680.
23. Liu, Z.T., et al., *The characterization of the optical functions of BCP and CBP thin films by spectroscopic ellipsometry.* Synthetic Metals, 2005. **150**(2): p. 159-163.
24. Greenham, N.C., R.H. Friend, and D.D.C. Bradley, *Angular-Dependance of the Emission From a Conjugated Polymer Light-Emitting Diode - Implications For Efficiency Calculations.* Advanced Materials, 1994. **6**(6): p. 491-494.
25. Khalfin, V.B., et al., *Weak microcavity effects in organic light-emitting devices.* 1998. **- 58**(- 7).
26. Wallace, W.L., R.P. Vanduyne, and F.D. Lewis, *Quenching of Aromatic Hydrocarbon Singlets and Aryl Ketone Triplets by Alkyl Disulfides.* Journal of the American Chemical Society, 1976. **98**(17): p. 5319-5326.
27. Harding, R.E., et al., *Non-radiative decay mechanisms in blue phosphorescent iridium(III) complexes.* Organic Electronics, 2008. **9**(3): p. 377-384.

6. Poly(dendrimer) Iridium Complexes

6.1 Introduction

In this chapter I overview the work that was done on iridum polymers for solution processable phosphorescent organic light emitting diodes. An introduction to phosphorescent polymers is given in Section 6.2 and experimental results are given in Sections 6.3, 6.4 and 6.5. Section 6.3 contains early work using $Ir(ppy)_2(acac)$ based polymers with and without dendrons to control aggregation in thin films. Section 6.4 covers work using the higher luminescent efficiency $Ir(ppy)_2(ptz)$ based polymer(dendrimer) and Section 6.5 discusses a poly(dendrimer) that uses double dendrons to better protect the cores from aggregation in the solid state and achieve higher efficiencies. A summary of all the materials used in this chapter is given in Section 6.6. Finally the conclusions are presented in Section 6.7.

6.2 Introduction to Phosphorescent Polymers

Much work has been done on the small molecule iridium complexes like *fac*-tris(2-phenylpyridine) iridium(III) or $Ir(ppy)_3$ which emits in the green [1, 2] for phosphorescent OLEDs. Typically these materials are deposited by thermal evaporation. Unfortunately, this technique is relatively costly and slow as it requires high vacuum but these small molecules are only slightly soluble in organic solvents and so are difficult to process via solution. In addition, solution processing can lead to aggregate formation in these materials as the molecules have more chance to order than if they are deposited into a glassy phase via thermal deposition.

Conjugated polymers, on the other hand, are readily solution processable. However they are not generally phosphorescent and so have limited maximum efficiencies in devices. This failing lead to the development of dendrimers, discussed in Chapter 3, with phosphorescent cores to provide a route to low cost highly efficient OLEDs. These devices have achieved 16% external quantum efficiency or ~80% internal quantum efficiency [3]. Unfortunately, unlike a polymer, dendrimers do not significantly modify the viscosity of their solvent when dissolved [4, 5]. These higher viscosities are required for ink-jet printing [6-8], which in turn allows patterned deposition of OLED materials that is required to produce a colour display. To overcome this limitation the idea of this project was to investigate phosphorescent poly(dendrimers) for use in OLEDs. The materials for this project were synthesised and chemically characterised by Wen-Yong Lai, Shih-Chun Lo and Paul Burn at the University of Queensland.

Phosphorescent polymers consist of two main components: the polymer backbone and the pendant iridium complexes. In much previous work conjugated polymers like poly(fluorene) have been used to provide the backbone [9-14]. Although the chosen polymers may be blue emitters this colour comes from the singlet state of the polymer. As the triplet state is lower lying this means that for green and blue emitting pendant iridium complexes back transfer to the polymer backbone often occurs, limiting the efficiency of devices [13-15]. These effects are illustrated in Figure 6.1. Though this problem is particularly pronounced in Poly(fluorene) due to the large

singlet-triplet energy splitting, this problem may also occur with other conjugated backbones for example poly(para-phenylene) [16] or poly(phenylacetylene) [17].

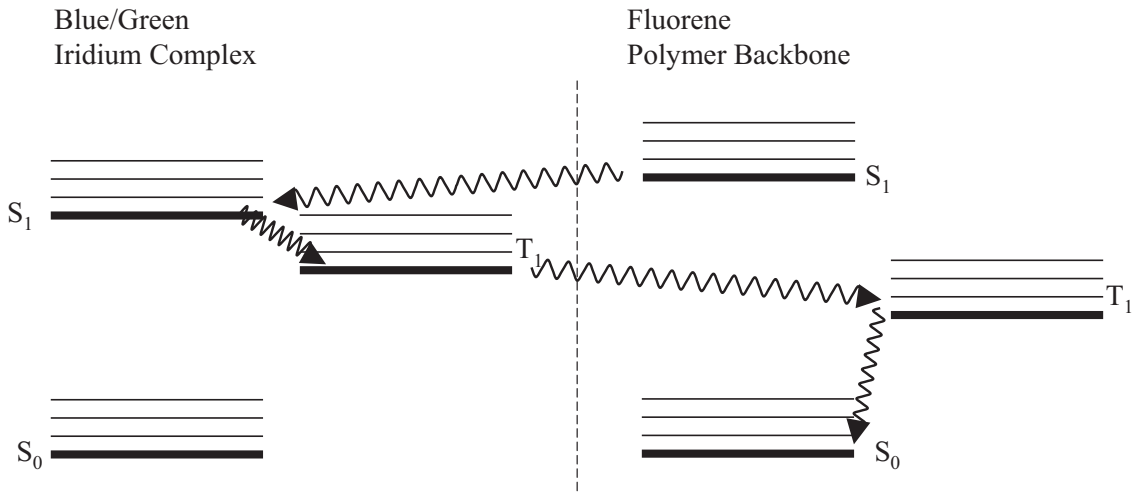

Figure 6.1 Diagram showing back transfer to the polymer backbone in conjugated poly(iridium) complexes.

A better approach is to use a non-conjugated polymer backbone as this does not have energy states that can quench triplet emission [18-26]. In Sections 6.3, 6.4 and 6.5 below and in Chapter 7 a non-conjugated poly-styrene backbone has been used to prevent quenching.

6.3 Ir(ppy)$_2$(acac) Based Polymers

The decision was taken to use an Ir(ppy)$_2$(acac) core, where ppy is 2-phenylpyridine and acac is acetoylacetonate, for the polymers initially. This was because Ir(ppy)$_2$(acac) has been successfully used to produce 90% internal quantum efficiency OLEDs in the past [27]. The electronic properties of this complex are otherwise rather similar to Ir(ppy)$_3$ as the acac ligand has rather large π-π* energy gap, compared to ppy due to its short conjugation and so does not contribute very much to the excited state properties [28].

The hetroleptic structure (where the ligands are different from one another) makes it easier to differentiate the ligand connected to the backbone from the other two during synthesis. This ensures one and only one linker ligand is attached to each core. The structure of the polymer **1** is shown in Figure 6.2 along with its unpolymerised

monomer **2** (referred to hereafter as the precursor) and a model compound designed to mimic the behavior of the individual monomers **3** (the monomer). Though this structure has no dendrons, the polymer nature of the material helps with solubility and all the materials are soluble enough in dichloromethane (DCM) and 1,2-dichloroethane that photophysical measurements could be made.

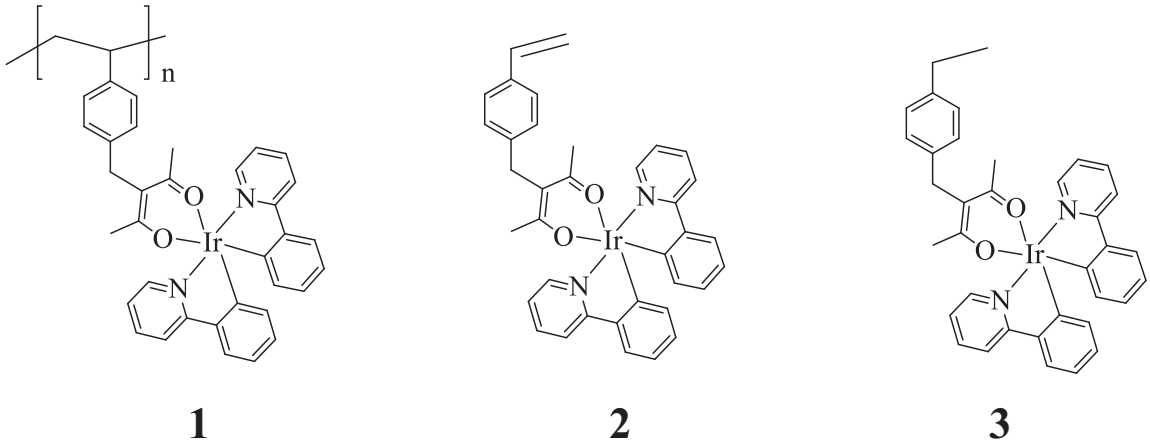

*Figure 6.2 The molecular structures of the Ir(ppy)$_2$(acac) polymer **1**, its precursor **2** and its monomer **3**.*

The synthesis of these materials is detailed in ref. [29]. The linker from the acac ligand to the polymer backbone contains a non-conjugated linkage and so the phenyl unit and the backbone should not extend their conjugation onto the complex. Nevertheless it was felt that the phenyl unit and its neighboring double bond in the precursor **2** would form a separated conjugated unit that might quench luminescence from the core. As a result the saturated monomer **3** is believed to better model the photophysics of the polymer's individual pendant groups.

6.3.1 Ir(ppy)$_2$(acac) Solution Properties

The solution absorption and photoluminescence spectra of materials **1-3** in degassed dichloromethane (DCM) are shown below in Figure 6.3. The emission spectra were excited at 360 nm. The strong absorption at less that 320 nm is due to the π-π* transitions on the ligands. The longer wavelength weaker absorption from 320 nm to 450 nm is due to the lower oscillator strength metal-to-ligand charge transfer singlet states. Finally the peak at 470 nm and longer wavelength absorption is assigned to the

metal to ligand charge transfer triplet state [28]. These peak positions are typical of green emitting iridium complexes. The absorption spectra of the materials are similar to each other which suggests no substantial change in the photophysical properties.

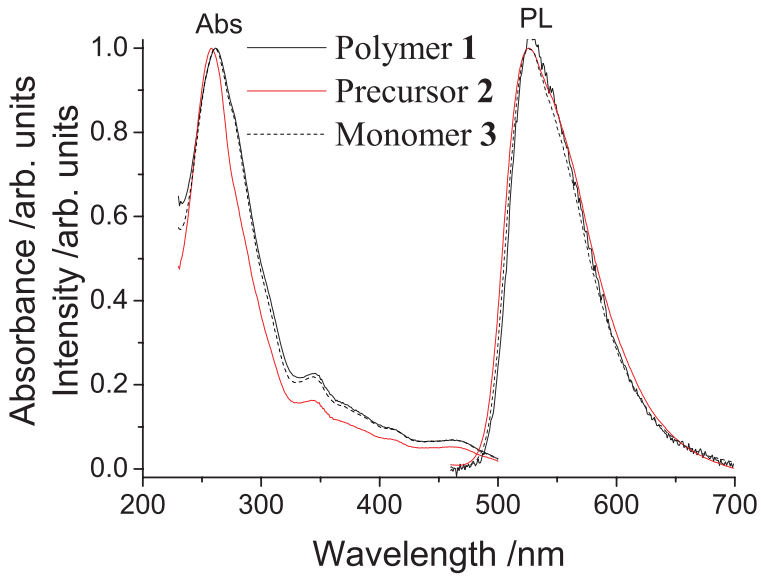

*Figure 6.3 Normalised solution absorption and photoluminescence spectra of compounds **1**, **2** and **3** in degassed DCM. The excitation wavelength was 360 nm.*

The emission spectrum of the polymer **1** peaks at 528 nm and the emission spectra of the precursor **2** and monomer **3** peak at 526 nm. The emission spectra are otherwise rather similar and all result in a yellow colour. This similarity implies that strong aggregation effects are not resulting in a significant red-shift of the material's emission on moving from the monomers to the polymer. Interestingly, the peak of the emission for $Ir(ppy)_2(acac)$ has been reported to be 516 nm in the literature. This suggests that the presence of the phenyl unit on the linker ligand has caused a red-shift in the emission despite the fact it is not part of the same conjugated system as the acac ligand.

The same degassed DCM solutions were used for time-resolved luminescence measurements via Time Correlated Single Photon Counting (discussed in Chapter 4). The resulting luminescence decays are shown in Figure 6.4. In each case the samples were excited at 355 nm and the detection monochromator was centred on 530 nm.

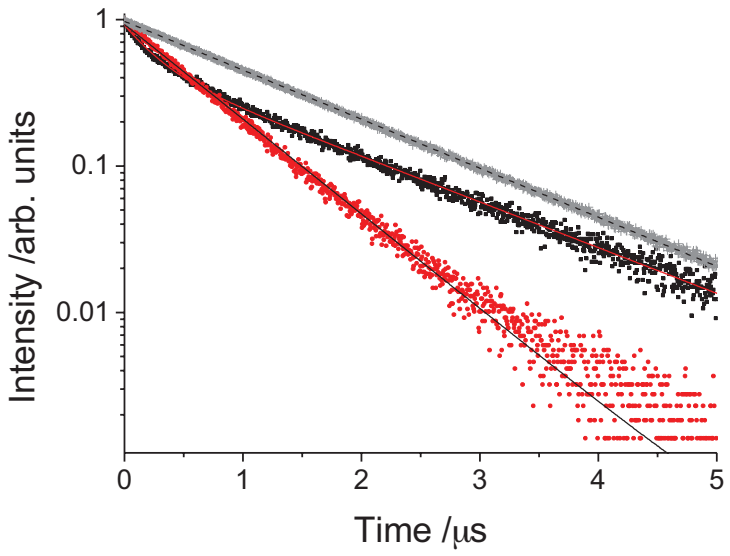

*Figure 6.4 Time-resolved luminescence of solutions of polymer **1** (black squares and red fit line), precursor **2** (red circles and black fit line) and monomer **3** (grey crosses and black fit line). Excitation was at 355 nm and detection centred at 530 nm.*

The precursor **2** and monomer **3** both had mono-exponential decay lifetimes of 670 ns and 1.3 μs respectively while polymer **1** had bi-exponetial lifetime with a short 260 ns component with 0.48 of the initial amplitude and longer 1.4 μs decay with 0.52 amplitude. The solution photoluminescence quantum yields of these materials are 42% for **2**, 52% for **3** and 34% for **1**. The mono-exponential decay of compound **2** and **3** indicate that they have only one emissive state while polymer **1** has a multi-exponential decay and so has more than one. The shorter initial lifetime of the polymer and the fact it has the lowest PLQY indicate that its luminescence is being quenched and that these extra states correspond to less emissive aggregates. These aggregates must be formed within the polymer chain as the solutions are of low concentration and so we would expect the individual molecules to be isolated from one another. This sort of multi-exponential lifetime has been observed before in iridium polymers in solution [10]. Polymer **1**'s longer decay component of 1.4 μs is close to that of the model monomer **3**'s 1.3 μs decay and so this appears to correspond to emission from non-aggregated cores in the polymer. The more rapid decay of precursor **2** and its lower PLQY than the model monomer **3** are attributed to

quenching by the phenyl and double bond conjugated system attached to the acac ligand.

6.3.2 $Ir(ppy)_2(acac)$ Film Properties

Neat films of materials **1**, **2** and **3**, and 6 wt% and 19 wt% of polymer **1** blended with 4,4'-N,N'-dicarbazolyl-biphenyl (CBP) were spin-coated from solutions of 1,2-dicholorethane onto quartz discs. 20 mg/ml concentrations were used, and spin-coated at 1200 rpm. CBP is a charge transport material that is often used in OLEDs to boost performance both by improving electron transport and reducing solid state aggregation by separating the emissive cores. The emission spectra of the films were recorded when excited at 325 nm and the spectra of the polymer **3** samples are shown in Figure 6.5. The PLQYs of the samples were also calculated using the Greenham method [30] described in Chapter 4.

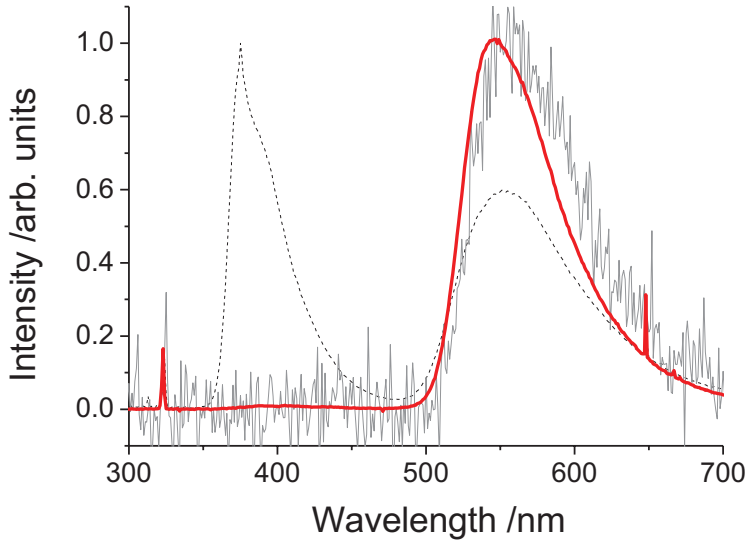

*Figure 6.5 The photoluminescence spectra of polymer **1** in neat film (grey line), 19 wt % in a CBP blend (thick red line) and 6 wt% in a CBP blend (dashed black line).*

The emission spectrum of the neat film of polymer **1** has a peak at 550-560 nm, the 19 wt% blend has an emission peak at 546 nm and the 6 wt% blend as two peaks at 375 nm and 552 nm. All of the green/yellow peaks are significantly red-shifted from the polymer **1**'s solution peak at 528 nm. The appearance of the peak at 375 nm in the 6

wt% blend corresponds to the emission of CBP and indicates the energy transfer from the host is incomplete. In the 19 wt% blend this peak has been greatly reduced indicating that the concentration of **1** in the 6 wt% is simply too low for efficient energy transfer.

The film PLQY values of neat films of **1**, **2** and **3** are similar and below 1%. This explains the poor signal to noise seen in the neat polymer's emission spectrum. The PLQY value of the 19 wt% blended film of polymer **1** is 7%, while the 6 wt% value cannot be used for comparison because of emission from the CBP. These results support the conclusion that there is very strong aggregation in the solid state for these materials which quenches luminescence. Although this quenching can be reduced by blending with CBP the 7% PLQY remains much lower than the solution value of 34% and so these materials are not suitable for making efficient OLEDs. This result is not entirely unexpected as non-dendronised iridium complexes often show strong quenching and low efficiency in neat films. For example non-dendronised $Ir(ppy)_3$ has a PLQY of only 12% in neat films compared to 22% for the comparible first generation dendrimer shown in **Error! Reference source not found.** [31].

6.3.3 Dendronised $Ir(ppy)_2(acac)$ Polymer Properties

In order to try and improve the film properties of these materials dendronised versions **1**, **2** and **3** where prepared and their structures are shown below as materials **4**, **5** and **6** respectively in Figure 6.6.

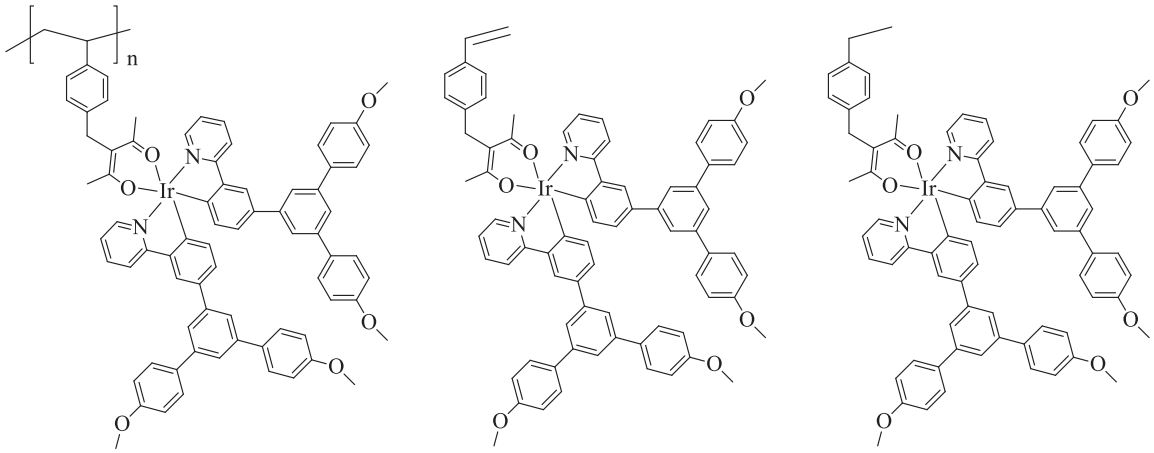

4 **5** **6**

*Figure 6.6 The molecular structures of the dendronised $Ir(ppy)_2(acac)$ polymer **4**, its precursor **5** and its monomer **6**.*

Solution and film photoluminescence measurements were made on these materials in the same way as for materials **1**-**3**, above. The solution absorption and emission spectra are shown in Figure 6.7. The absorption peak at 270 nm is assigned to π-π* transitions in the dendrons and ligands. The other absorption peaks are assigned as above for Figure 6.3. The emission peaks of these materials are at 536 nm for the polymer **4** and 534 nm for the precursor **5** and monomer **6**. These peaks are all red shifted by 6 nm compared to the undendronised counterparts. This difference results from the increased conjugation length on the dendrimers due to the meta-linked dendrons attached to the ppy ligands.

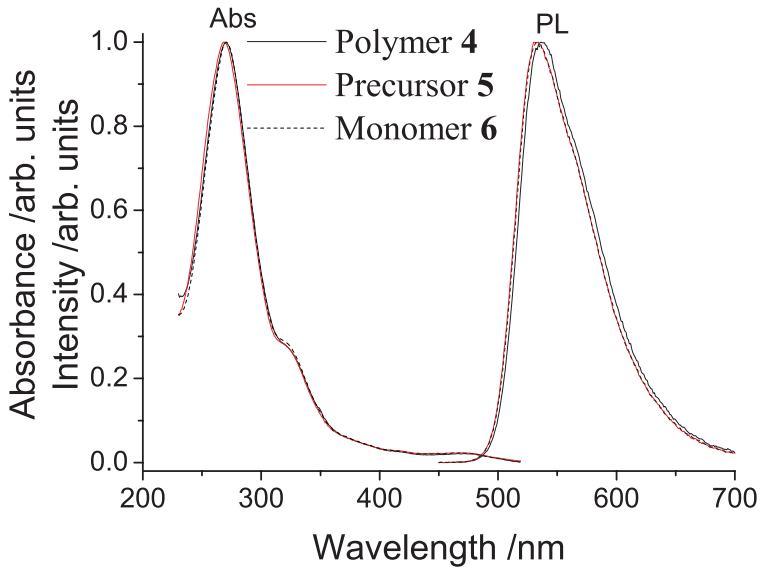

*Figure 6.7 Normalised solution absorption and photoluminescence spectra of compounds **1**, **2** and **3** in degassed DCM. The excitation wavelength was 360 nm.*

The film spectra of polymer **4** and a 20 wt% blend of polymer **4** in CBP are shown in Figure 6.8. A concentration of 20 mg/ml in 1,2-dichloromethane was used to spin-coat films at 1200 rpm. The emission peak for the neat polymer film is 554 nm and for the blended film it is 548 nm. The CBP still shows some residual blue emission in the 20 wt% blended film, however it is small enough that this sample can be used to assess the photoluminescence quantum yield.

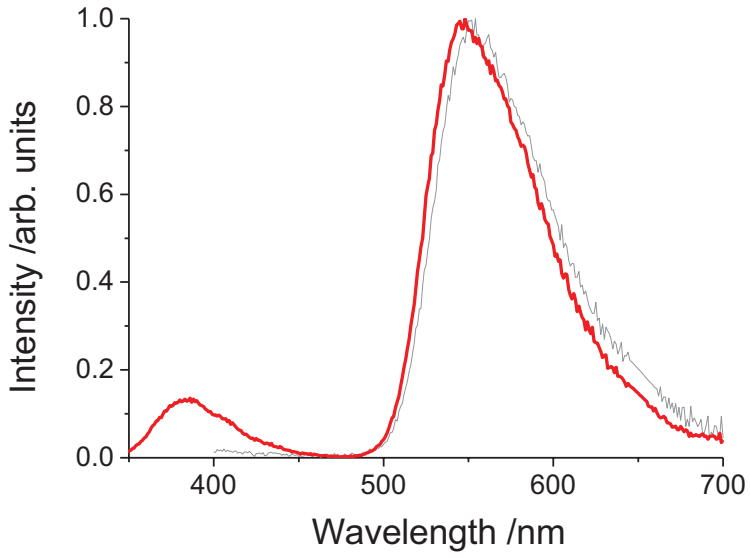

*Figure 6.8 The photoluminescence spectra of polymer **4** in neat film (grey line) and 20 wt % in a CBP blend (thick red line).*

A comparison of the solution and film PLQYs of the dendronised and undendronised materials is shown in Table 6.1. As can be seen the solution PLQYs are similar despite the addition of the dendrons however there is an approximate factor 2 improvement in the film PLQY in the dendronised materials.

Material	Type	Solution PLQY (360 nm)	Film PLQY (325 nm)	~20 wt% CBP Blended Film PLQY
1	Core Polymer	34%	0.9%	7.0%
2	Core Precusor	42%	0.7%	
3	Core Monomer	52%	0.6%	
4	Dendrimer Polymer	30%	1.9%	18%
5	Dendrimer Precusor	37%	1.1%	
6	Dendrimer Monomer	53%	-	

Table 6.1 PLQY values for the Ir(ppy)2(acac) polymers in solution (excited at 360 nm) and film (excited at 325 nm).

6.4 $Ir(ppy)_2(ptz)$ Based Poly(Dendrimers)

Intra and inter-chain aggregation means that the solution PLQY of the pendant iridium monomers sets the upper limit on the efficiency of any iridium polymer. The unexpectedly low solution PLQY of the $Ir(ppy)_2(acac)$ based materials led to a search for a higher efficiency heteroleptic core. The next core tried kept the 2-phenylpydridyl (ppy) ligands but used a phenyltriazolyl (ptz) linker ligand to replace the acetoylacetonate (acac) ligand. Like acetoylacetonate, phenyltriazolyl is a higher band gap ligand than 2-phenylpydridyl, for example $Ir(ptz)_3$ cores have been used as a blue/green emitting material in solution processible dendrimers [32, 33]. This higher energy means it should not interfere very much with the excited state properties of the core. The structure of this core, **7**, is shown in Figure 6.9 along with the poly(dendrimer) **8** based on it. The structure of the dendrimer monomer **9** is also shown. The synthesis of these materials is described in ref. [5].

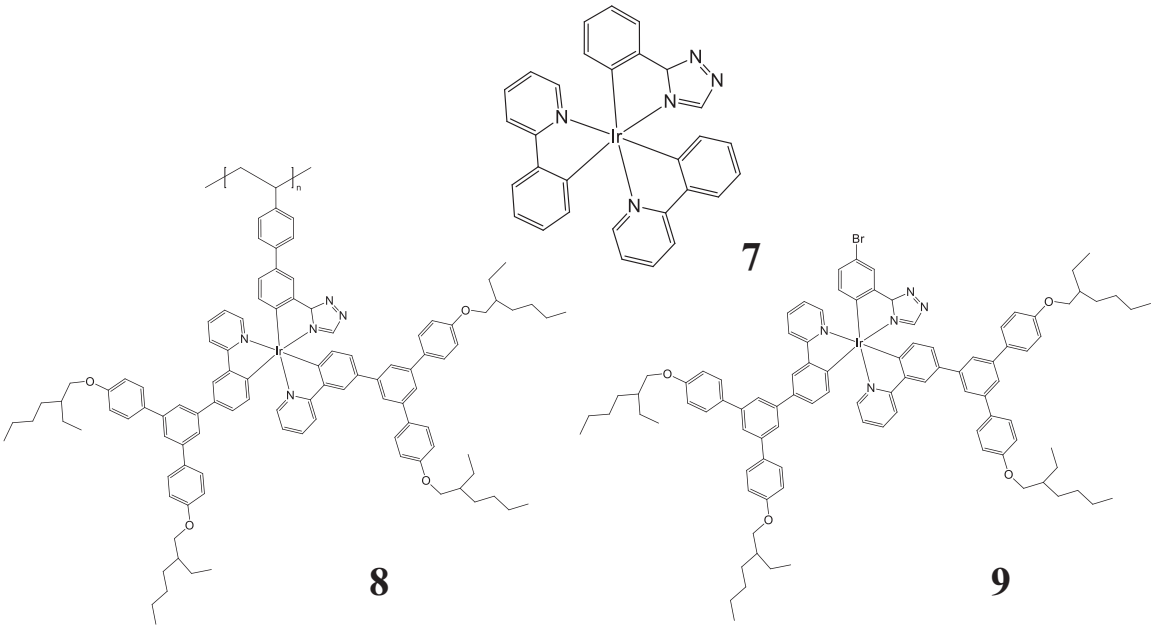

*Figure 6.9 The molecular structures of the $Ir(ppy)_2(ptz)$ based materials. The core **7**, the polymer dendrimer **8** and its monomer **9**.*

6.4.1 $Ir(ppy)_2(ptz)$ Solution Properties

The solution absorption and photoluminecscene of these materials is shown in Figure 6.10. As in Figure 6.3 the absorption below 320 nm in core 7 is assigned to π-π*

transistions in the ligands. The absorption peaks at 270 nm to 280 nm in the polymer **8** and monomer **9** stronger because of absorption due to π-π* transistions in the dendrimers. The longer wavelength absorption peaks are assigned as before. The photoluminescence peak of **7** and **9** is at 510 nm where as the peak of the polymer **8** is at 518 nm. We would expect some red-shifting of the emission due to the addition of the dendrons in **8** and **9** as well as possible intra-molecular aggregation in **8**. In monomer **9** however some blue shifting is expected due to the inductive effect of the bromine atom. Therefore we cannot know if the red-shifting of polymer **8** is due to aggregation or simply because it lacks the bromine atom.

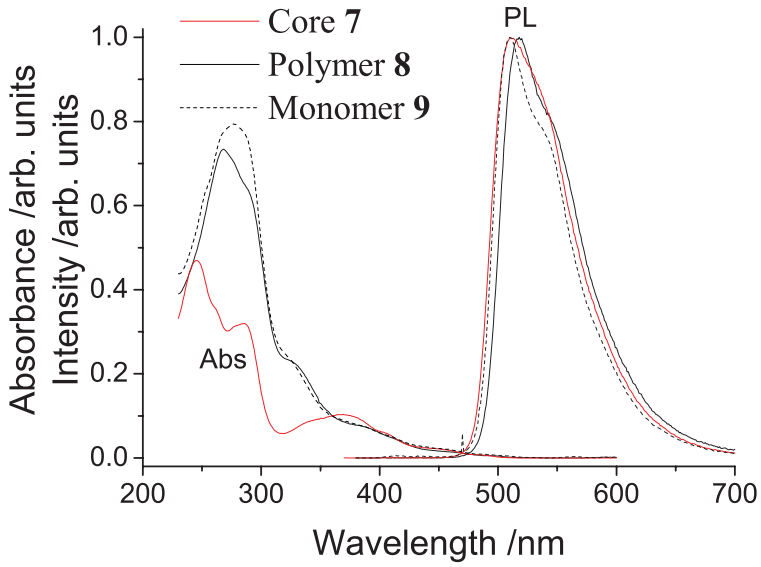

*Figure 6.10 Normalised solution absorption and photoluminescence spectra of the core 7, the polymer **8** and the monomer **9** in degassed DCM excited at 360 nm. The absorption spectra were normalised at 360 nm.*

The solution PLQY values of these materials were determined when excited at 360 nm. The core **7** has a PLQY of 82% where as monomer **9** has a PLQY of 92%. The polymer has a reduced PLQY of 61%. This reduced PLQY is assigned to aggregation along the polymer chain. However this solution PLQY is approximately a factor 2 better than the 34% and 30% values for the $Ir(ppy)_2(acac)$ polymer and poly(dendrimer) in Section 6.3.

Figure 6.11 shows the time-resolved luminescence data for these materials in degassed DCM solutions. Monomer **9**'s decay is fit well by a mono-exponential decay of 1.6 µs while polymer **8**'s decay is multi-exponential with 0.58 initial intensity 1.0 µs component and 0.42 1.95 µs component. As before this is attributed to a single emissive state for the monomer and multiple aggregated and non-aggregated states in the polymer. The faster decay of the polymer is consistent with its lower PLQY and both are consistent with quenching by aggregates.

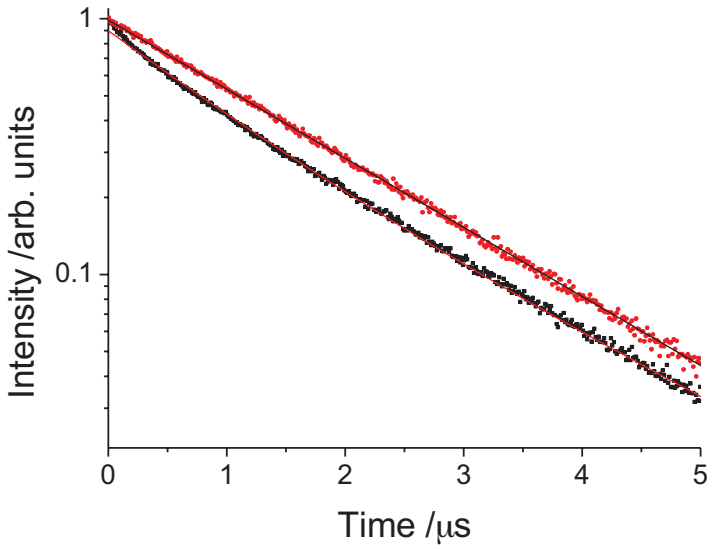

*Figure 6.11 TCSPC measurements of solutions of polymer **8** (black squares and red fit line) and monomer **9** (red circles and black fit line). Excitation was a 393 nm and detection centred at 530 nm.*

6.4.2 Ir(ppy)$_2$(ptz) Film Properties

Film PL measurements were made on polymer **8** in neat and 20 wt% blend in CBP films. The films were spun at 1200 rpm from 20 mg/ml concentration solutions in DCM. This was in order to determine its PLQY in the solid state in order to see if it was a suitable OLED material. The film photoluminescence spectra (excited at 325 nm) are shown in Figure 6.12. The neat film has an emission peak at 523 nm which is slightly longer than the 518 nm peak in solution. The CBP blended film has a slightly shorter wavelength peak than the neat film at 521 nm.

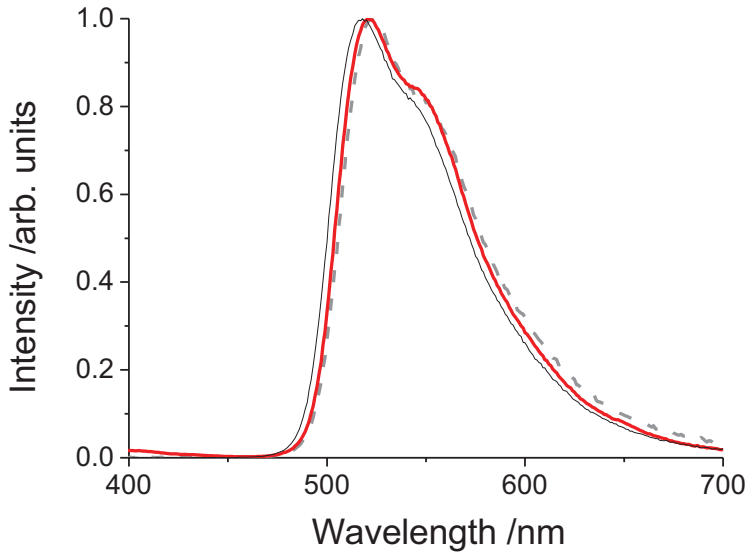

*Figure 6.12 The photoluminescence spectra of polymer **8** (excited at 325 nm) in neat film (thick dashed grey line) and 20 wt % in a CBP blend (thick red line). Polymer **8**'s solution spectrum excited at 360 nm (thin black line) is shown for comparison.*

The film PLQY value of the neat film is 13% by the Greenham method [30] or 16% by the Suzuki method [34] (both discussed in Chapter 4). The blended film PLQYs are 42% and 40% respectively. The reduction of PLQY and red-shifting in the neat film compared to the solution is consistent with aggregation. However the $Ir(ppy)_2(ptz)$ poly(dendrimer) **8** has considerably higher film PLQY than either the $Ir(ppy)_2(acac)$ undendronisied material **1** or the poly(dendrimer) **4** in Section 6.3. This higher PLQY results from using both a more emissive core and the dendron's ability to reduce concentration quenching.

6.4.3 $Ir(ppy)_2(ptz)$ OLED Devices

As a result of the high film PLQY of 20 wt% of polymer **8** blended with CBP it was decided to use this film as the basis of an OLED device. Bi-layer devices, as described in Chapter 3, use a 1,3,5-tris(2-N-phenylbenzimidazolyl)benzene (TPBI) hole-blocking layer to achieve charge balance between electrons and holes without requiring extensive optimisation. This makes it easier to see what the achievable efficiency of an emissive material is quickly. Therefore it was decided to make a bi-

layer OLED device following the protocol described in Chapter 4 with a blended emissive layer spun at 2000 rpm from a 20 mg/ml DCM solution.

The electroluminescence spectrum is shown in Figure 6.13, the current/voltage and brightness/current curves are shown in Figure 6.14, the external quantum efficiency/voltage and power efficiency/voltage curves are shown in Figure 6.15 below.

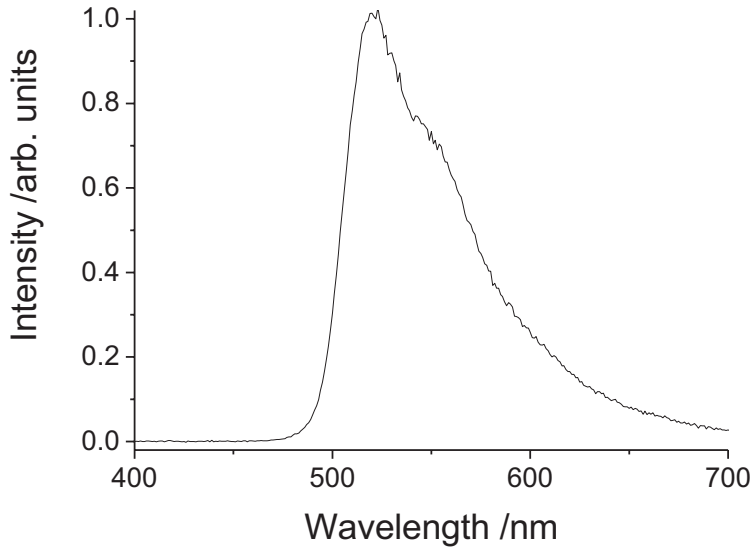

Figure 6.13 Emission spectrum of bi-layer OLED containing 20 wt% of polymer ***8*** *in a CBP blend. Drive voltage 20 V.*

Figure 6.13 shows the EL peak is at 523 nm. The CIE coordinates are (0.34, 0.62), which correspond to yellow/green emission. The emission peak is the same as the neat film and 2 nm red-shifted from that of the blended film. The EL spectrum can be particularly sensitive to aggregation effects as the charge carriers have a chance to become stuck in trap states before excitons form meaning the system has longer to find the lowest available energy states than in PL. The fact that there is not significant red-shifting of the EL spectrum compared to the PL spectrum is a good sign that deleterious aggregation effects are not too strong.

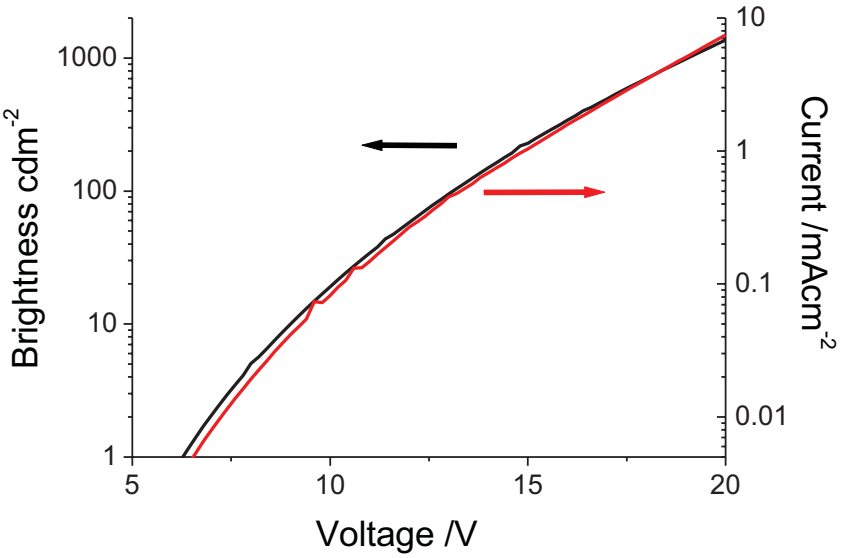

*Figure 6.14 Brightness (black) and current (red) of the OLED containing 20 wt% of polymer **8** in CBP.*

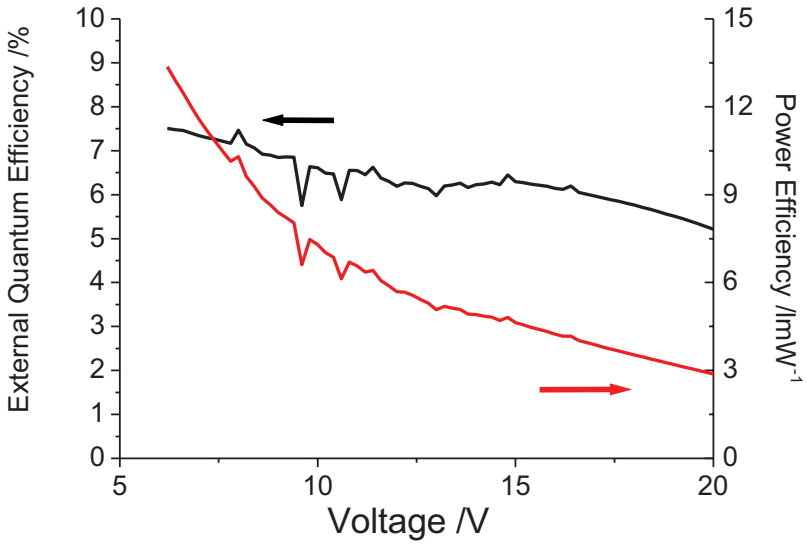

*Figure 6.15 External quantum efficiency (black) and power efficiency (red) of OLEDs with 20 wt% of polymer **8** in CBP as emissive layer.*

The brightness curve and the current density curve shown in Figure 6.14 almost overlap indicating that the current efficiency of the devices is approximately constant with increasing drive voltage. This is confirmed by the mostly flat external quantum efficiency curve in Figure 6.15 which drops from 6.2% (21.8 cd/A) at 13.2 V at 100 cd/m^2, to 5.5% (19.3 cd/A) at 19.0V, which corresponds to 1,000 cd/m^2. 100 cd/m^2 is

normally taken as the benchmark brightness for a display application. Unfortunately the drive voltage of 13.2 V for this brightness and the turn on voltage (brightness 1 cd/m^2) of 6.2 V are a little too high for device applications and negatively impact the power efficiency. These values could be reduced by reduction and optimisation of the layer thicknesses and improved charge injection at the cathode for applications in actual devices.

The external quantum efficiency of 6.2% is ~80% of the theoretical maximum efficiency of 8% arrived at by assuming 20% out-coupling efficiency, perfect charge recombination and using the 40% PLQY value of the blended film. This suggests that the bi-layer structure has done a good job of balancing the electron and hole currents but that some further optimisation is possible.

6.5 Doubly Dendronised Ir(ppy)$_2$(ptz) Polymer

The dendrimer concept uses the dendrimer arms to protect the emissive core from aggregating with its neighbours via steric interactions. Nevertheless the most efficient dendrimer OLEDs still make use of a charge transporting host like CBP or 4,4',4''-tris(N-carbazoyl)triphenylamine (TCTA) to increase the film PLQY and device efficiency by helping to separate the cores [3]. These blended devices achieved 16% EQE. Another solution that has been used is to add a second set of dendrons to each ligand, thereby better encapsulating each core and protecting it from its neighbours [35]. This has allowed 13.6% EQE to be achieved in neat film devices.

As the Ir(ppy)$_2$(ptz) poly(dendimer) in Section 6.4 was already achieving close to its theoretical maximum OLED efficiency it was decided to try and improve the film luminescence quantum yields and thus the device efficiencies of the poly(dendrimers) by adopting a double-dendron structure. The structures of the polymer and its corresponding polymer are shown as materials **10** and **11** in Figure 6.16 below.

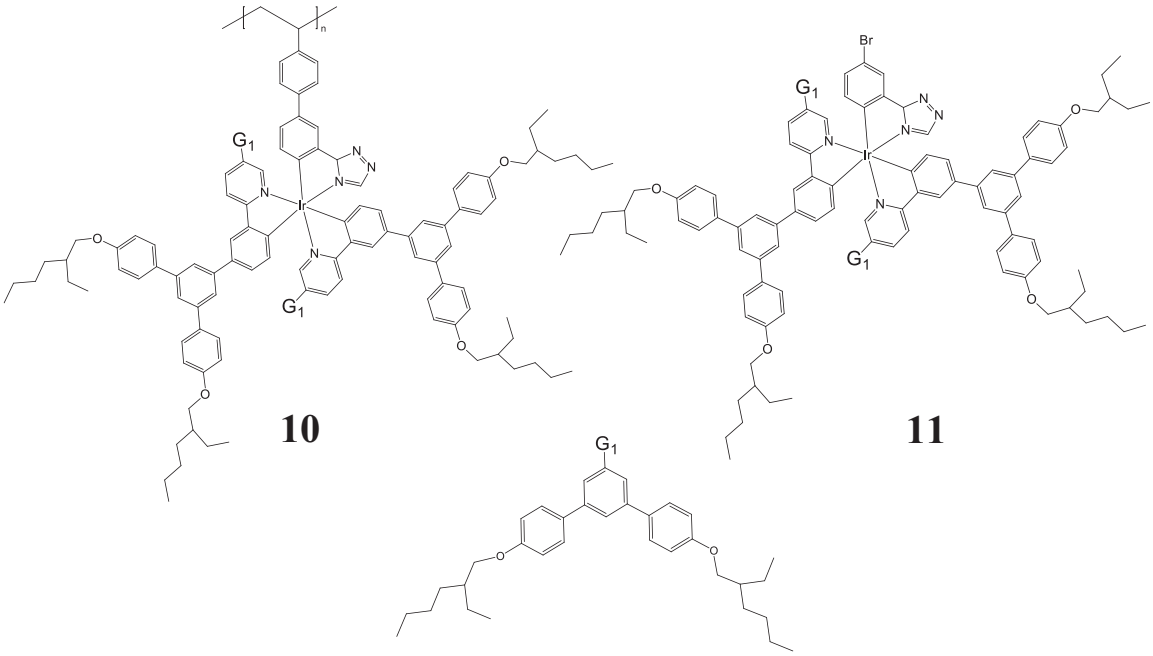

*Figure 6.16 The molecular structures of the Ir(ppy)$_2$(ptz) double dendron materials: poly(dendrimer) **10** and its monomer **11**.*

6.6.1 Double Dendron Solution Properties

The solution absorption and emission spectra in degassed DCM of double dendron materials **10** and **11** are compared against the single dendron polymer **8** in Figure 6.17 below. The absorption spectra are assigned as before. The absorption below 370 nm is stronger in the double dendron materials **10** and **11** because this corresponds to the π-π* transitions in the ligands and dendrons and so the increased absorption is the result of the extra dendrons.

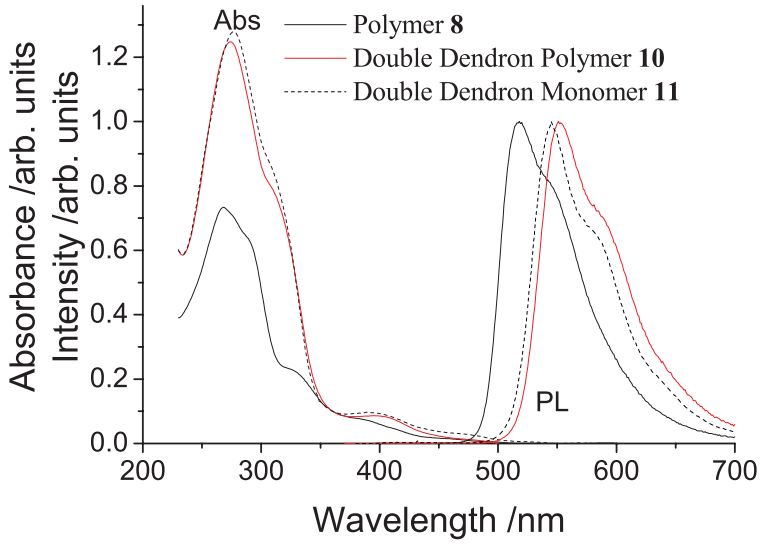

*Figure 6.17 Normalised solution absorption and photoluminescence spectra of single dendron polymer **8** and double dendron polymer **10** and the double dendron monomer **11** in degassed DCM excited at 360 nm. The absorption spectra were normalised at 360 nm.*

The photoluminescence peaks in the double dendron materials are at 545 nm for monomer **11** and 551 nm for polymer **10**. This is a significant red-shift from the single dendron polymer **8**'s peak at 518 nm, which is due to the increased conjugation due to adding the second dendrons at the para positions to the phenyl pyridine ligands. The conjugation is extended by a greater extent than the addition of the first set of dendrons to the meta positions that was observed in the $Ir(ppy)_2(acac)$ ligands in Section 6.3.3. This red-shift is consistent with earlier observations in double dendrimers [35].

The solution PLQY of monomer **11** is 94% which is comparable with monomer **9**'s value of 92%. Polymer **10**'s PLQY is 67% which is slightly higher than the 61% value for polymer **8** but still within the experimental error of ~10% of the total. Therefore there is no strong evidence that the double dendron structure has reduced aggregation in the solution phase.

Time-resolved measurements on these solutions are shown in Figure 6.18. The monomer **11** has a mono-exponenital decay of 2.1 μs while both polymers have bi-

exponential decays. This is slower than the single dendron monomer **9** decay time of 1.6 μs. **8** has a faster decay with 0.58 1.0 μs component and 0.42 1.95 μs component and **10** has a slower decay than **8** with 0.23 1.1 μs and 0.77 1.8 μs components. It is clear from these measurements and the photoluminescence measurements that the addition of the second dendrons has changed the photophysics of the cores resulting in red-shifted emission and a longer decay time in double dendron monomer **11** than in monomer **9**. This means that while polymer **10**'s photoluminescence lifetime appears to have more mono-exponential character than polymer **8** is difficult to compare the polymers as we would expect the double dendron materials to have a longer lifetime in any case and fitting the decay curves assuming only two emissive environments is probably only an approximation to the true decay profile.

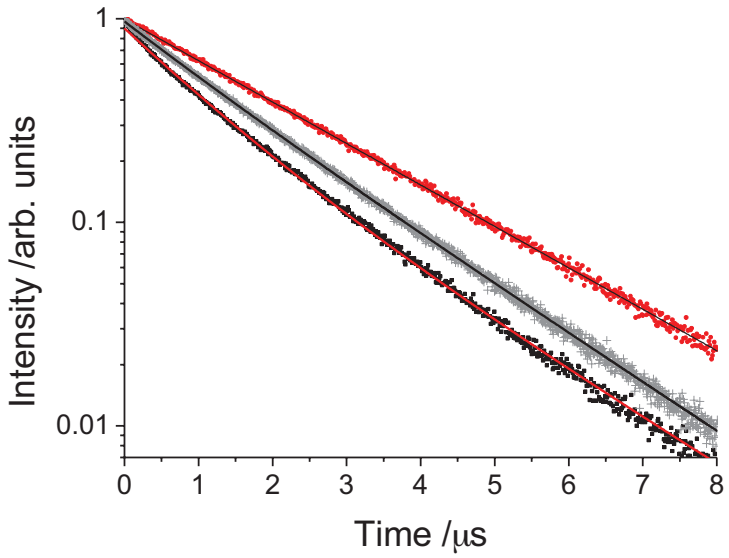

*Figure 6.18 TCSPC measurements of solutions of polymer **8** (black squares and red fit line), double dendron polymer **10** (grey crosses and black fit line) and monomer **11** (red circles and black fit line). Excitation was at 393 nm and detection centred at 530 nm.*

6.5.2 Double Dendron Film Properties

Figure 6.19 below shows how the neat and blend film photoluminescence spectra compare to the solution spectra for polymer **10**. These films were spun from 20 mg/ml DCM solutions at 1200 rpm. The peak in solution is at 551 nm and this is red-shifted

slightly to 555 nm in the neat film. In the 20 wt% CBP film the red-shifting is reduced to 553 nm.

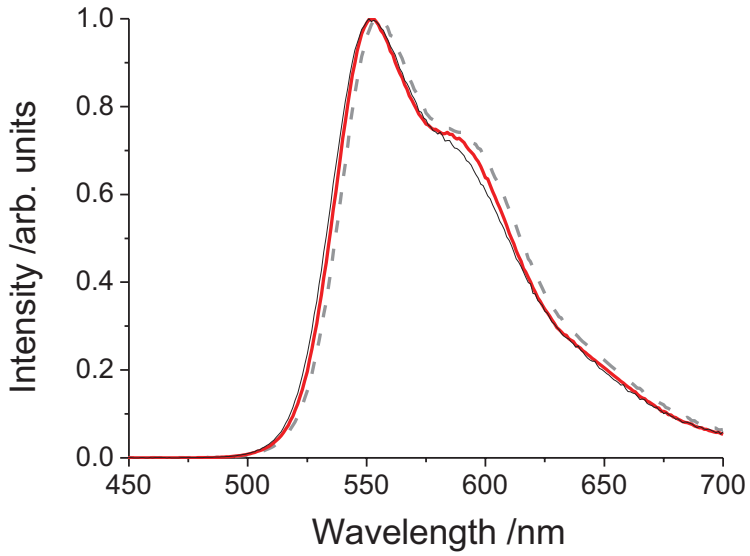

*Figure 6.19 The photoluminescence spectra of polymer **10** (excited at 325 nm) in neat film (thick dashed grey line) and 20 wt % in a CBP blend (thick red line). Polymer **10**'s solution spectrum excited at 360 nm (thin black line) is shown for comparison.*

The film PLQY values of these materials were measured using the Suzuki method [34]. The film PLQY value do show evidence for aggregation effects in the neat film where the PLQY of polymer **10** drops from 67% in solution to 47%. However in 20 wt% CBP blended films the aggregation does not appear to be strong enough to cause any quenching of the emission and the film PLQY remains 67%. These results show much less quenching than for the single dendron polymer **8** where the solution PLQY of 61% drops to 16% and is still only 40% in the 20 wt% CBP blended film.

6.5.3 Double Dendron OLED Devices

As the film PLQY value of double dendron poly(dendrimer) **10** are significantly higher than for the single dendron poly(denrimer) **8** it was decided to try both neat film and 20 wt% CBP layers in bi-layer OLEDs similar to those described in Section 6.4.3. However due to the high turn on voltage of the polymer **8** devices the solution concentration was reduced to 10 mg/ml in DCM spun at 2000 rpm.

The electroluminescence spectra of the neat and blended devices are shown in Figure 6.20. The peak emission of the neat film occurs at 555 nm and the blended film emission peaks at 554 nm which are both very close to the film photoluminescence and not significantly red-shifted from the solution peak at 551 nm. The CIE coordinates of the neat device are (0.48, 0.51) and the blended device has (0.46, 0.53), which both correspond to yellow emission.

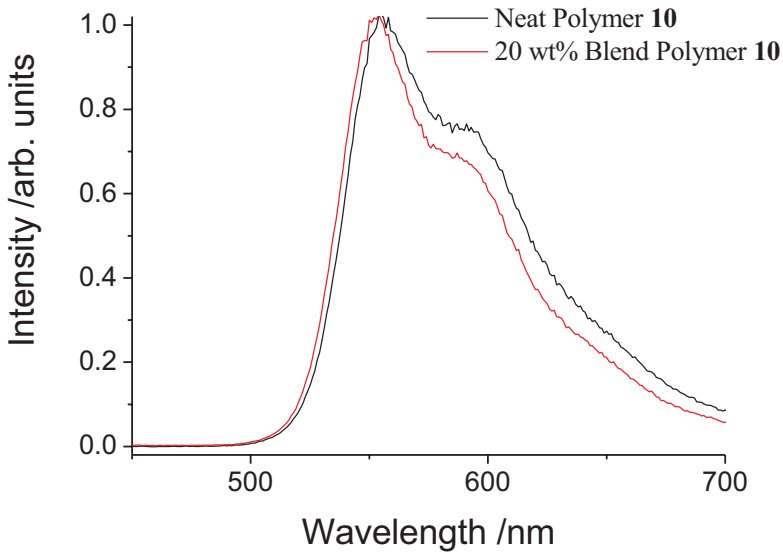

*Figure 6.20 Emission spectrum of bi-layer OLEDs with polymer **10** in neat and 20 wt% CBP blended emissive layers. Drive voltage 12 V.*

The brightness and current vs. voltage curves of the OLEDs are shown in Figure 6.21 and the external quantum efficiency and power efficiency curves are shown in Figure 6.22. The current and brightness curves of the blended film almost overlay however for both devices the current rises more steeply than voltage resulting in decreasing external quantum efficiency with increasing voltage. At 100 cd/m^2 the blended device achieves 12.1% EQE (39.3 cd/A) at 7.4 V which results in a power efficiency of 16.7 lm/W. The neat devices have lower efficiency and achieve 9.3% EQE (28.1 cd/A) at 6 V giving 14.7 lm/W at the same brightness. Both these results are superior to the single dendron blended OLEDs presented above in Section 6.4.3. In addition the blended device achieves a higher EQE at 100 cd/m^2 than the highest value that has previously been reported in a phosphorescent polymer OLED at any brightness (11.8%) [20] or 35 cd/A [25]

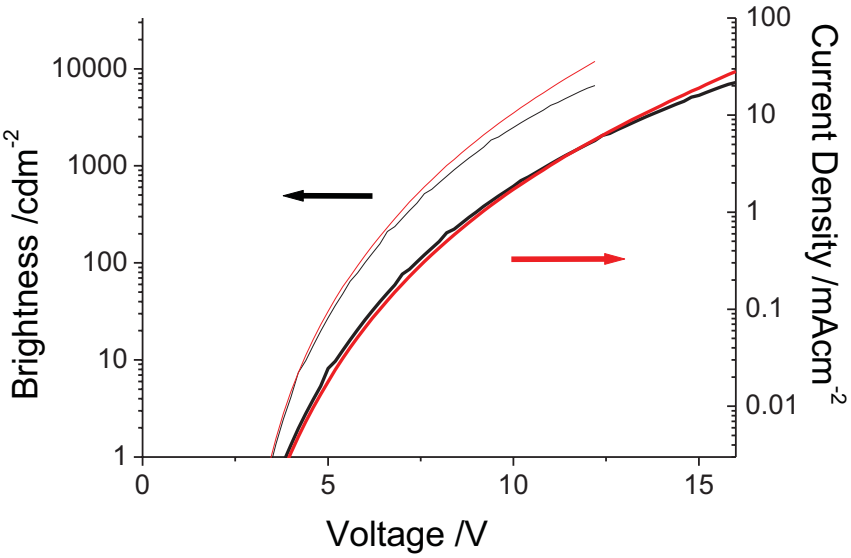

*Figure 6.21 Brightness (black) and current (red) of OLED containing neat films of polymer **10** (thin lines) and 20 wt% of polymer **10** in CBP(thick lines).*

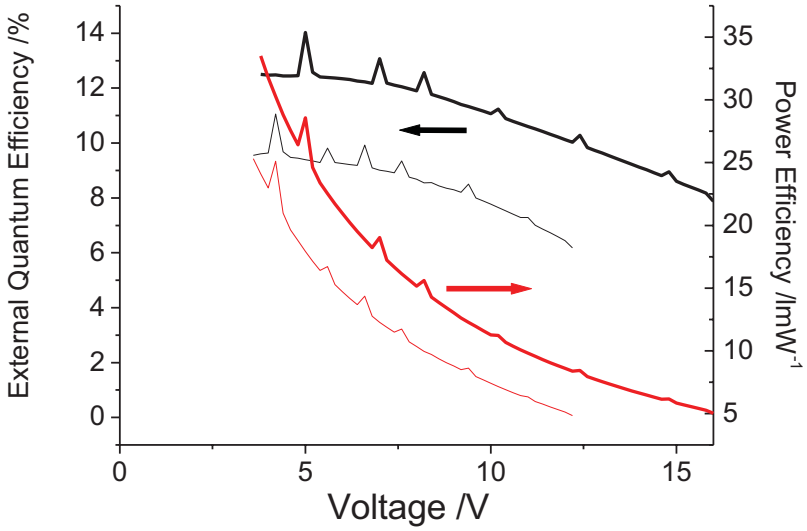

*Figure 6.22 External quantum efficiency (black) and power efficiency (red) of OLEDs with neat films of polymer **10** (thin lines) and 20 wt% of polymer **10** blended with CBP (thick lines).*

Figure 6.23

6.6 Summary of Materials

Material No.	Description	Solution PLQY	Solution TRL /μs	Neat Film PLQY	Neat Film OLED @100 cd/m^2	20 wt% CBP Blended Film PLQY	20 wt% CBP Blended Film OLED @100 cd/m^2
1	$Ir(ppy)_2(acac)$ polymer	34%	48% 0.26, 52 % 1.4	0.9%		7.0%	
2	Precursor	42%	0.67	0.7%			
3	Monomer	52%	1.3	0.6%			
4	$Ir(ppy)_2(acac)$ single dendron polymer	30%	40% 0.30, 60% 1.8	1.9%		18%	
5	Precursor	37%	1.5	1.1%			
6	Monomer	53%	1.9				
7	$Ir(ppy)_2(ptz)$ core	82%					
8	Single dendron polymer	61%	58% 1.0, 42% 1.95	16%		40%	6.2%, 21.8 cd/A at 13.2 V
9	Monomer	92%	1.6			56%	
10	Doubly dendronised $Ir(ppy)_2(ptz)$ polymer	67%	58% 1.0, 42% 1.95	47%	9.3%, 28.1 cd/A at 6.0 V	67%	12.1%, 39.3 cd/A at 7.4 V
11	Monomer	94%	2.1	41%		73%	

Table 6.2 An overview of the properties of all the materials discussed in this chapter. TRL stands for time resolved luminescence and the percentage figures quoted for OLEDs correspond to their external quantum efficiencies.

6.7 Conclusions

Phosphorescent materials are desirable for OLED applications because they allow the harvesting of singlet and triplet excitons and thus 100% internal quantum efficiency to be achieved and using a dendrimer architecture, to solubilise phosphorescent small molecules and protect their cores from aggregation in the solid state, others have achieved highly efficient solution processable dendrimer OLEDs. However, unlike

fluorescent polymers, these molecules do not give their solutions the viscosity necessary for ink-jet printing. This requires us to develop phosphorescent polymers that can be used to produce highly efficient ink-jet printable devices.

Using a non-conjugated polymer backbone to prevent quenching of the phosphorescence, the properties of these materials have been explored over the course of this chapter. The materials have been developed starting with a $Ir(ppy)_2(acac)$ core and no dendrons. The resulting polymer was found to produce high enough viscosity solutions to allow inkjet printing [29]. It was then demonstrated that adding dendrons to the core reduced aggregation quenching in the solid state resulting in a factor 2 increase in solid state performance. Unfortunately these materials still suffered from low photoluminescence quantum yields and unexpectedly long wavelength emission, possibly due to problems with the acac ligand.

By switching to a $Ir(ppy)_2(ptz)$ core the solution photoluminescence quantum yield was increased by a factor of 2 while retaining the required viscosity for inkjet printing [5]. The dendrimer structure allowed a blended film quantum yield of 40% which was high enough to allow OLED devices with 6.2% EQE at 100 cd/m^2 to be made. The aggregation in the solid state was further reduced by adding extra dendrons to make double dendron materials and, while these showed only a modest improvement in solution they had, greatly improved film PLQY to 67%. As film PLQY is a very important parameter for OLED devices this resulted in greatly improved OLEDs with 12.1% EQE (39.3 cd/A) at 100 cd/m^2. These doubly dendronised polymer OLEDs showed a higher efficiency than the 11.8% EQE [20] or 35.1 cd/A [25] of the best previously reported phosphorescent polymer devices.

Throughout this chapter the solution quantum yield of the monomer materials has been higher than the polymers and the time-resolved luminescence data has showed the polymers contain multiple emissive environments. This is because the polymers have closely spaced pendant iridium complexes that can concentration quench. This intrachain aggregation does not seem to be significantly affected by using no-dendrons, single dendrons or double dendrons and so an alternative strategy, of separating the iridium cores on the polymers using spacer groups and creating a co-polymer, will be discussed in the next chapter.

1. King, K.A., P.J. Spellane, and R.J. Watts, *Excited-State Properties of a Triply Ortho-Metalated Iridium(III) Complex.* Journal of the American Chemical Society, 1985. **107**(5): p. 1431-1432.
2. Baldo, M.A., et al., *Very high-efficiency green organic light-emitting devices based on electrophosphorescence.* Applied Physics Letters, 1999. **75**(1): p. 4-6.
3. Lo, S.C., et al., *Green phosphorescent dendrimer for light-emitting diodes.* Advanced Materials, 2002. **14**(13-14): p. 975.
4. Gunning, J.P., et al., *The development of poly(dendrimer)s for advanced processing.* Polymer Chemistry, 2010. **1**(5): p. 730-738.
5. Lai, W.Y., et al., *A Phosphorescent Poly(dendrimer) Containing Iridium(III) Complexes: Synthesis and Light-Emitting Properties.* Macromolecules, 2010. **43**(17): p. 6986-6994.
6. Tekin, E., et al., *Ink-jet printing of luminescent ruthenium- and iridium-containing polymers for applications in light-emitting devices.* Macromolecular Rapid Communications, 2005. **26**(4): p. 293-297.
7. Singh, M., et al., *Inkjet Printing-Process and Its Applications.* Advanced Materials, 2010. **22**(6): p. 673-685.
8. Shimoda, T., et al., *Inkjet printing of light-emitting polymer displays.* Mrs Bulletin, 2003. **28**(11): p. 821-827.
9. Sandee, A.J., et al., *Solution-processible conjugated electrophosphorescent polymers.* Journal of the American Chemical Society, 2004. **126**(22): p. 7041-7048.
10. Evans, N.R., et al., *Triplet energy back transfer in conjugated polymers with pendant phosphorescent iridium complexes.* Journal of the American Chemical Society, 2006. **128**(20): p. 6647-6656.
11. Zhen, H.Y., et al., *Electrophosphorescent chelating copolymers based on linkage isomers of naphthylpyridine-iridium complexes with fluorene.* Macromolecules, 2006. **39**(5): p. 1693-1700.
12. Jiang, J.X., et al., *High-efficiency electrophosphorescent fluorene-alt-carbazole copolymers N-grafted with cyclometalated Ir complexes.* Macromolecules, 2005. **38**(10): p. 4072-4080.
13. Chen, X.W., et al., *High-efficiency red-light emission from polyfluorenes grafted with cyclometalated iridium complexes and charge transport moiety.* Journal of the American Chemical Society, 2003. **125**(3): p. 636-637.
14. Sudhakar, M., et al., *Phosphorescence quenching by conjugated polymers.* Journal of the American Chemical Society, 2003. **125**(26): p. 7796-7797.
15. Schulz, G.L., et al., *Enhancement of phosphorescence of Ir complexes bound to conjugated polymers: Increasing the triplet level of the main chain.* Macromolecules, 2006. **39**(26): p. 9157-9165.
16. Yang, W., et al., *Synthesis of electrophosphorescent polymers based on para-phenylenes with iridium complexes.* Synthetic Metals, 2005. **153**(1-3): p. 189-192.
17. Vicente, J., et al., *Synthesis and Luminescence of Poly(phenylacetylene)s with Pendant Iridium Complexes and Carbazole Groups.* Journal of Polymer Science Part a-Polymer Chemistry, 2010. **48**(17): p. 3744-3757.
18. Tokito, S., M. Suzuki, and F. Sato, *Improvement of emission efficiency in polymer light-emitting devices based on phosphorescent polymers.* Thin Solid Films, 2003. **445**: p. 353–357.

19. Tokito, S., et al., *High-efficiency phosphorescent polymer light-emitting devices.* Organic Electronics, 2003. **4**: p. 105–111.
20. Suzuki, M., et al., *Highly efficient polymer light-emitting devices using ambipolar phosphorescent polymers.* Applied Physics Letters, 2005. **86**(10): p. 103507.
21. Deng, L., et al., *Living radical polymerization of bipolar transport materials for highly efficient light emitting diodes.* Chemistry of Materials, 2006. **18**(2): p. 386-395.
22. Furuta, P.T., et al., *Platinum-functionalized random copolymers for use in solution-processible, efficient, near-white organic light-emitting diodes.* Journal of the American Chemical Society, 2004. **126**(47): p. 15388-15389.
23. Wang, X.Y., et al., *Polymer-based tris(2-phenylpyridine)iridium complexes.* Macromolecules, 2006. **39**(9): p. 3140-3146.
24. Wang, X.Y., A. Kimyonok, and M. Weck, *Functionalization of polymers with phosphorescent iridium complexes via click chemistry.* Chemical Communications, 2006(37): p. 3933-3935.
25. Thesen, M.W., et al., *Hole-Transporting Host-Polymer Series Consisting of Triphenylamine Basic Structures for Phosphorescent Polymer Light-Emitting Diodes.* Journal of Polymer Science Part a-Polymer Chemistry, 2010. **48**(15): p. 3417-3430.
26. Thesen, M.W., et al., *Investigation of Spacer Influences in Phosphorescent-Emitting Nonconjugated PLED Systems.* Journal of Polymer Science Part a-Polymer Chemistry, 2010. **48**(2): p. 389-402.
27. Adachi, C., et al., *Nearly 100% internal phosphorescence efficiency in an organic light-emitting device.* Journal of Applied Physics, 2001. **90**(10): p. 5048-5051.
28. Hay, P.J., *Theoretical studies of the ground and excited electronic states in cyclometalated phenylpyridine Ir(III) complexes using density functional theory.* Journal of Physical Chemistry A, 2002. **106**(8): p. 1634-1641.
29. Lai, W.Y., et al., *A study on the preparation and photophysical properties of an iridium(III) complexed homopolymer.* Journal of Materials Chemistry, 2009. **19**(28): p. 4952-4959.
30. Greenham, N.C., et al., *Measurement of Absolute Photoluminescence Quantum Efficiencies in Conjugated Polymers.* Chemical Physics Letters, 1995. **241**(1-2): p. 89-96.
31. Namdas, E.B., et al., *Photophysics of Fac-tris(2-phenylpyridine) iridium(III) cored electroluminescent dendrimers in solution and films.* Journal of Physical Chemistry B, 2004. **108**(5): p. 1570-1577.
32. Lo, S.C., et al., *Blue phosphorescence from iridium(III) complexes at room temperature.* Chemistry of Materials, 2006. **18**(21): p. 5119-5129.
33. Lo, S.C., et al., *Solution-Processible Phosphorescent Blue Dendrimers Based on Biphenyl-Dendrons and Fac-tris(phenyltriazolyl)iridium(III) Cores.* Advanced Functional Materials, 2008. **18**(19): p. 3080-3090.
34. Suzuki, K., et al., *Reevaluation of absolute luminescence quantum yields of standard solutions using a spectrometer with an integrating sphere and a back-thinned CCD detector.* Physical Chemistry Chemical Physics, 2009. **11**(42): p. 9850-9860.
35. Lo, S.C., et al., *Encapsulated cores: Host-free organic light-emitting diodes based on solution-processible electrophosphorescent dendrimers.* Advanced Materials, 2005. **17**(16): p. 1945-+.

7. Phosphorescent Copolymer Dendrimers

7.1 Introduction

In this chapter I will discuss a continuation to the work on phosphorescent polymers for ink jet printable OLEDs that was started in Chapter 6. In this chapter a copolymer approach was used to control intra-chain aggregation that was observed in the homo-polymers in Chapter 6, which reduced their efficiency as light emitters. These interactions manifested themselves as decreases in photoluminescence efficiency of the polymers compared to their monomers and multiple lifetime components appearing in time resolved luminescence measurements.

In order to reduce these interactions higher energy spacer units are inserted between the phosphorescent cores. The higher band gap energy of these spacers means they should not suffer from back transfer of triplet states from the iridium complexes [1, 2] and any excited states formed on the spacer units will be transferred to the emissive cores. Previous work on iridium based phosphorescent copolymers has been done by

others [1, 3-11] however these authors only made use of pendant iridum complexes which were susceptible to aggregation, limiting device efficiency.

As many of the materials in this chapter are related to those in the previous chapter on phosphorescent polymers the material numbers will continue on from those in the previous chapter. Once again the materials were made and chemically characterised by Wen-Yong Lai, Shih-Chun Lo and Paul Burn at the University of Queensland. The spacer unit that was used initially was poly(styrene) and single dendron copolymers use it as a spacer unit are discussed in Section 7.2, including solution, film and OLED device results. As poly(styrene)'s high HOMO-LUMO gap required additional charge transporting CBP to be added to make OLED devices it was decided to use charge transporting PVK spacer units to make copolymers based on dendronless cores, single dendron emissive units and doubly dendronised units. These materials are detailed in Section 7.3. Finally the conclusions from this work are summarised in Section 7.4.

7.2 Poly(styrene) copolymers

The polymers described in Chapter 6 are all based on a non-conjugated poly(styrene) backbone. This material is regularly used as an inert host for organic materials due to the fact it does not quench photoluminescence and is readily available. Therefore it was a logical choice as a spacer unit for separating the iridium cores and preventing intra-chain aggregation and quenching.

The poly(styrene)/poly(dendrimer) copolymer was synthesised using 99 poly(styrene) spacer units to every 1 dendrimer unit using the single dendron $Ir(ppy)_2(ptz)$ polymer **8** described in Chapter 6 Section 6.4 as a basis. The structure of this copolymer (**12)** is shown in Figure 7.1 along with polymer **8** and monomer **9** for comparison.

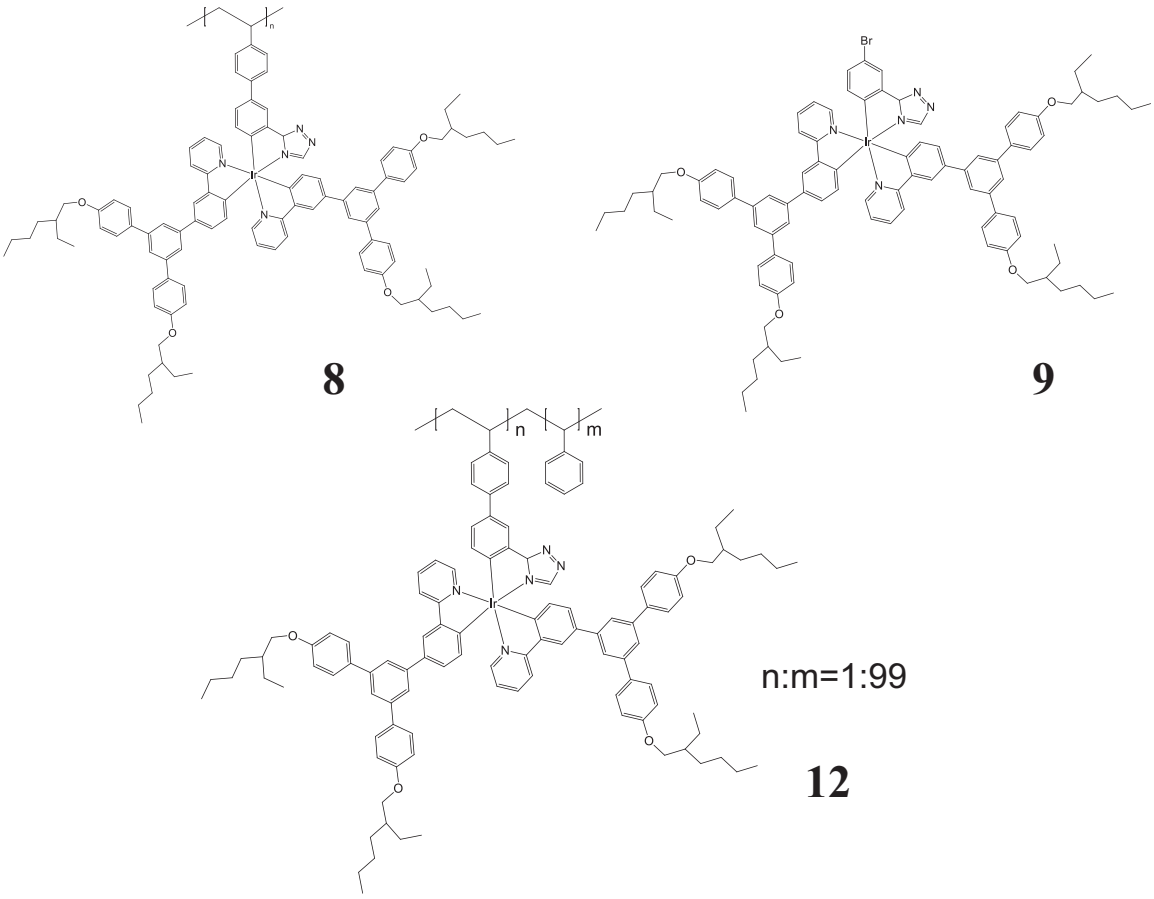

*Figure 7.1 Molecular structure of $Ir(ppy)_2(ptz)$ single dendron based copolymer **12**.*

7.2.1 Solution Properties - Poly(styrene) co-polymer

The dichloromethane (DCM) solution absorption and photoluminescence spectra of **12** were measured and are compared to the homo-polymer **8** and the dendrimer monomer **9** in Figure 7.2. The absorption peaks above 320 nm are assigned to the metal to ligand charge transfer states of the iridium complexes and the peaks below 320 nm are assigned to π-π* type transistions in the ligands, dendrons and the poly(styrene) backbone [12]. The sharp peak in the copolymer's absorption at 269 nm coincides with one of the longer wavelength peaks in the absorption of poly(styrene) in solution [13] and the extra poly(styrene) in the copolymer is the reason why this peak is unusually sharp compared to the absorption of the homo-polymer and monomer.

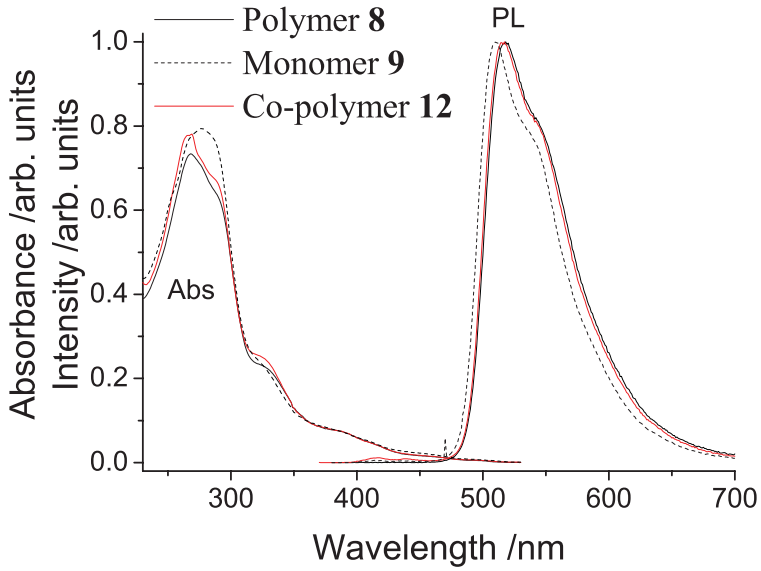

*Figure 7.2 Normalised solution absorption and photoluminescence spectra of polymer **8**, monomer **9** and copolymer **12** in degassed DCM. Absorption spectra were normalised at 360 nm. The excitation wavelength was 360 nm.*

The emission spectra show that the monomer **9**, with its peak at 510 nm, is blue shifted compared to the peaks of polymers **8** and **12**. This is likely to be due to the inductive effect of its bromine substituent. The copolymer **12** has a very slightly bluer peak at 517 nm compared to the peak of polymer **8** at 518 nm. This indicates that aggregation effects in polymer **8** are not responsible for significant red-shifting of the polymer compared to copolymer **12** with its spacer units.

The solution photoluminescence quantum yield of **12** was 94%, which is comparable to monomer **9** (92%) and a significant improvement on polymer **8** (61%). This suggests that intra-molecular interaction in polymer **8** have been eliminated in **12** leading to a PLQY that is comparable to the isolated molecule.

In order to better understand the intra-chain interactions in polymers **8** and **12** time correlated single photon counting was performed on these solutions. Monomer **9** is also shown for comparison. The results are shown below in Figure 7.3. The copolymer **12** has a mono-exponential decay of 1.5 μs which is close to the 1.6 μs for monomer **9**. Polymer **8** has a multi-exponential decay with 0.58 pre-exponential factor

1.0 μs componemt and 0.42 1.95 μs components. This multi-exponential decay occurs because aggregates have created multiple emissive species in **8** which have been eliminated by the poly(styrene) spacer groups in copolymer **9** giving mono-exponential decay.

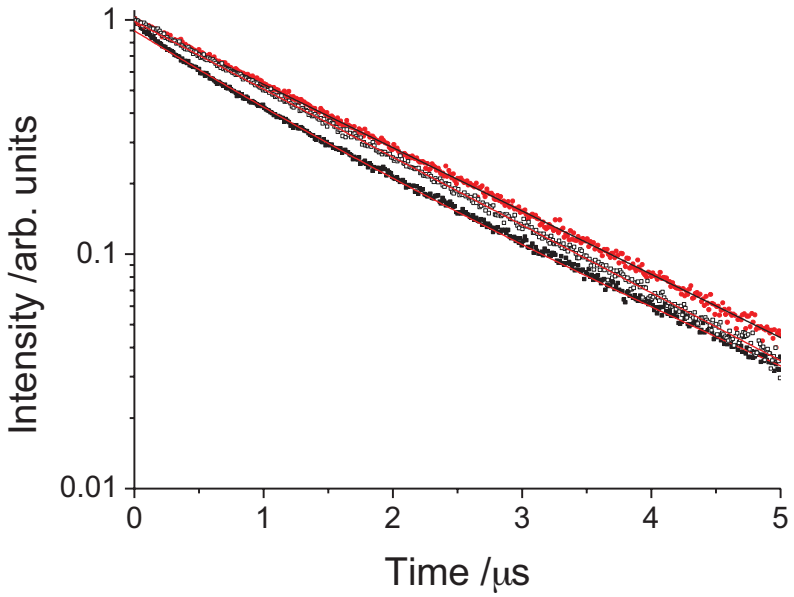

*Figure 7.3 Time resolved luminescence of solutions of polymer **8** (black filled squares, red fit line), monomer **9** (red circles, black fit line) and copolymer **12** (black open squares, red fit line). Excitation was at 393 nm and detection centred at 530 nm.*

7.2.2 Film Properties - Poly(styrene) co-polymer

In order to investigate the usefulness of copolymer **12** in OLEDs, photophysical measurements were made on films. Neat and 20 wt% blends of the copolymer in a 4,4'-N,N'-dicarbazolyl-biphenyl host were spin-coated at 1200 rpm from 20 mg/ml solutions in dichloromethane (DCM). The emission spectra of the neat and blended films are shown in Figure 7.4. The solution spectrum is shown for comparison and so is the neat film spectrum of polymer **8**.

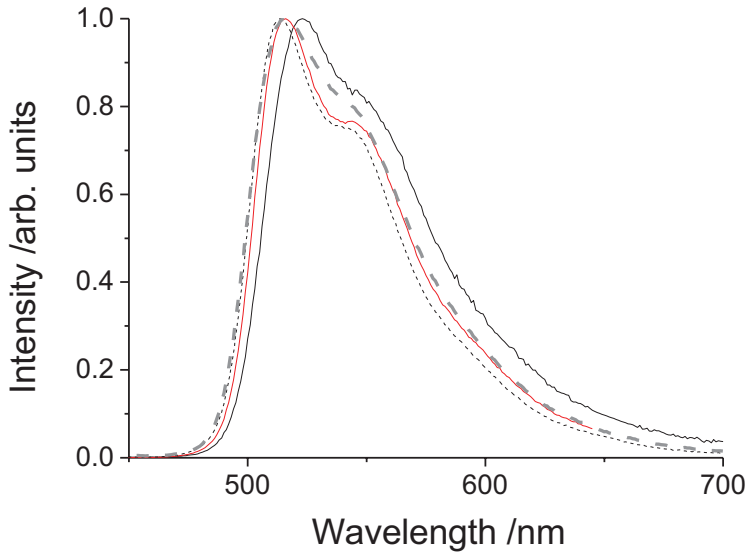

*Figure 7.4 Neat and 20 wt% in CBP blended film emission spectra of copolymer **12** (red solid line and black dashed line) and a comparison with a neat film of homopolymer **8** (solid black line). All films were excited at 325 nm. Also shown for comparison is the copolymer **12** solution spectrum excited at 360 nm (dashed thick grey line).*

As can be seen from Figure 7.4 the emission spectra of copolymer **12** are very similar whether it is in solution or in neat or blended films. The emission peak is at 517 nm in dilute solution and 516 nm in neat film but it slightly blue-shifted to 514 nm in blended films.

Film PLQY for the neat film of polymer **8** is only 13% by the Greenham method [14], compared to 51% for copolymer **12**. In addition the blended film PLQY of polymer **8** was 42% compared to 62% for copolymer **12**. The additional spacer units have improved both the solution and film PLQY values by preventing aggregation.

7.2.3 OLED Device Properties - Poly(styrene) co-polymer

Due to the increased film photoluminescence quantum yield it was hoped that OLEDs made with copolymer **12** would show an improvement on those made with homopolymer **8**. As in Chapter 6, bilayer devices with a 1,3,5-tris(2-N-

phenylbenzimidazolyl)benzene (TPBI) hole blocking layer were made following the protocol in Chapter 4. The 20 wt% of the copolymer was blended with CBP and dissolved in DCM at a concentration of 10 mg/ml. The CBP host was used both to increase the film PLQY but also because the polystyrene spacer groups will not contribute to charge transport due to their high HOMO – LUMO energy gap.

The electroluminescence spectrum of the blended OLED at 15 V is shown below in Figure 7.5. The emission peaks at 516 nm which is close to the solution peak at 516 nm and the blended film photoluminescence peak at 514 nm.

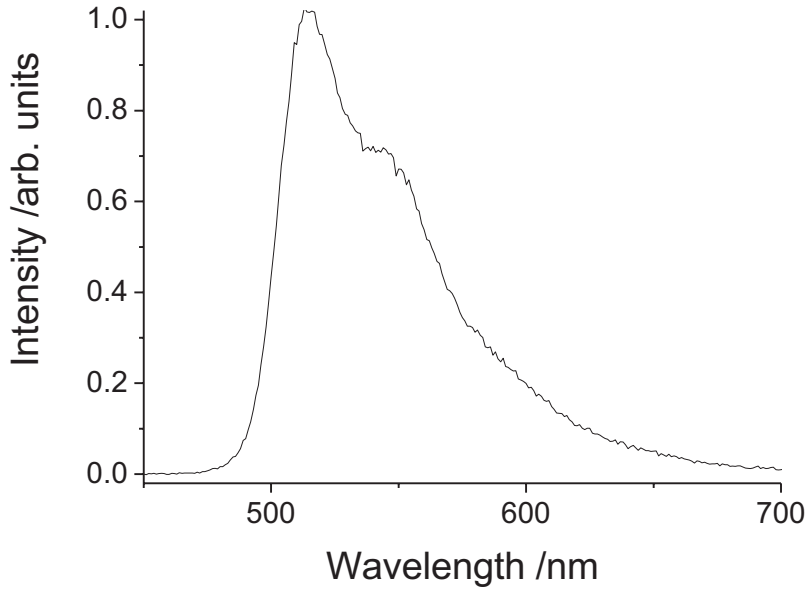

*Figure 7.5 Emission spectrum of bilayer OLED containing 20 wt% of copolymer **12** in a CBP blend. Drive voltage 15 V.*

The brightness and current vs. voltage plots for this OLED are shown in Figure 7.6 and the external quantum efficiency and power efficiency curves are shown in Figure 7.7. The efficiency seems to increase following turn on as the brightness rises faster than the current up to about 10-11 V where the EQE peaks. This increasing efficiency may indicate that the charge carrier's are not balanced at low drive voltages due to a barrier to injection.

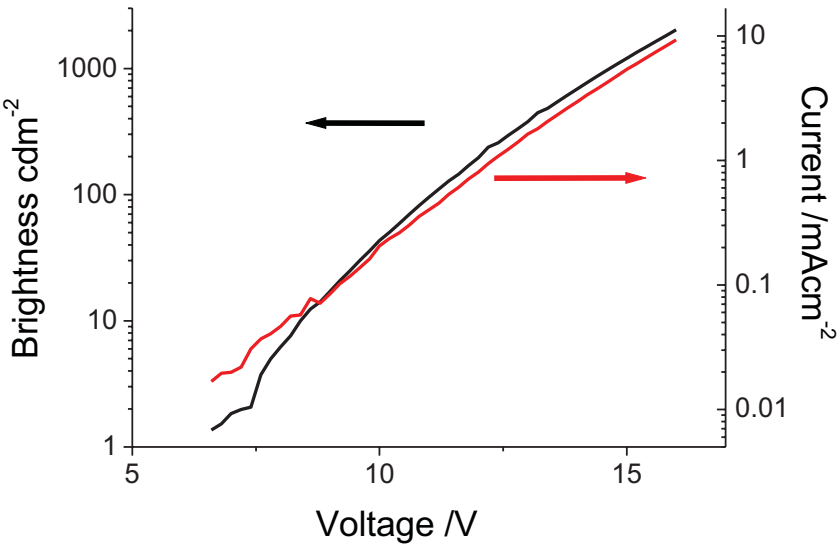

*Figure 7.6 Brightness (black) and current (red) of OLED containing 20 wt% of polymer **12** in CBP.*

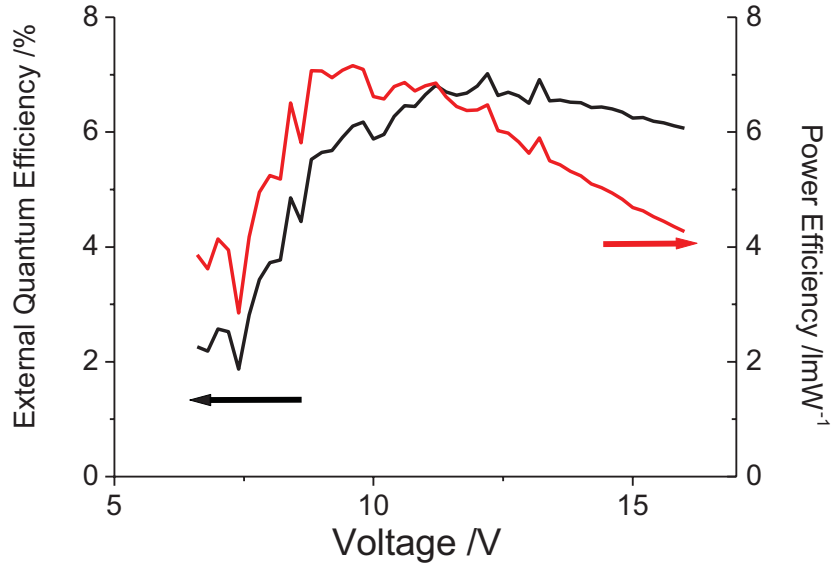

*Figure 7.7 External quantum efficiency (black) and power efficiency (red) of OLEDs with 20 wt% of polymer **12** in CBP as emissive layer.*

The efficiency of the device at 100 cd/m^2 is 6.6% external quantum efficiency (23.8 cd/A), 6.8 lm/W at 11.0 V. Assuming at 20% out coupling efficiency the estimated maximum efficiency from the blended film PLQY is 12.4% EQE. Using this figure

these devices are operating about 50% of optimal efficiency. It is likely that this is because charge balance has not been achieved, perhaps because the poly(styrene) units are reducing hole transport through the emissive layer. These results are, however, an improvement on homopolymer **8** blended film devices which achieved 100 cd/m^2 at 6.2% EQE (21.8 cd/A) and 13.2 V. This is because the copolymer has achieved an increased blended film PLQY due to its spacer units which reduce inter-molecular and intra-molecular aggregation effects.

7.3 Poly(carbazole) copolymers

In order to try and produce better copolymer materials for devices it was decided to try and use charge transporting spacer units to separate the emissive units. As many charge transport materials used in OLEDs contain the carbazol moiety [15] the decision was taken to use 9-vinylcarbazole as the spacer unit. When used to form a homo-polymer, poly(9-vinylcarbazole), this material is often known as PVK or PVCz and is commonly used as a hole transport material [15, 16]. It was decided to try these materials without dendrons, with single dendrons and with double dendrons to see what effect this had on aggregation.

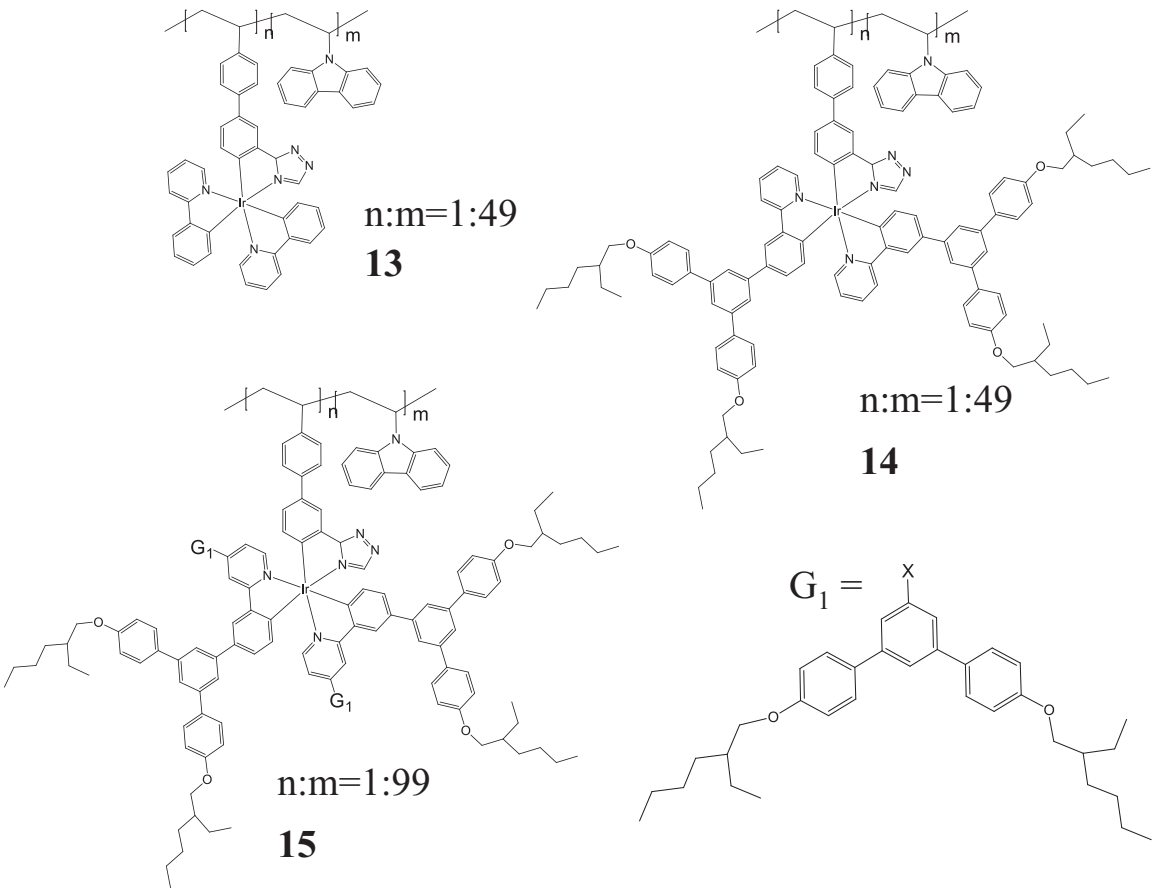

*Figure 7.8 Molecular structure of Ir(ppy)$_2$(ptz) poly(9-vinylcarbazole) based copolymers **13**, **14** and **15** featuring core, single and double dendron structures respectively.*

7.3.1 Solution Properties - Poly(carbazole) co-polymers

The emission spectra of the copolymers in dilute DCM solutions is shown in Figure 7.9. These spectra were normalised at 330 nm so that the absorption due to the PVK type units would be clearly shown. As before absorption due to the metal-to-ligand charge transfer states of the cores are responsible for the absorption at longer than 320 nm, however below 350 nm the absorption is dominated by π-π* transitions in the PVK units of the polymers. This can be seen in the fact that double dendrimer copolymer **15** has lower long wavelength absorption as it contains approximately half as many iridium cores as the other two copolymers.

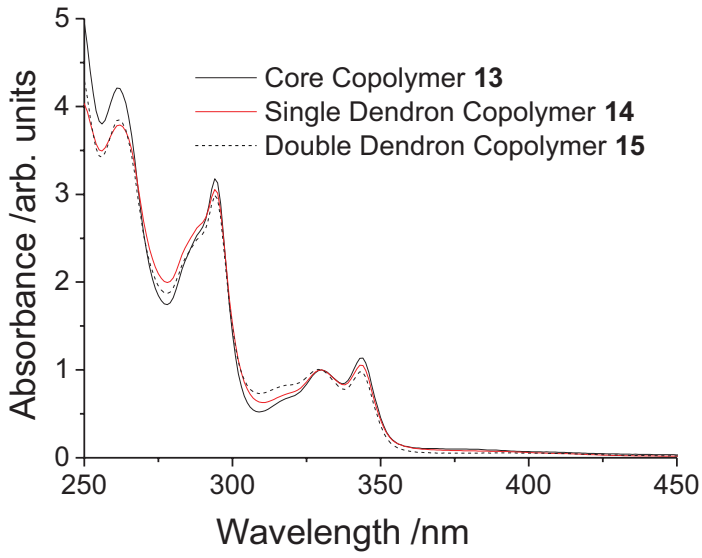

Figure 7.9 Normalised solution absorption spectra in DCM. All spectra were normalised at 330 nm.

The absorption of PVK is reported in the literature to have peaks at 330 nm and 343 nm [16] which correspond to the features seen at 329-330 nm and 343-344 nm in the three copolymers. The π-π* transition from the dendrons and the iridium ligands are expected to appear below 320 nm and have been observed in $Ir(ppy)_3$ and $Ir(ppy)_3$ based dendrimers to give a peak around 290 nm in solution [17]. However this is also the location of a peak in PVK's absorption. Therefore the peak at 294 nm in the copolymer materials is attributed to both. As there is not much difference between the spectra of the co-polymers most of the absorption is attributed to the more numerous PVK units.

The photoluminescense spectra of the same solutions of the copolymers in degassed DCM is shown below in Figure 7.10. The peaks in the emission spectrum are at 512 nm for the core copolymer **13**, 516 nm for the dendrimer copolymer **14** and 551 nm for the double dendron copolymer **15**. The core copolymer **13**'s emission spectrum is very slightly red-shifted from 510 nm for the isolated core **7** in solution. This is likely to be due to extra conjugation from the addition of the extra phenyl unit at the meta postion to the phenyltriazolyl linker ligand. The single-dendron copolymer **14**'s peak at 516 nm is close to the 518 nm emission peak for the single dendron homopolymer **8**

and the 517 nm for the poly(styrene) copolymer **9**. We would expect the core copolymer's peak to be slightly blue shifted due to reduced conjugation as it lacks the meta linked phenylene dendrons. Copolymer **15**'s peak is significantly redshifted thanks to the extra conjugation length due to the para linked second pair of dendrons [18]. Its emission peak at 551 nm is at the same wavelength of the emission peak of the double dendron homopolymer **10** at 551 nm.

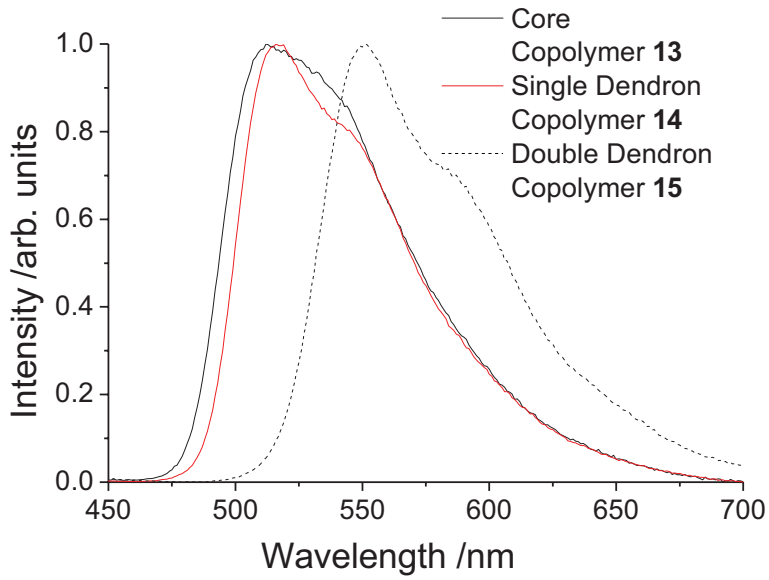

*Figure 7.10 Normalised photoluminescence spectra of copolymers **13**, **14** and **15** in degassed DCM. The solutions were excited at 360 nm.*

When excited at 360 nm the solution PLQY values for these samples were 69%, 64% and 64% for materials **13**, **14** and **15** respectively. These values are comparable to single dendron homopolymer **8** (61%) and double dendron homopolymer **10** (67%). This is significantly lower than the PLQYs of the core and the single dendron and double dendron monomers (materials **7**, **9** and **11**, PLQY values 82%, 92% and 94% respectively). As with the emission spectra there does not appear to be any evidence that the copolymer structure has reduced intra-chain aggregation unlike in case of the single dendron poly(styrene) copolymer **12**, which has a solution PLQY of 94%.

In order to investigate this further, solution TCSPC measurements were performed on the samples. The results of these measurements together with mono-exponential fit lines are shown in Figure 7.11. All the copolymers were well fit by mono-exponential

decays. Core copolymer **13** had a decay time of 1.5 μs. The single dendron copolymer **14** had a decay time of 1.1 μs, which is shorter than corresponding monomer **9** and polystyrene copolymer **12**'s decay times of 1.6 μs and 1.5 μs respectively. The double dendron copolymer **15** also had a decay time of 1.8 μs shorter than its monomer **11's** 2.1 μs decay.

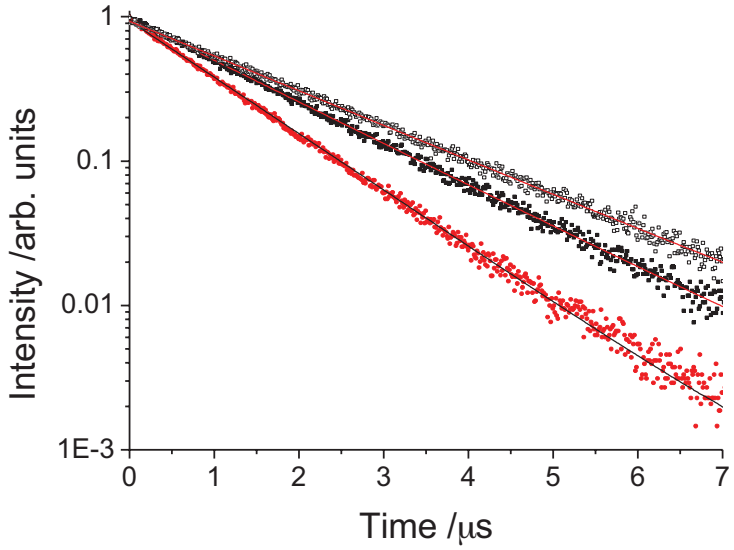

*Figure 7.11 Time resolved luminescence of solutions of core copolymer **13** (black filled squares, red fit line), single dendron copolymer **14** (red circles, black fit line) and double dendron copolymer **15** (black open squares, red fit line). Excitation was a 393 nm and detection centred at 530 nm.*

The fact that emission spectra are redshifted, PLQY values are reduced and lifetimes are shorter in the copolymer are consistent with each other. However, it is surprising that multi-exponential decays due to aggregated species have not appeared. This does however suggest that there is reduced oscillator strength or an increased non-radiative rate in the copolymers. The radiative and non-radiative lifetimes are calculated in Table 7.1 below.

Material	Description	Total decay rate /μs	PLQY	Radiative Lifetime /μs	Non-Radiative Lifetime /μs
7	Core	-	82%	-	-
13	Core PVK copolymer	1.5	69%	2.2	4.8
9	Single Dendron Monomer	1.6	92%	1.7	20.0
12	Single Dendron poly(sytrene) copolymer	1.5	94%	1.6	25.0
14	Single Dendron PVK copolymer	1.1	64%	1.7	3.1
11	Double Dendron Monomer	2.1	94%	2.2	35.0
15	Double Dendron PVK copolymer	1.8	64%	2.8	5.0

Table 7.1 The radiative and non-radiative lifetimes of the PVK based copolymers and their monomers in degassed DCM solutions. Poly(styrene) copolymer 12 is also included for comparison.

It is clear from the table that the radiative rates are similar for the monomers and their corresponding copolymers, however, the non-radiative lifetime has shortened dramatically in the PVK based materials. We would not expect change in the radiative lifetimes of the materials as nothing in the material structure would suggest a change in the emissive properties of the core. The increased non-radiative rate seems unlikely to be from non-emissive aggregates because of the mono-exponential decays of these materials in solution. Vibration of the molecules can also cause an increase in the non-radiative rate however the copolymerisation should not have an effect on the core rigidity.

It is possible that the increased non-radiative rate could result form triplet back transfer to the 9-vinylcarbazole units. While the 9-vinylcarbazole carbazole monomer has a triplet energy of 3.02 eV (corresponding to 415 nm) measured by cyclic voltammetry [15], poly(9-vinylcarbazole) has a triplet energy of ~2.5 eV (corresponding to ~500 nm) measured by phosphorescence at 77K [19, 20]. This may be the results of aggregation of the PVK units. As a result some higher energy excitations on the iridium cores could back transfer onto the PVK units where they would not emit light. This would reduce the PLQY while still leaving mono-exponential decay. Similar behaviour has been observed in blue emitting dendrimers

where the dendrons have comparable triplet energy to the phosphorescent core [21]. In dilute solution the triplets could not escape from the molecule and so the result was and increased lifetime as the triplet could not decay radiatively while on the dendrons. In the solid state however the PLQY was significantly reduced as the triplet could now escape and find lower energy trap states. It seems likely that the many repeating PVK units would allow a fraction of the excitations to escape and find a lower energy aggregated part of the PVK chain.

However, we would expect these effects to be strongly reduced in the lower energy double dendron copolymer **15** as the lower triplet energy should reduce back transfer to the PVK. Instead the reduction in PLQY is similar to higher energy polymers **13** and **14** and the PLQY and emission wavelength remain comparable to double dendron homopolymer **10**. This indicates that the effect is the same strength in the double dendron copolymer as the others and suggests back transfer to the PVK spacer units may not be the cause of the reduced luminescence.

Finally it may be the case that the neighbouring PVK units on the polymer are π-stacking with the linker ligand of the emissive cores and reducing the luminescence. However in order to avoid this creating multiple emissive environments in the time resolved luminescence this structure must either be non-emissive or must be formed in a uniform fashion along the polymer chain.

7.3.2 Film Properties - Poly(carbazole) co-polymers

It was hoped the presence of charge transfer spacer units, to control aggregation and allow hole-transport, would allow highly efficient neat film OLED devices to be fabricated. To check that the copolymers had efficient emission in neat films photoluminescence measurements were made on films spun at 1200 rpm from 20 mg/ml solutions in DCM. The emission spectra of the copolymers is shown in Figure 7.12.

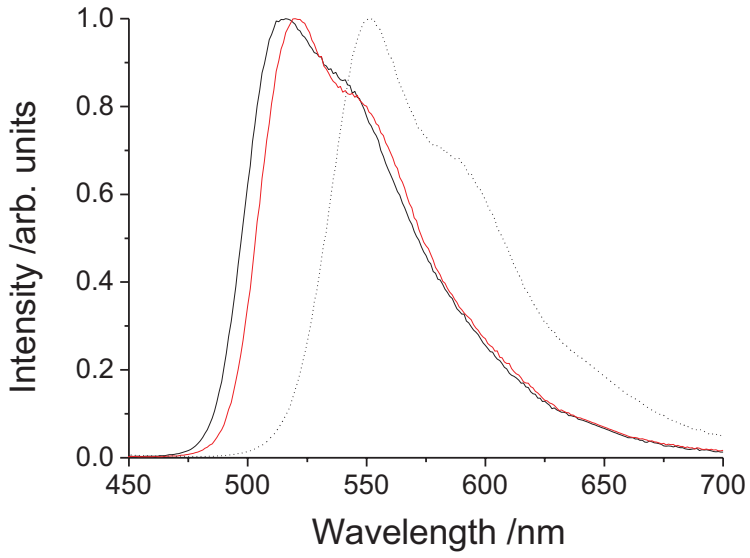

*Figure 7.12 Neat film emission spectra of copolymers **13** (black line), **14** (red line) and **15** (dotted line). All films were excited at 325 nm.*

The emission peak of copolymer **13** is at 516 nm, slightly red-shifted from the solution emission at 512 nm. Copolymer **14** is similarly red-shifted from 516 nm to 520 nm. However double dendron polymer **15** has maintained its emission peak at 551 nm on going from solution to film. The emission peak of single dendron copolymer **14** is still on the blue side of neat films of corresponding homopolymer **8** which has its peak at 523 nm in neat film and 521 nm in 20wt% blended films with CBP. Similarly copolymer **15** has bluer emission than neat films of homopolymer **10** (555 nm) and 20 wt% blended films in CBP (553 nm).

The neat film PLQY values of these materials were measured using the Suzuki method [22] with 325 nm excitation. Copolymer **13** was found to have a PLQY of 46%, copolymer **14** 49% and copolymer **15** 57%. This is a significant improvement on the single dendron homo-polymer **8**'s PLQY of 16% and copolymer **15** shows and improvement on double dendron homopolymer **10**'s value of 47%. For comparison blended films of homopolymers **8** and **10** have PLQYs of 40% and 67% which are similar to the copolymers. The copolymers appear to show a trend of increasing PLQY with the addition of single and then double dendrons, which we might expect from increased steric protection of the cores.

7.3.3 Neat OLED Device Properties - Poly(carbazole) co-polymers

The copolymers were then tried in bilayer OLEDs with TPBI as the hole blocking layer and a neat film of the copolymer, spin-cast at 2000 rpm from a 10 mg/ml DCM solution, was used as the emissive layer. The hole transporting PVK units were expected to allow good hole transport to the TBPI interface while electrons would be slowed before they reached the anode allowing for a high quantum efficiency.

The emission spectra of the devices are shown in Figure 7.13, the current-voltage plots are shown in Figure 7.14, the brightness-voltage curves are shown in Figure 7.15 and the external quantum efficiency-voltage curves are shown in Figure 7.16 below.

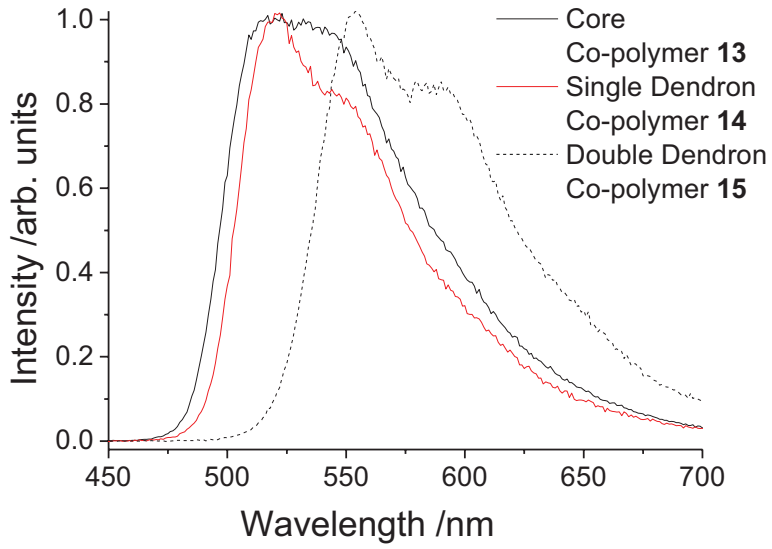

*Figure 7.13 Emission spectra of neat bilayer OLEDs of copolymers **13**, **14** and **15**. The drive voltage was 12 V for all devices.*

The peak of the electroluminescence was at 517 nm for core copolymer **13** and it had CIE coordinates of (0.35, 0.60) which correspond to yellow/green emission. This is only 1 nm longer wavelength than its neat film spectrum and close to its 512 nm solution peak. However the emission spectrum was unusually broad compared to its solution and film spectra and showed a significant red-tail which can indicate lower energy aggregated states. Copolymer **14** has its emission peak at 522 nm and has CIE coordinates of (0.35, 0.61) which is yellow/green. This is again comparable to the neat film photoluminescence peak at 520 nm and here the emission is narrower in shape

than copolymer **13**. Copolymer **15** has an emission peak at 554 nm which is again only slightly red-shifted from its neat film peak at 551 nm. Its CIE coordinates are (0.48, 0.52) which are significantly more yellow than the other two materials.

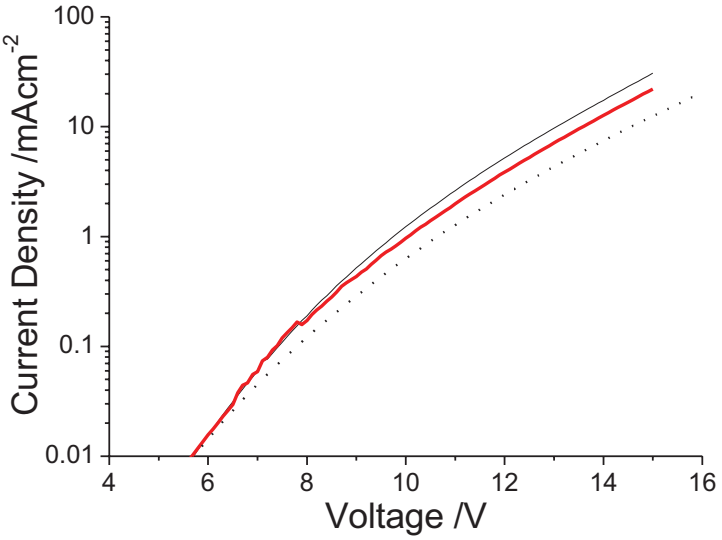

*Figure 7.14 Current vs. voltage plots for neat bilayer layer OLEDs of copolymers **13** (black line), **14** (red line) and **15** (dotted line).*

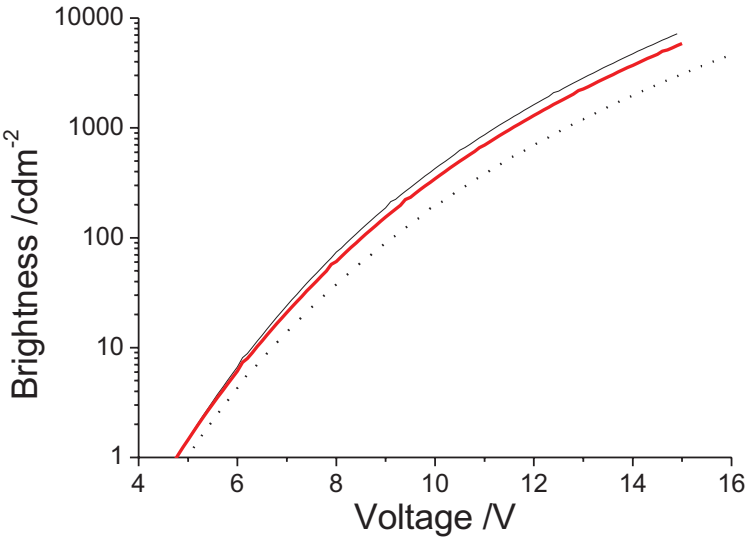

*Figure 7.15 Brightness vs. voltage plots for neat bilayer layer OLEDs of copolymers **13** (black line), **14** (red line) and **15** (dotted line).*

The both the current/voltage and brightness/voltage curves show that these devices have only moderate turn-on voltages, achieving 1 cd/m^2 at 4.8 V for **13** and **14**, and 5 V for **15**.

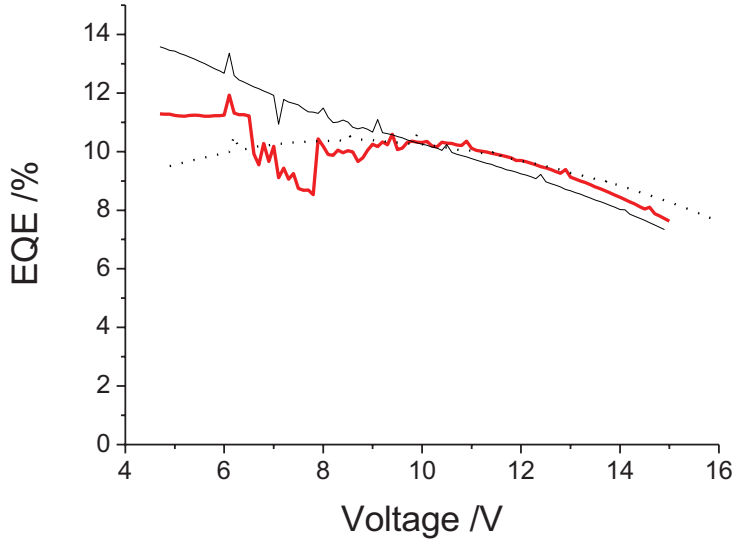

*Figure 7.16 EQE vs. voltage plots for neat bilayer layer OLEDs of copolymers **13** (black line), **14** (red line) and **15** (dotted line).*

The performances of the devices at 100 cd/m^2 brightness were: **13** EQE 11.0% (37.3 cd/A), 14.1 lm/W at 8.3V; **14** EQE 10.0% (34.8 cd/A), 12.9 lm/W at 8.5 V; **15** EQE 10.4% (31.0 cd/A), 10.7 lm/W at 9.1 V. The device's EQEs are rather similar and meet or exceed the theoretical maximum given by the material's neat film PLQYs of 9.2% for polymer **13**, 9.8% for **14** and 11.4% for **15** assuming 20% out coupling. This indicates that the devices are achieving excellent charge balance.

7.3.4 Blended Film Properties - Poly(carbazole) co-polymers

Despite the presence of a large number of spacer units in the copolymers it was decided that the film PLQY was limiting device performance and this might be improved by blending them with CBP. As the polymers already contained many carbazole units it was decided that a 50 wt% blend would be sufficient dilution of the emissive cores to eliminate aggregation effects. The emission spectra of these films were measured using a Hammastu C9920-02 PLQY measurement system during the determination of their PLQY via the Suzuki method [22] with excitation at 325 nm. The photoluminescence spectra are shown in Figure 7.17.

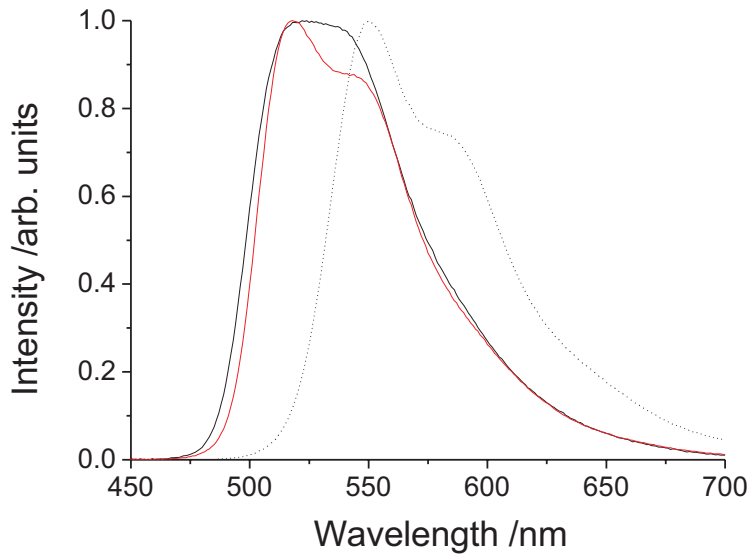

*Figure 7.17 Film emission spectra of copolymers **13** (black line), **14** (red line) and **15** (dotted line) 50wt% blended into CBP. All films were excited at 325 nm.*

For the core copolymer **13** the spectrum has a peak at 522 nm which is unusually broad compared to the neat film photoluminescence in Figure 7.12 and is similar to the broad spectrum the neat film devices shown under electroluminescence in Figure 7.13. The emission peak is red-shifted compared to neat films and neat film OLEDs which peak at 516 nm and 517 nm respectively. However the red-tail of the emission is less pronounced in the blended film than in the neat film OLED spectrum. The dendronised copolymer **14** has its emission peak at 518 nm, which is slightly blue shifted from the emission peak in neat films at 520 nm. Similarly double-dendron copolymer **15** has an emission peak at 550 nm in the blended film and 551 nm.

The PLQY values for these blended films of copolymers **13**, **14** and **15** are 64%, 61% and 73% respectively, which are significant increases on the neat film PLQYs of 46%, 49% and 57%. These values have no decrease in the PLQY despite the increased broadening and red-shifting in the emission spectrum in the copolymer **13** blended films and instead show blending with CBP has increased luminescence efficiency in all the materials probably through reduced aggregation.

7.3.5 Blended OLED Device Properties - Poly(carbazole) co-polymers

Blended OLED devices with 50 wt% of CBP as the emissive layer and a TPBI electron transporting layer were fabricated using copolymers **13**, **14** and **15**. However only copolymer **15** based devices gave satisfactory light emission (>100 cd/m^2 brightness) and so these are the devices detailed below. The emission spectrum is shown in Figure 7.18, the brightness and current vs. voltage curves are shown in Figure 7.19 and the external quantum efficiency and luminous efficiency are shown in Figure 7.20.

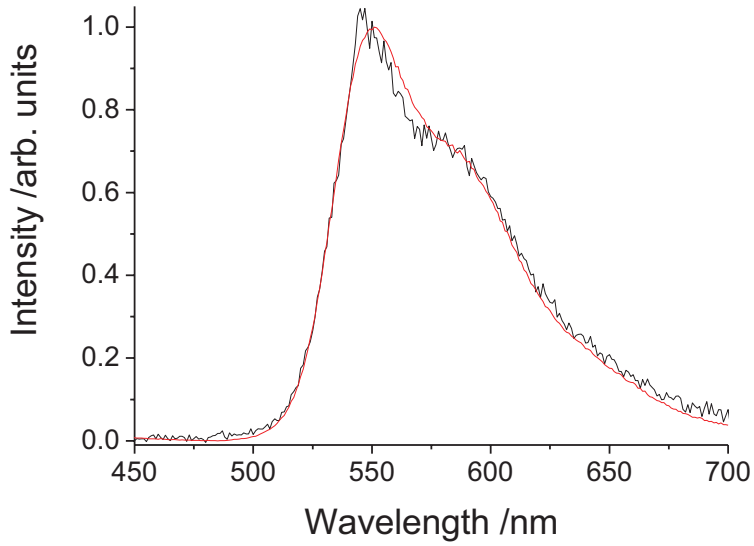

*Figure 7.18 The black line shows the emission spectrum of bilayer OLEDs with 50 wt% of copolymer **15** blended with CBP as the emissive layer at a drive voltage of 12 V. The red line shows the solution photoluminescence spectrum of **15** for comparison.*

The OLEDs emission peak at 546 nm and the device has CIE coordinates of (0.44, 0.54), which is yellow/green. The emission peak is bluer than the neat film device for **15**, which has more yellow CIE coordinates of (0.48, 0.52) and a peak at 554 nm. This shows that there was some aggregation in the neat film OLED that has been reduced by blending. The peak emission of the blended device is close to the photoluminescence peak in the blended film at 550 nm and is comparable to the solution emission spectrum of copolymer **15** at 551 nm. The slight blue shifting of the

spectral peak is attributed to noise in the measurement as the emission spectrum otherwise corresponds closely to the solution emission spectrum of **15**.

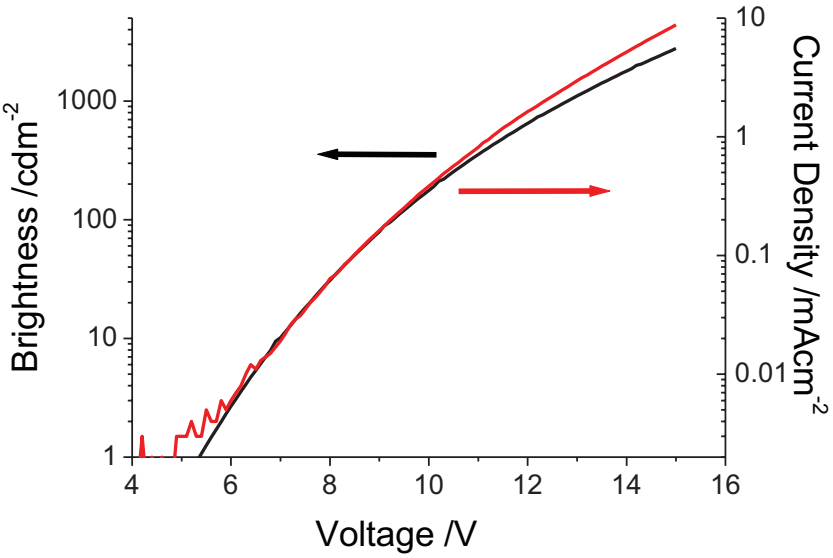

*Figure 7.19 Current and brightness vs. voltage plots for bilayer OLEDs with 50 wt% of copolymer **15** blended with CBP as the emissive layer.*

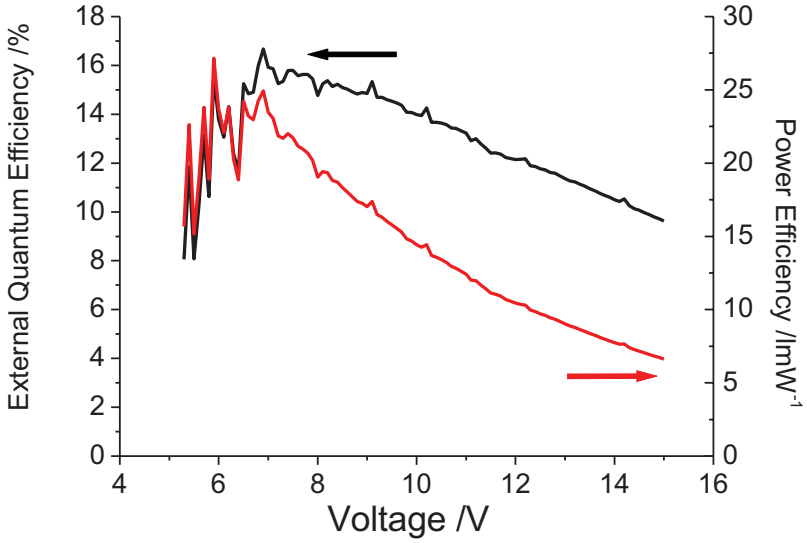

*Figure 7.20 EQE and power efficiency curves for bilayer OLEDs with 50wt% of copolymer **15** blended with CBP as the emissive layer.*

The brightness and current curves in Figure 7.19 show that the current increases more rapidly than brightness at voltages over 10 V indicating a decrease in current efficiency with voltage. This is confirmed by the external quantum efficiency plot in

Figure 7.20. The efficiency at 100 cd/m^2 brightness is 14.7% EQE (48.3 cd/A) and 16.3 lm/W power efficiency at 9.3 V. At 1000 cd/m^2 the efficiency has reduced to 11.6% EQE (38 cd/A) with 9.3 lm/W power efficiency at 12.8 V.

The efficiency of 14.7% is close to the 14.6% estimated value that would be achieved with 20% light extraction with the blended film PLQY of 73% assuming perfect charge balance. This indicates that the balance of electrons and holes in the devices is close to optimal. This efficiency is a significant increase on the neat copolymer devices which achieved 11.0% EQE using of copolymer **13** and 10.3% EQE using copolymer **15** at 100 cd/m^2. This increase is largely because of the increased photoluminescence quantum yield from 57% to 73% on blending the films of **15** with 50 wt% CBP because of reduced aggregation.

Unfortunately the devices have a relatively high drive voltage for 100 cd/m^2 of 9.3V which is significantly higher than the 5 V drive voltage for the double dendron homopolymer **10** in blended devices. This means the copolymer blend's power efficiency of 16.3 lm/W at 100 cd/m^2 is actually lower than the 16.7 lm/W power efficiency of the blended homopolymer **10** devices despite the fact that the EQE of the homopolymer blend is only 12.1%. This higher drive voltage can simply be attributed to the increased thickness of the **15** blended film which is 120 nm thick, compared to the 70 nm emissive layer thickness for blends of polymer **10**. By reducing the layer thickness and further optimising the device the higher quantum efficiency of the **15** blended film devices should result in a significant increase in power efficiency in optimised devices.

7.4 Summary of Materials

Material No.	Description	Solution PLQY	Solution TRL /μs	Neat Film PLQY	Neat Film OLED @100 cd/m^2	20 wt% CBP Blended Film PLQY	20 wt% CBP Blended Film OLED @100 cd/m^2
8*	Single dendron polymer	61%	58% 1.0, 42% 1.95	16%		40%	6.2%, 21.8 cd/A at 13.2 V
9*	Monomer	92%	1.6			56%	
12	Single dendron poly(styrene) copolymer	94%	1.5	51%		67%	6.6% 23.8 cd/A, 11.0 V
10*	Doubly dendronised polymer	67%	58% 1.0, 42% 1.95	47%	9.3%, 28.1 cd/A at 6.0 V	67%	12.1%, 39.3 cd/A at 7.4 V
11*	Monomer	94%	2.1	41%		73%	
13	Core poly(carbazole) copolymer	69%	1.5	46%	11.0% 37.3 cd/A at 8.3V	64%	
14	Single Dendron poly(carbazole) copolymer	64%	1.1	49%	10.0% 34.8 cd/A at 8.5 V	61%	
15	Doubly dendronised poly(carbazole) copolymer	64%	1.8	57%	10.4% 31.0 cd/A at 9.1 V	73%	14.7% 48.3 cd/A 9.3 V

Table 7.2 An overview of the properties of all the materials discussed in this chapter. Starred materials were discussed in detail in Chapter 6. TRL stands for time resolved luminescence and the percentage figures quoted for OLEDs correspond to their external quantum efficiencies.

7.5 Conclusions

In solution the copolymer structures have resulted in phosphorescent polymers with increased photo luminescent quantum yields compared to the homopolymers in Chapter 6 and as a result these materials are more suitable for applications in light

emitting diodes. This has been demonstrated by the fabrication of devices with higher external quantum efficiencies than in comparable homo-polymers, achieving a maximum efficiency of 14.7% at 100 cd/m^2. This result is significantly higher than the previous best reported quantum efficiency for a phosphorescent polymer of 11.8% [5].

The improvement in solution quantum yields can be seen most clearly in copolymer **12**, with its poly(styrene) spacer units and single dendron emissive core. In this material the addition of the spacer groups have increased the PLQY from 61% for, comparable homopolymer **8**, to 94% which is comparable to the monomer's PLQY of 92%. This lack of intra-chain interactions is confirmed by the mono-exponential photoluminescence lifetime.

Copolymer **12** remained impressive in films, showing significant improvements over polymer **8**, giving 51% PLQY in neat film and 67% in blended films of **12** compared to only 16% and 40% for **8**. However the polystyrene spacer units were effectively insulating and appear to have impeded hole transport in blended bilayer OLED devices resulting in a EQE of 6.6% at 100 cd/m^2, approximately 50% of the estimated maximum given the blended film PLQY. While this was better than 6.2% EQE for polymer **8** it suggested that copolymers with hole transporting units might be better for devices.

Using poly(carbazole) as the spacer units met the requirement of high energy hole transporting spacer units. However the photoluminescence quantum yields of these materials in film were less promising at only 61%-69%, compared to >90% for the monomers and the poly(styrene) spacer copolymer. Time resolved luminescence showed that the materials did have mono-exponential decays, indicating only one emissive state was present, but that they had increased non-radiative decay rates without changing the radiative rates. This suggests that the poly(carbazole) units have in some way provided a non-radiative de-excitation pathway in these materials.

Fortunately the poly(carbazole) materials did not suffer a significant decrease in photoluminescence quantum yield in neat or blended films, which set the upper limit on OLED efficiency. By controlling intra-core interactions through the use of the

carbazole units and dendrons these materials gave 11.0% EQE in neat films and 14.7% EQE (48.3 cd/A) in blended films at 100 cd/m^2. This is a significant improvement on using double dendrons to control interactions in a homopolymer alone which only gave 9.0% and 12.1% EQE respectively. This makes means this device has a significantly higher current efficiency than the 11.8% EQE [5] or 35.1 cd/A [10] of the best literature reports for a phosphorescent polymer.

It is unclear that the dendon's have made a significant improvement to the performance of these materials as the neat and blended film PLQYs of the core only, single dendron and double dendron materials are similar. There is however a slight upward trend with increasing number of dendrons from 46%, 49% to 57% in neat film and 64%, 61%, 73% in blended film. Critically it appears that the double dendron structure has allowed the creation of high brightness OLEDs when blended with CBP, which was not the case for the other two materials. The combination of double dendrons and the poly(carbazole) spacer units in copolymer **15** has resulted in the highest blended film PLQY of any of any of the materials presented in Chapter 6 or 7 and this has lead to its very high OLED external quantum efficiency which corresponds to an estimated internal quantum efficiency of ~75% in a solution processable device.

1. Chen, X.W., et al., *High-efficiency red-light emission from polyfluorenes grafted with cyclometalated iridium complexes and charge transport moiety.* Journal of the American Chemical Society, 2003. **125**(3): p. 636-637.
2. Sudhakar, M., et al., *Phosphorescence quenching by conjugated polymers.* Journal of the American Chemical Society, 2003. **125**(26): p. 7796-7797.
3. Tokito, S., M. Suzuki, and F. Sato, *Improvement of emission efficiency in polymer light-emitting devices based on phosphorescent polymers.* Thin Solid Films, 2003. **445**: p. 353–357.
4. Tokito, S., et al., *High-efficiency phosphorescent polymer light-emitting devices.* Organic Electronics, 2003. **4**: p. 105–111.
5. Suzuki, M., et al., *Highly efficient polymer light-emitting devices using ambipolar phosphorescent polymers.* Applied Physics Letters, 2005. **86**(10): p. 103507.
6. Sandee, A.J., et al., *Solution-processible conjugated electrophosphorescent polymers.* Journal of the American Chemical Society, 2004. **126**(22): p. 7041-7048.
7. Jiang, J.X., et al., *High-efficiency electrophosphorescent fluorene-alt-carbazole copolymers N-grafted with cyclometalated Ir complexes.* Macromolecules, 2005. **38**(10): p. 4072-4080.

8. Zhen, H.Y., et al., *Electrophosphorescent chelating copolymers based on linkage isomers of naphthylpyridine-iridium complexes with fluorene.* Macromolecules, 2006. **39**(5): p. 1693-1700.
9. Jiang, J.X., et al., *High-efficiency white-light-emitting devices from a single polymer by mixing singlet and triplet emission.* Advanced Materials, 2006. **18**(13): p. 1769-+.
10. Thesen, M.W., et al., *Hole-Transporting Host-Polymer Series Consisting of Triphenylamine Basic Structures for Phosphorescent Polymer Light-Emitting Diodes.* Journal of Polymer Science Part a-Polymer Chemistry, 2010. **48**(15): p. 3417-3430.
11. Thesen, M.W., et al., *Investigation of Spacer Influences in Phosphorescent-Emitting Nonconjugated PLED Systems.* Journal of Polymer Science Part a-Polymer Chemistry, 2010. **48**(2): p. 389-402.
12. Hay, P.J., *Theoretical studies of the ground and excited electronic states in cyclometalated phenylpyridine Ir(III) complexes using density functional theory.* Journal of Physical Chemistry A, 2002. **106**(8): p. 1634-1641.
13. Torkelson, J.M., et al., *Fluorescence and Absorbance of Polystyrene in Dilute and Semidilute Solutions.* Macromolecules, 1983. **16**(2): p. 326-330.
14. Greenham, N.C., et al., *Measurement of Absolute Photoluminescence Quantum Efficiencies in Conjugated Polymers.* Chemical Physics Letters, 1995. **241**(1-2): p. 89-96.
15. Brunner, K., et al., *Carbazole compounds as host materials for triplet emitters in organic light-emitting diodes: Tuning the HOMO level without influencing the triplet energy in small molecules.* Journal of the American Chemical Society, 2004. **126**(19): p. 6035-6042.
16. Zhang, C., et al., *Blue Electroluminescent Diodes Utilizing Blends of Poly(p-phenylphenylene vinylene) in Poly(9-vinylcarbazoyl).* Synthetic Metals, 1994. **62**(1): p. 35-40.
17. Namdas, E.B., et al., *Photophysics of Fac-tris(2-phenylpyridine) iridium(III) cored electroluminescent dendrimers in solution and films.* Journal of Physical Chemistry B, 2004. **108**(5): p. 1570-1577.
18. Lo, S.C., et al., *Encapsulated cores: Host-free organic light-emitting diodes based on solution-processible electrophosphorescent dendrimers.* Advanced Materials, 2005. **17**(16): p. 1945-+.
19. Kawamura, Y., S. Yanagida, and S.R. Forrest, *Energy transfer in polymer electrophosphorescent light emitting devices with single and multiple doped luminescent layers.* Journal of Applied Physics, 2002. **92**(1): p. 87-93.
20. Rippen, G., G. Kaufmann, and W. Klopffer, *Luminescence of Poly(n-vinylcarbazole) Films at 77K. Fluorescence, Phosphorescence and Delayed Fluorescence.* Chemical Physics, 1980. **52**(1-2): p. 165-177.
21. Lo, S.C., et al., *High-Triplet-Energy Dendrons: Enhancing the Luminescence of Deep Blue Phosphorescent Iridium(III) Complexes.* Journal of the American Chemical Society, 2009. **131**(46): p. 16681-16688.
22. Suzuki, K., et al., *Reevaluation of absolute luminescence quantum yields of standard solutions using a spectrometer with an integrating sphere and a back-thinned CCD detector.* Physical Chemistry Chemical Physics, 2009. **11**(42): p. 9850-9860.

8. UV Enhanced Hybrid Photodiodes

8.1 Introduction

Chapters 5 to 7 have focused on light emitting materials and devices, however in this chapter I will focus on using organic semiconductors in devices for detecting light. A commonly used technology for light detection in the visible uses silicon p-n junctions. This has high sensitivity in the visible at relatively low cost while being directly compatible with silicon CMOS processing technologies. This has allowed a proliferation of low cost multi-pixel visible imaging technologies like CCDs which can be used in applications from taking pictures to compact multi-channel spectrometers.

Unfortunately, silicon detectors work best in the visible and near infra-red and do not have sensitivity in the ultraviolet (UV). These wavelengths are useful for applications in spectroscopy [1], astronomy [2] and nuclear physics [3]. Silicon's low UV response is due to its of the high refractive index and the strong absorption of silicon at these wavelengths. This means that much incident light is reflected and the rest absorbed in the first few nanometers away from the p-n junction, where electron and holes can be separated and converted into photocurrent. The refractive index and absorption coefficient of intrinsic silicon are shown in Figure 8.1 (taken from the publication by Green and Keevers [4]).

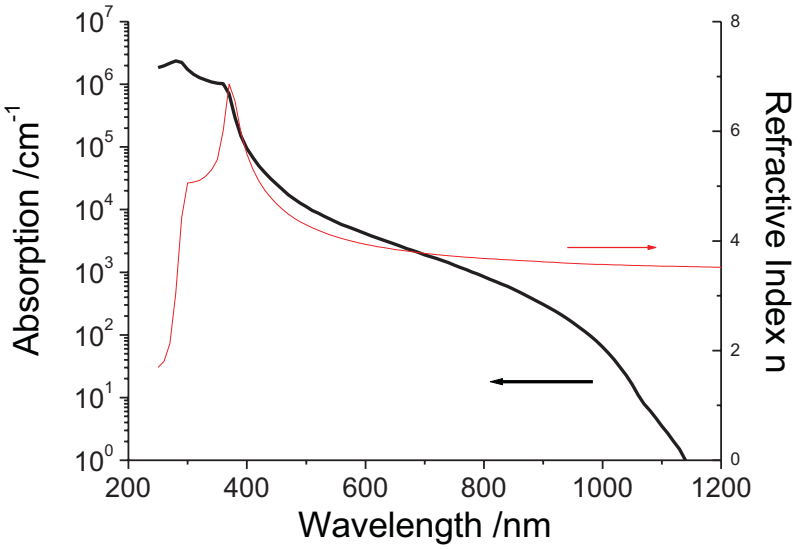

Figure 8.1 The absorption and refractive index of intrinsic silicon. Ref. [4].

Alternatives to silicon for 200-400 nm UV detection exist in the form of wider band gap semiconductor inorganic materials such as SiC and GaP [5]. These have been joined by evaporated organic UV detectors [6-8]. Unfortunately all these devices are difficult to make into multi-pixel imaging devices and the devices tend to have a rather narrow spectral sensitivity. In addition the inorganic devices can be significantly more expensive than their silicon counterparts.

As a result of these shortcomings silicon is often coated with a downconversion layer that absorbs the incident UV light and re-emits it at a longer wavelength where the silicon detector has sensitivity. Using a sufficiently thin layer, to avoid pixel cross-talk, this approach can be used in multi-pixel devices such as CCD spectrometers. In order to qualify as a successful enhancement layer a material must thus have strong absorption over a range of UV wavelengths, high photoluminescence quantum yield (PLQY), and a long emission wavelength, so that the sensitivity of the photodiode to the emission is maximised. In addition it would be desirable if this layer was transparent at visible wavelengths where silicon devices already have high sensitivity.

Many of these properties are fulfilled by organic semiconductors, and some of these materials also have the advantage that they can be solution processed allowing for low cost techniques for applying an enhancement layer [9]. This would result in creating a

"hybrid" device, which uses both organic and inorganic materials [10]. Organic enhancement layers that have been tried in the past, but have mostly been deposited by the relatively high cost method of thermal evaporation. Materials that have been reported included aluminum tris-8-hydroxyquinoline (Alq_3), N,N'-diphenyl-N,N'-bis-(3-methylphenl)-1,1'-biphenyl-4,4'-diamine, and bis-(8-hydroxyquinaldine)-chlorogallium (Gaq2'Cl) [11], lumogen and coronene [12-14]. Evaporated lumogen (which is commonly used in sensitising commercial CCDs) achieves 20-30% quantum efficiency across the UV, and coronene has achieved 30-40% efficiency. Though some patent literature has reported the idea of using the solution processable organic semiconducting polymer poly[2,7-(9,9-dioctylfluorene)] (PFO) [15] the responsivity of this device was still observed to fall by a factor of 100 from 500 nm to 250 nm indicating that this early effort was not very successful. Therefore I decided to see if it was possible to improve on these results.

In Section 8.2 I will discuss the experimental methods used in this chapter. In Section 8.3 I will discuss the absorption and luminescence properties of the enhancement layers used and their effect on the performance of photodiodes. Section 8.4 will focus on a simple model that can be used to explain the response of UV photodiodes given the optical and photophysical properties of the enhancement layer. Finally the conclusions are presented in Section 8.5.

8.2 Photodiode Fabrication and Testing

The photodiodes used for enhancement in this experiment were Silonex SLSD-71N5 photodiodes. These were chosen because they were not encapsulated and so the enhancement layer could be directly spin coated on top of the transparent silicon oxide layer on top of the devices. This layer was found to be 68 nm thick using a J.A. Woolam Co. Inc. M-2000DI spectrosoptic ellipsometer. It provided good wetting properties and did not interfere with light coupling into the device. The enhancement layers were spin coated from toluene or dicholoromethane solutions directly on top of the photodiodes for device performance and reflectivity measurements and onto quartz discs for absorption and photoluminescence measurements. Film thickness measurements were made using a Veeco DekTak 150 surface profilometer.

The devices were characterised using two chopped beams from a Varian Cary 300 spectrophotometer which alternated at 30 Hz. This arrangement is shown in Figure 8.2. Initially a photodiode of known responsivity was placed in each arm of the instrument and these were connected to a pair of Stanford Research Systems (USA) SR830 DSP lock-in amplifiers. The lock-ins were triggered by the photodiode in the reference channel (a Newport 818-UV photodetector), using an Agilent 54624A oscilloscope to produce a trigger pulse so that both lock-in amplifiers were synchronised to the reference channel of the Cary 300's chopper wheel. By using this synchronous technique I was able to measure small signals and thus use a low power source, and remove any background from stray light. The amplitude of the current at zero bias was recorded for the photodiodes in both channels. The Newport 818-UV photodiode was checked against a photodiode which had been calibrated by the National Physical Laboratory in order to check the correct amplitude and spectral response of the setup before the sample devices were tested.

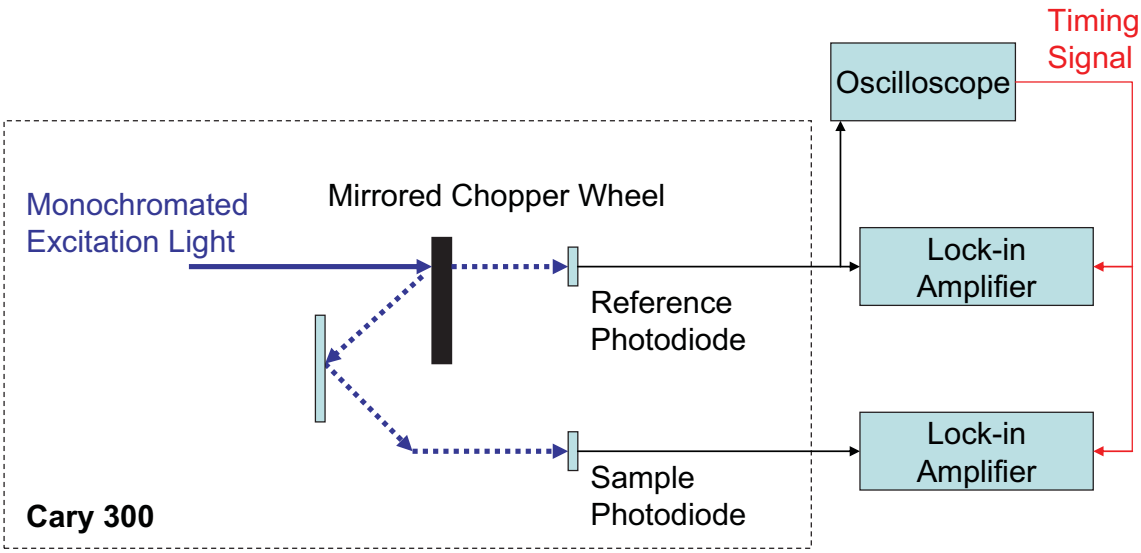

Figure 8.2 The experimental setup for measuring the spectral responsively of the photodiodes.

The reflectivity of the photodiodes was measured using the Varian Cary 300's absolute reflectivity attachment which measures the reflectivity of a sample to light incident on it at an angle of 7 degrees to the normal.

8.3 Results

8.3.1 Poly(fluorene) Enhancement Layer

The chemical structure of poly[2,7-(9,9-dioctylfluorene)] (PFO) [16-18] is shown in Figure 8.3. This material is a commonly used blue light emitting polymer with a good photoluminescence quantum yield of around 50% in thin films [18]. Therefore, PFO seemed a suitable candidate for a solution processable enhancement layer. The PFO used in these measurements was ADS129BE purchased from American Dye Source. In all cases below the PFO films were spin coated from toluene solutions at a concentration of 10 mg/ml at 2000 rpm. The absorption and emission spectra of the material is shown in Figure 8.4. The quantum efficiency of devices enhanced using a 53 nm film PFO is shown in Figure 8.5.

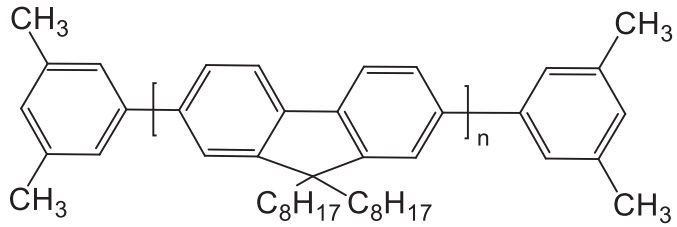

Figure 8.3 Molecular Structure of poly[2,7-(9,9-dioctylfluorene)](PFO).

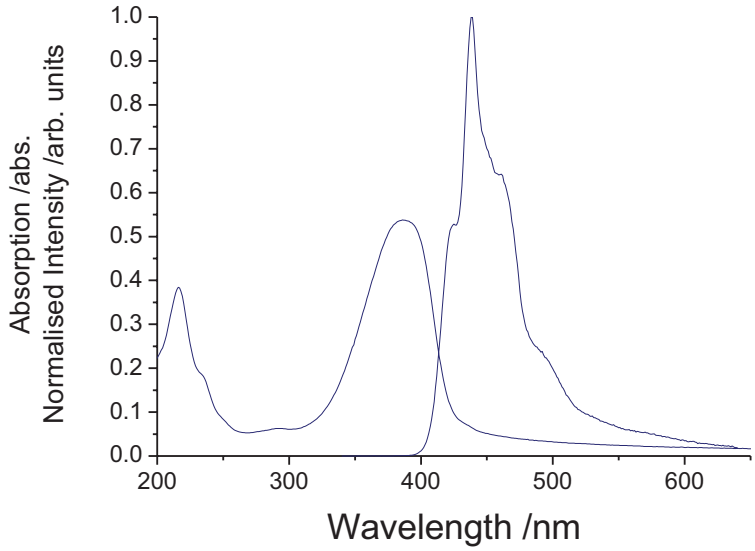

Figure 8.4 Absorption and emission spectra of a 53 nm thick film of PFO. The emission spectrum was excited at 325 nm.

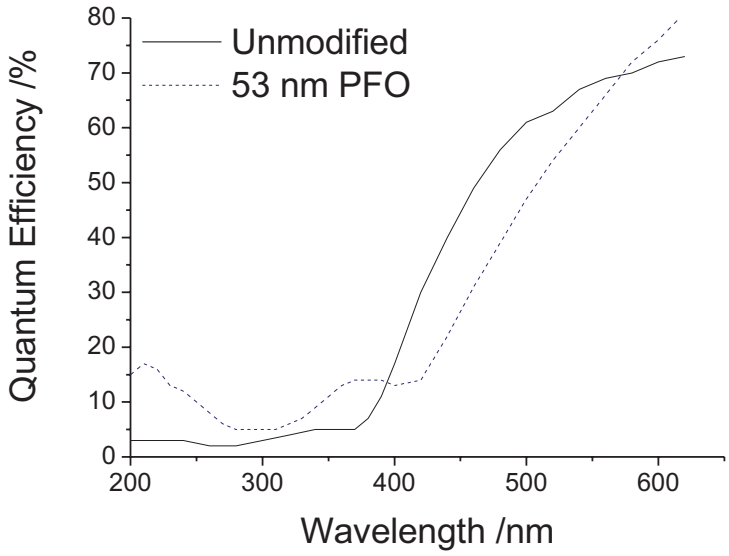

Figure 8.5 The quantum efficiency of an unmodified photodiode and a photodiode enhanced with a 53 nm layer of PFO.

Figure 8.5 shows that the performance of the photodiode has been enhanced from 200-390 nm by applying the PFO layer. This leads to a performance of up to 17% at 210 nm for the enhanced photodiode compared to 3% for the unmodified device, an improvement of >5 times. There is another peak in the quantum efficiency of the PFO device of 14% at 370 nm which compares favourably to 5% for the unenhanced photodiode. These peaks in the enhancement correspond to the peaks in PFO's absorption spectrum (Figure 8.4), which shows that for a film of 53 nm thickness the amount of luminescence is limited by the amount of light being absorbed at other wavelengths. Notably, there is a gap in both the absorption and enhancement in the range of 250-350 nm. The maximum UV quantum efficiency of 17% is also quite modest and this results from both the fact that the peak of the PFO emission spectrum is at 439 nm, which is not at the peak quantum efficiency of the unmodified photodiode and that only 50% of the collected photons can be re-emitted to be collected by the photodiode because that is the PLQY value.

At longer wavelengths of 400-560 nm the unmodified photodiode outperforms the PFO coated photodiode while the enhanced photodiode has higher responsivity at >560 nm. This is due to the fact a wavelength scale dielectric film has been added to the top of the photodiode. This changes the anti-reflection properties of the silicon

oxide layer on top of the device and shifts them to longer wavelengths. A 68 nm thickness of silica would be expected to enhance absorption at ~400 nm and so these photodiodes have been designed to have increased blue response by using this layer to increase absorption at these wavelengths. By adding the PFO layer and increasing this dielectric layer thickness this anti-reflection peak has been shifted towards the red, so the enhanced device outperforms the unmodified device in the yellow/red part of the spectrum.

8.3.2 $(F8)_9BT$ Co-polymer Enhancement Layer

In order to improve on the performance of the PFO device it was necessary to shift the emission wavelength to longer wavelengths, to use the region where the photodiodes are most sensitive, and to increase the material's PLQY value. Fortunately a poly(fluorene) based co-polymer which uses 90% (9,9-dioctylfluorenyl-2,7-diyl) and 10% (1,4-benzo-{2,1',3}-thiadiazole) units ($(F8)_9BT$) was available which addresses both of these issues. This material was purchased from American Dye Source with the name ADS233YE. The addition of the (1,4-benzo-{2,1',3}-thiadiazole) units creates units of the polymer that behave like the green emitting polymer F8BT [19]. Both these polymers are shown in Figure 8.6. Energy is transferred by Förster energy transfer from the blue emitting PFO like units to these longer wavelength emitting units and so the emission of the polymer is entirely yellow. This is shown in Figure 8.7, were the emission peaks at 552 nm in a 26 nm thick film. Films of $(F8)_9BT$ were spin coated from a 10 mg/ml concentration toluene solutions spin coated at 2000 rpm. In addition to this longer wavelength emission the co-polymer also has an excellent PLQY value of 80% [10] which has made it very useful in the fields of organic lasers [10] and amplifiers [20].

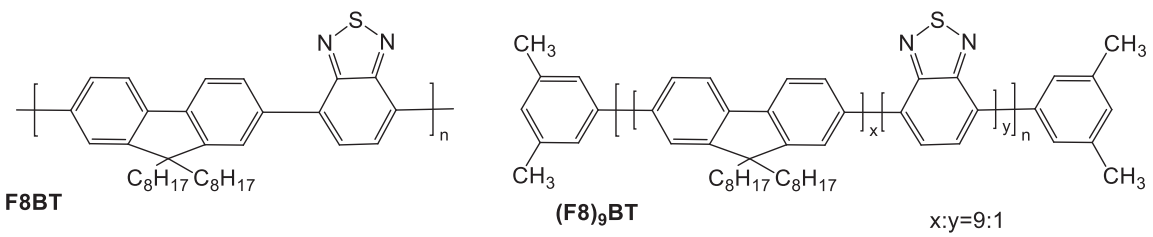

Figure 8.6 The material structures of polymers F8BT and $(F8)_9BT$.

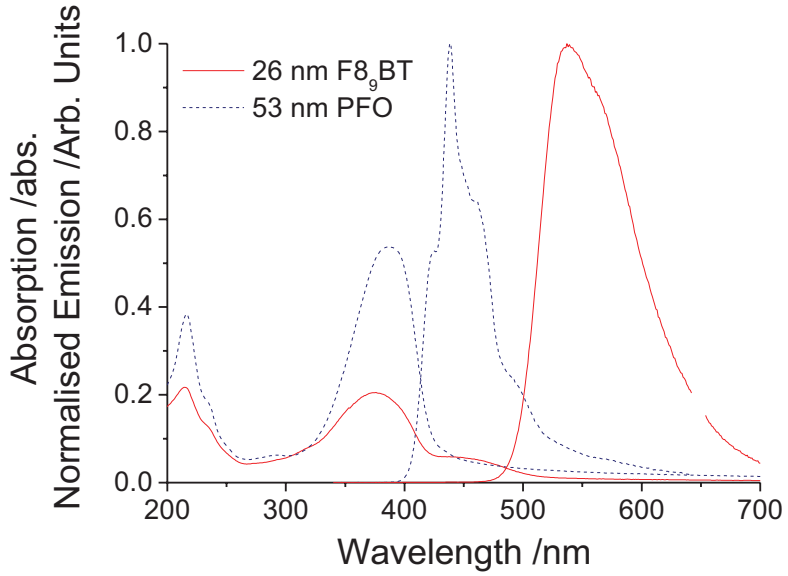

Figure 8.7 The absorption and emission spectra of a 26 nm thick film of $(F8)_9BT$. The emission spectra were excited at 325 nm.

As can be seen from Figure 8.7 the absorption spectra of $(F8)_9BT$ and PFO are rather similar with peaks at 216 nm and at ~380 nm. This is expected as the majority of the co-polymer is PFO units. There is some additional absorption at ~460 nm that corresponds to the added 1,4-benzo-{2,1',3}-thiadiazole units and the resulting lower energy absorption and emission. The emission peak of the $(F8)_9BT$ is at 537 nm which is significantly longer than 439 nm peak in the PFO emission. The photodiode should have a higher internal quantum efficiency at these longer wavelengths and so the responsivity should be increased.

The quantum efficiency of $(F8)_9BT$ enhanced photodiodes in shown in Figure 8.8. Despite using a thinner 26 nm film than the 53 nm film that was used for PFO the enhancement in the UV quantum efficiency is higher. It peaks at 36% at 200 nm and 31% at 370 nm which is greater than twice the performance of the PFO enhanced device (quantum efficiency 15% and 14% respectively). Although the combination of higher PLQY and longer wavelength emission have improved the quantum efficiency the PFO device's dip in performance at 250-300 nm remains as the $(F8)_9BT$ also does not absorb strongly in this region.

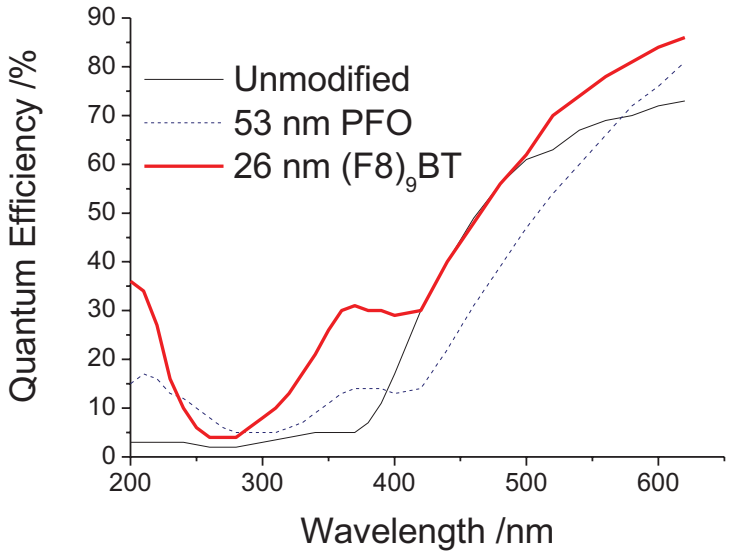

Figure 8.8 The quantum efficiency of a photodiode enhanced with a 26 nm layer of $(F8)_9BT$. The PFO enhanced and unmodified photodiodes are shown for comparison.

8.3.3 $(F8)_9BT$ CBP Blend Enhancement Layer

In order to enhance the absorption of the $(F8)_9BT$ in the 250-300 nm region and thus give a more even spectral response, 20wt% of the co-polymer was blended with 4,4'-N,N'-dicarbazolyl-biphenyl (CBP). This is a high energy host material that was used for making OLEDs in Chapters 6 and 7, and has good UV absorption. It was hoped that energy would be absorbed by the CBP and would then transfer via a Förster process to the longer wavelength emitting $(F8)_9BT$ and thus achieve a large Stokes shift between absorption wavelength and emission wavelength. The absorption and emission spectra of a 46 nm thick film of the blend is shown in Figure 8.9. The blended films were prepared by spin casting from dichloromethane solutions. The 46 nm film shown in Figure 8.9 was spin coated from a solution with 10 mg/ml concentration at 3,000 rpm.

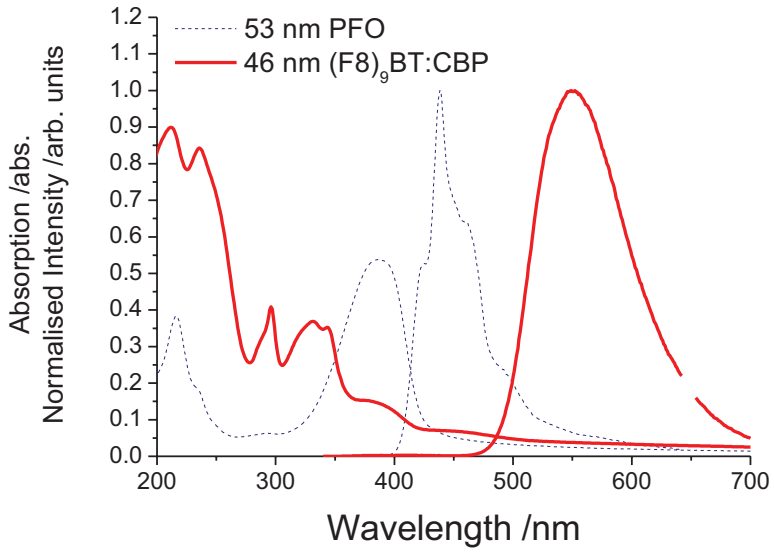

Figure 8.9 The absorption and emission spectra of a blended film of 20 wt% of $(F8)_9BT$ in CBP. PFO film absorption and emission spectra are shown for comparison. Emission spectra were excited at 325 nm.

The emission of the CBP blended $(F8)_9BT$ shows no blue emission from either the CBP or the PFO units and instead gives a single peak at 552 nm which is slightly red-shifted from the neat $(F8)_9BT$'s peak at 537 nm. However, otherwise the emission spectrum is similar. The absorption spectrum is significantly different from the PFO and neat $(F8)_9BT$ and the absorption has been increased at all wavelengths below 350 nm. Both these results show the CBP is performing its function of enhancing UV absorption and allowing energy transfer to the yellow emitting $(F8)_9BT$ co-polymer. In addition to these measurements film PLQYs for the CBP blend were measured to be 84±10% using the Greenham method [21]. This is comparable to 80% value reported for neat films of $(F8)_9BT$ [10].

This blend was used to enhance photodiodes in three different layer thicknesses: 63 nm, 100 nm and 153 nm spin coated from DCM solutions at 3,000 rpm from 10 mg/ml, 1,200 rpm from 10 mg/ml and 1,200 rpm from 20 mg/ml respectively. The results are shown in Figure 8.10. These devices show good quantum efficiencies of 55%, 60% and 61% respectively at 200 nm. The 100 nm device achieves 34-60% quantum efficiency over the entire 200-620 nm range measured and the 153 nm device gives >49% quantum efficiency at all wavelengths less than 360 nm. This

compares favourably to commercial silicon CCDs using evaporated lumogen which can achieve 20-30% quantum efficiency in the UV [14, 22]. These results show that the dip at 250-300 nm in performance due to poor absorption of the PFO and $(F8)_9BT$ has been eliminated by using the blended enhancement layer.

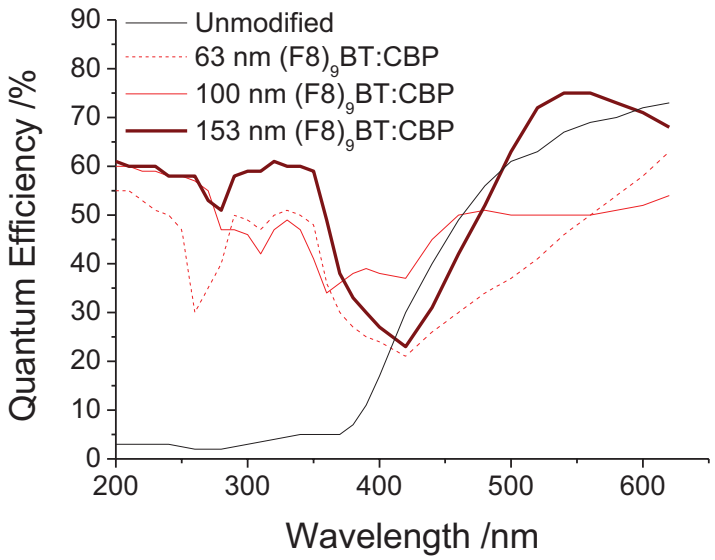

Figure 8.10 The quantum efficiencies of photodiodes enhanced with various thicknesses of 20 wt% blends of co-polymer $(F8)_9BT$ in a CBP host. An unmodified photodiode is shown for comparison.

As commericial devices are often assessed using responsitivity of the detector in terms of Amps of photocurrent produced per Watt of incident power Figure 8.10 has been re-plotted in terms of responsivity in Figure 8.11 below.

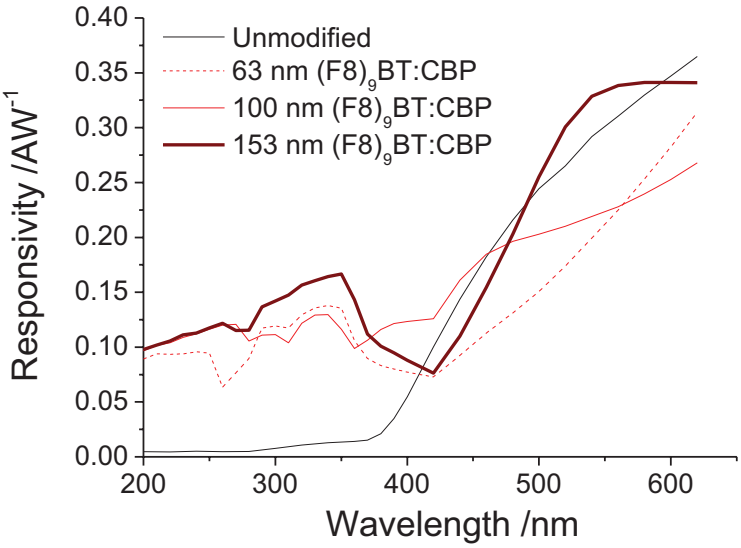

Figure 8.11 The A/W responsivities of the photodiodes enhanced with various thicknesses of 20 wt% blends of co-polymer (F8)$_9$BT in a CBP host together with an unmodified photodiode for comparison.

8.4 Modelling

As has been discussed above there are several factors affecting the quantum efficiency of an enhanced photodiode at a given wavelength. These include the absorption of the enhancement layer, the quantum efficiency of that layer and the internal quantum efficiency of the silicon photodiode for the emitted light. We can think about this problem more rigorously by considering what happens to an individual photon of wavelength λ as it is incident on the device. The resulting processes are shown in Figure 8.12. Incident light is either transmitted $T(\lambda)$ (1), absorbed $A(\lambda)$ (2) or reflected $R(\lambda)$ (3). The light that is absorbed is re-emitted with an efficiency given by the PLQY Φ_{PL} (4). This light is then either captured by the photodiode β or escapes from the device $(1-\beta)$ (5). Transmitted light or fluorescence from the enhancement layer is then converted into a photocurrent using the devices internal quantum efficiency (6). For the transmitted light this is simply the internal quantum efficiency at the wavelength of the incident light $G(\lambda)$ but for the captured fluorescence this is a weighted average of the internal quantum efficiency across the fluorescence spectrum of the enhancement layer Q.

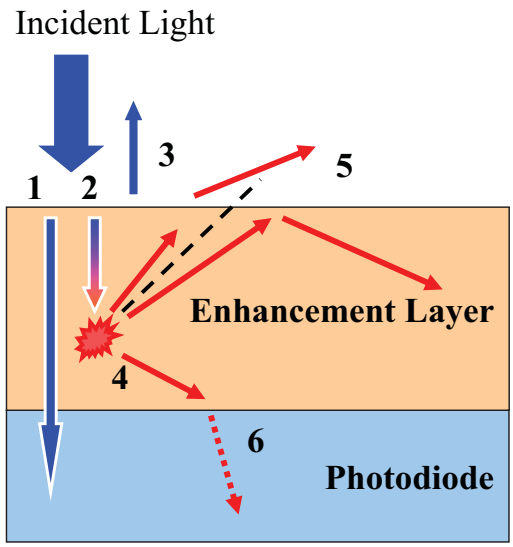

Figure 8.12 The processes for a photon incident on the enhancement layer in the model for the enhanced photodiodes: 1. transmission, 2. absorption, 3. reflection, 4. re-emission, 5. escape from the device and 6. conversion to photocurrent at the internal quantum efficiency of the photodiode. The white dashed line shows the critical angle above which photons are totally internally reflected and captured by the photodiode.

The reflectivity $R(\lambda)$ of the devices can be directly measured, as can the absorbance $\alpha(\lambda)$ of a film of the enhancement layer on a silica substrate. These can both be used to calculate the fraction of incident light that is absorbed $A(\lambda)$ and transmitted $T(\lambda)$ using Equations 8.1 and 8.2 below.

$$A(\lambda) = (1 - R(\lambda))(1 - 10^{-\alpha(\lambda)}) \quad [8.1]$$

$$T(\lambda) = (1 - R(\lambda))10^{-\alpha(\lambda)} \quad [8.2]$$

The fraction of light coupled into the photodiode β can be calculated following a method similar to that for the light extraction efficiency of OLEDs discussed in Chapter 3. As in the OLED case any light emitted in an upward direction can escape from the device provided it is not emitted at an angle greater than the critical angle for total internal reflection. Any light emitted above this angle is captured by the strongly absorbing silicon photodiode. Unlike the OLED case there is no reflective layer so light emitted downwards is all captured directly. Assuming iso-tropic emission and

performing an integral over all solid angles the fraction of light captured is given by Equation 8.3. The refractive index of the CBP used in the enhanced photodiodes has a refractive index of 1.75 at the wavelengths of the fluorescence, as determined from previous elipsometry work [23]. Thus the fraction of captured light is estimated to be 91%.

$$\beta = \frac{1}{2}\left(1 + \sqrt{1 - \frac{1}{n^2}}\right) \qquad [8.3]$$

The internal quantum efficiency of the photodiode $G(\lambda)$ can be calculated by dividing the external quantum efficiency $E_{Bare}(\lambda)$ of the unmodified photodiode by the fraction of incident light at a given wavelength that is absorbed $(1 - R_{Bare}(\lambda))$.

Using this value the effective internal quantum efficiency of the photodiode to the fluorescence of the enhancement layer Q can be calculated using the fluorescence emission spectrum $L(\lambda)$ as shown in Equation 8.4.

$$Q = \frac{\int G(\lambda)L(\lambda)d\lambda}{\int L(\lambda)d\lambda} \qquad [8.4]$$

Using all these contributions together the external quantum efficiency of the enhanced photodiodes $E(\lambda)$ can be calculated using Equation 8.5.

$$E(\lambda) = A(\lambda)\Phi_{PL}\beta Q + T(\lambda)G(\lambda) \qquad [8.5]$$

Overall this method is similar to that used by Garbozov [11] however unlike their reported method, this one does not split the spectrum into two parts based on the point at which the internal quantum efficiency becomes negligible and takes transmitted light into account across the entire spectrum.

The reflectivity spectra of the $(F8)_9BT$:CBP blend enhanced photodiodes are shown in Figure 8.13. There is a minimum in the reflectivity of the unmodified photodiode at 475 nm which can be attributed to the anti-reflection quarter wavelength peak resulting from the 68 nm silicon oxide layer. For the enhanced photodiodes in the >400 nm region, where the films are mostly transparent, the different layer thicknesses show significant differences in reflectivity due to the thin film effects of the dielectric. Increasing layer thickness shifts the 475 nm anti-reflection of the unmodified photodiode to a longer wavelength of 557 nm in the 63 nm film. In the thicker films the λ/4 peak is shifted outside of the wavelength range of the measurement. The high reflectivity at 420 nm of the 153 nm and 63 nm thick films explain the dip in the quantum efficiency of those devices at that wavelength (Figure 8.10). In addition the relatively flat response of the 100 nm film is explained by the fact that the film reflectivity maximum around 610 nm, where the internal quantum efficiency of the silicon photodiode is highest, thus offsetting this peak in the devices performance.

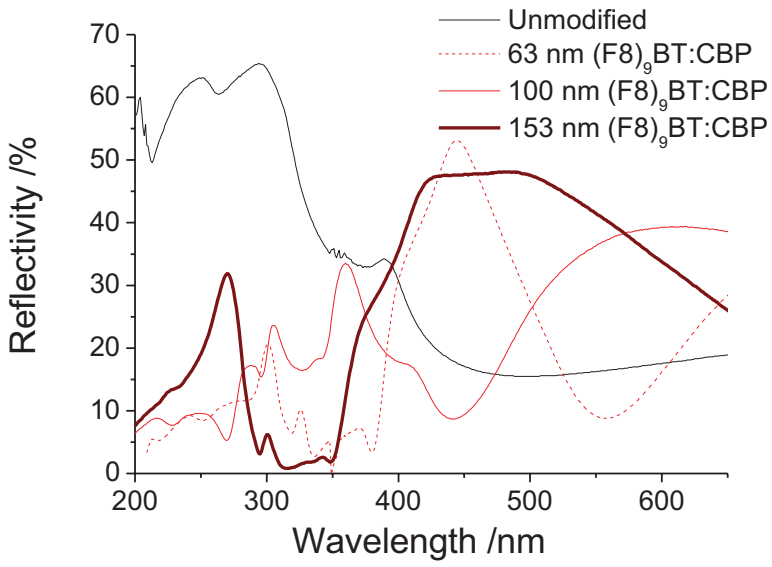

Figure 8.13 Reflectivity spectra of the 20 wt% $(F8)_9BT$ in CBP blend devices.

Using the reflectivity of the unmodified photodiode and its external quantum efficiency the internal quantum efficiency was calculated and it is shown in Figure 8.14 below. These results show that the internal quantum efficiency is flat below 360 nm at a value of approximately 6%. Some of this may be the result of a systematic

error if the monochromator was letting through some light of longer wavelengths. The internal quantum efficiency at the emission peak of PFO (440 nm) is 49% and this increases to 80% at 550 nm where the $(F8)_9BT$'s emission peaks. This shows that there has been a significant improvement in the responsivity of the photodiodes by red-shifting the emission of the enhancement layer.

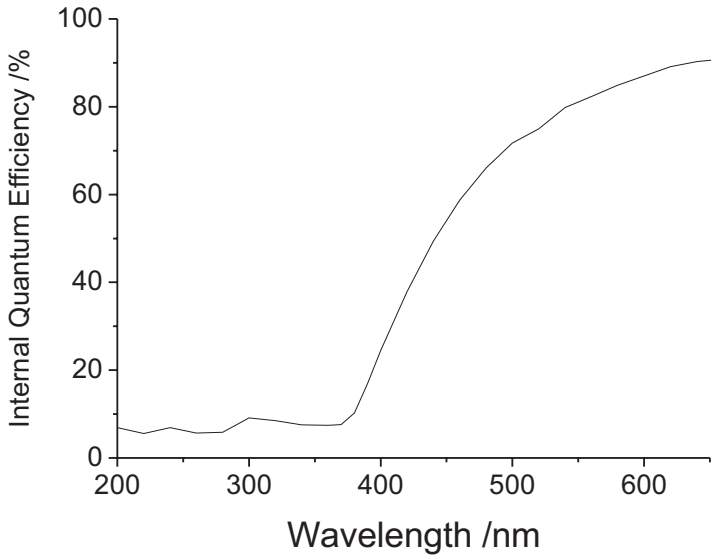

Figure 8.14 The calculated internal quantum efficiency of the photodiodes.

Using the reflectivity spectra, internal quantum efficiency, absorption and fluorescence properties of the enhancement layers the expected enhancement factors of these films were calculated using Equation 8.5. These results are compared to the experimental measurements below in Figure 8.15. Wavelengths of 200-250 nm the experimental and theoretical results are in close agreement however in the range of 250-350 nm the model appears to systematically underestimate the experimental quantum efficiency. This may be because the absorption is measured using transmission through thin films and in the actual device reflections at the top of the silicon may allow some of the incident light to be reflected giving another opportunity for absorption. According to the model at 320 nm the fraction of incident light absorbed by the 63 nm film is 62% compared to 37% which is transmitted. Therefore an increase of approximately 60% of the model value could occur due to reflections from the silicon. The model predicts 42% for the quantum efficiency and the

experimental value is 50%, a 20% increase. For the thicker 100 nm film 65% is absorbed and 18% is transmitted according to the model, so the quantum efficiency could be increased by up to 28%. Here the model predicts 43% and the experiment gives 47%, a smaller increase of 10%. Finally for the thickest 153 nm film we expect 85% of the light to be absorbed from the model and 9% transmitted allowing a maximum increase in quantum efficiency of 10%. The model predicts 54% and the actual value is 61% and increase of 12%. From these values it seems plausible that much of this discrepancy is caused by failing to account for UV light being reflected from the silicon back into the enhancement layer.

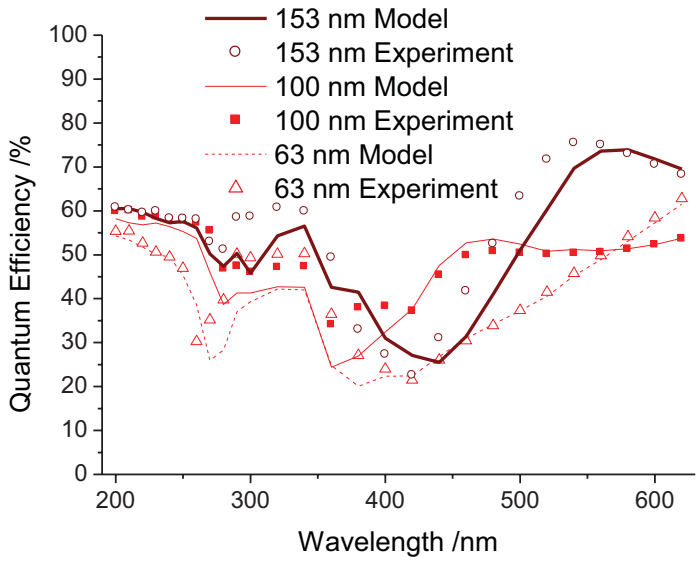

Figure 8.15 The experimental and expected quantum efficiencies of the $(F8)_9BT$:CBP blend enhanced photodiodes. These use the measured value of 84% for the PLQY of the enhancement layer.

Above 400 nm, in the region where the films are transparent, the peaks and dips corresponding to the anti- and pro- reflection points appear to be shifted to longer wavelengths in the model than is experimentally observed. This is likely to be due to the fact the reflectivity is measured at an angle of 7 degrees and not at normal incidence thus a red-shifting of these peaks is expected due to the increased path length in the dielectric.

A better calculation would measure or model reflectivity of the photodiodes at normal incidence and possibly include a more reliable estimate of the amount of light absorbed taking reflections at the silicon interface into account. Despite these issues the model does a reasonable job of fitting the data. This shows that the simple estimate of the coupling efficiency based on the refractive index of the enhancement layer and the escape cone model of light out coupling, has generated results which are consistent with experiment.

8.5 Conclusions

In this Chapter I have discussed the creation of hybrid organic-inorganic photodetectors that use a highly emissive layer to down convert incident UV light to wavelengths that can be detected by low cost silicon photodiodes. By making use of energy transfer, I have used a high energy host and a longer wavelength emitting guest. This gives good, even, UV absorption and long wavelength emission. This ~550 nm emission make use of the region where the silicon photodiodes have good internal quantum efficiency. This has enabled the fabrication of devices with up to 61% quantum efficiency at 200 nm wavelength or 60-34% quantum efficiency over the 200-620 nm wavelength range.

These results show that solution processed organic semiconductors can be used to produce devices, that can match or beat the performance of lumogen based commercial UV enhanced silicon CCDs. I have also shown that these performances can be achieved using ~100 nm thick films that will be thin enough for multi-pixel applications. By using solution processing, these devices will be easier to manufacture than their thermally evaporated counterparts. In addition I have shown that the performance of these devices can be estimated using a simple model using an escape cone model for the fraction of light captured from the enhancement layer and coupled into the silicon photodiode.

The blends of organic materials can easily be optimised both in terms of composition and layer thickness to give absorption and thin film interference that are most suitable for the wavelength range required for a given application. The current results and this

flexibility mean that this work has applications in making higher sensitivity and lower cost UV enhanced CCDs than are currently used commercially.

1. Jones, D.G., *Photodiode Array Detectors in UV-Vis Spectroscopy. Part 1.* Analytical Chemistry, 1985. **57**(9): p. 1057-&.
2. Joseph, C.L., *Advances in astronomical UV image sensors and associated technologies*, in *Photodetectors: Materials and Devices Ii*, G.J. Brown and M. Razeghi, Editors. 1997. p. 244-258.
3. Soukhanovskii, V.A., et al., *Compact collimated vacuum ultraviolet diagnostics for localized impurity measurements in fusion boundary plasmas.* Review of Scientific Instruments, 2001. **72**(8): p. 3270-3276.
4. Green, M.A. and M.J. Keevers, *Optical-Properties of Intrinsic Silicon at 300 K.* Progress in Photovoltaics, 1995. **3**(3): p. 189-192.
5. Monroy, E., F. Omnes, and F. Calle, *Wide-bandgap semiconductor ultraviolet photodetectors.* Semiconductor Science and Technology, 2003. **18**(4): p. R33-R51.
6. Su, Z.S., et al., *High response organic ultraviolet photodetector based on blend of 4,4 ', 4 "-tri-(2-methylphenyl phenylamino) triphenylaine and tris-(8-hydroxyquinoline) gallium.* Applied Physics Letters, 2008. **93**(10).
7. Lin, H.W., et al., *Highly efficient visible-blind organic ultraviolet photodetectors.* Advanced Materials, 2005. **17**(20): p. 2489-+.
8. Ray, D. and K.L. Narasimhan, *High response organic visible-blind ultraviolet detector.* Applied Physics Letters, 2007. **91**(9).
9. Forrest, S.R., *The path to ubiquitous and low-cost organic electronic appliances on plastic.* Nature, 2004. **428**: p. 911.
10. Yang, Y., G.A. Turnbull, and I.D.W. Samuel, *Hybrid optoelectronics: A polymer laser pumped by a nitride light-emitting diode.* Applied Physics Letters, 2008. **92**(16): p. 163306.
11. Garbuzov, D.Z., et al., *Organic films deposited on Si p-n junctions: Accurate measurements of fluorescence internal efficiency, and application to luminescent antireflection coatings.* Journal of Applied Physics, 1996. **80**(8): p. 4644-4648.
12. Blouke, M.M., et al., *Ultraviolet Downconverting Phosphor for Use With Silicon CCD Imagers.* Applied Optics, 1980. **19**(19): p. 3318-3321.
13. Kristianpoller, N. and D. Dutton, *Optical Properties of "Liumogen": A Phosphor for Wavelength Conversion.* Applied Optics, 1964. **3**(2): p. 287.
14. Cowens, M.W., et al., *Coronene and Liumogen as VUV Sensitive Coatings for Si CCD Imagers - A Comparison.* Applied Optics, 1980. **19**(22): p. 3727-3728.
15. Vardeny, Z.V., S.A. Jeglinski, and P.A. Lane, *Enhanced Radiation Detectors Using Luminescent Materials.* United States Department of Energy, 2001(US Patent Application 6211524 B1).
16. Ranger, M., D. Rondeau, and M. Leclerc, *New well-defined poly(2,7-fluorene) derivatives: Photoluminescence and base doping.* Macromolecules, 1997. **30**(25): p. 7686-7691.
17. Bradley, D.D.C., et al., *Influence of aggregation on the optical properties of a polyfluorene*, in *Optical Probes of Conjugated Polymers*, Z.V. Vardeny and L.J. Rothberg, Editors. 1997. p. 254-259.
18. Redecker, M., et al., *Nondispersive hole transport in an electroluminescent polyfluorene.* Applied Physics Letters, 1998. **73**(11): p. 1565-1567.

19. Stevens, M.A., et al., *Exciton dissociation mechanisms in the polymeric semiconductors poly(9,9-dioctylfluorene) and poly(9, 9-dioctylfluorene-co-benzothiadiazole).* Physical Review B, 2001. **63**(16).
20. Amarasinghe, D., et al., *High-Gain Broadband Solid-State Optical Amplifier using a Semiconducting Copolymer.* Advanced Materials, 2009. **21**(1): p. 107-110.
21. Greenham, N.C., et al., *Measurement of Absolute Photoluminescence Quantum Efficiencies in Conjugated Polymers.* Chemical Physics Letters, 1995. **241**(1-2): p. 89-96.
22. Garnir, H.P. and P.H. Lefebvre, *Quantum efficiency of back-illuminated CCD detectors in the VUV region (30-200 nm).* Nuclear Instruments & Methods in Physics Research Section B-Beam Interactions with Materials and Atoms, 2005. **235**: p. 530-534.
23. Liu, Z.T., et al., *The characterization of the optical functions of BCP and CBP thin films by spectroscopic ellipsometry.* Synthetic Metals, 2005. **150**(2): p. 159-163.

9. Conclusion

One of the many useful applications of semiconductor materials is optoelectronics, the science of inter-converting light and electricity. Examples of these devices include LEDs, solar cells, CCD cameras and compact solid state lasers. This thesis has focused on the photophysics and applications of light emitting organic semiconductors, with a particular emphasis on light emitting diodes.

Organic semiconductors are made from conjugated carbon based systems and through organic chemistry many possible molecular structures can be synthesised and investigated. This allows the materials properties to be easily tuned for specific applications. One important issue with organic semiconductors is that they can suffer from concentration quenching of their luminescence, and this can be a particular problem in the solid state. This can reduce the efficiency of light emitting devices and so it is important to control it. In this thesis I have investigated materials which use a number of different strategies for controlling concentration quenching: in Chapter 5 by twisting molecules to prevent π stacking, in Chapter 6 by using bulky dendrons to sterically protect emissive cores [1] and in Chapter 7 by using high energy spacer units to prevent aggregation along a polymer chain. Another strategy is host-guest blending which separates the chromophores in a higher energy host which can be optimised for charge transport. This approach is used to augment the dendrimer materials in Chapters 6 and 7 and is also used in Chapter 8 to increase the coverage of the absorption spectrum of the enhancement layers.

In addition organic materials can be made soluble and are generally amorphous which makes low cost solution processing of devices on rigid or flexible substrates [2]. The ability to deposit devices on large areas at low cost makes these materials suitable for large area solar cells and low glare lighting installations. If the solution properties of these materials can be sufficiently controlled they can be deposited via ink-jet printing allowing the printing of transistors for processing [3] or light emitting diodes for displays [4]. Chapters 6 and 7 covered the development of high efficiency emissive layers for ink-jet printable OLEDs by polymerising successful dendrimer materials so that higher viscosity solutions, suitable for printing, could be achieved. Taking

advantage of the ease of deposition via solution processing is also part of the theme of Chapter 8, where I have shown how an efficient UV enhancement layer can be spin coated onto silicon photodiodes.

In Chapter 5 I showed how a planar molecule (triphenylene) could be prone to π-stacking, leading to red-shifted emission in the solid state and multiple emissive lifetimes in the time-resolved luminescence. By adding extra methyl groups the hexamethyltriphenylene (HMTP) molecule was twisted out of one plane due to steric crowding [5]. This prevented both the concentration dependent red-shifting of the emission spectrum in solution and made sure there was only one emissive state. I also showed how the strength of the optical transitions of molecules can be affected by changing their shape. Triphenylene has a symmetry that makes the S0 to S1 transition rather weak [6-8] and by changing the shape of the molecule this increased both the absorption and emission dipole moments from 0.7 D to 3.6 D and 0.5 D to 2.1 D respectively. This resulted in a ~20 times increase in the radiative de-excitation rate, and taken with the reduced aggregation effects this meant that HMTP became a moderately efficient emitter in the solid state with a photoluminescence quantum yield (PLQY) of 31%.

Futher work in this area would investigate the reasons why HMTP has higher film PLQY (31%) than solution (5%) and the possible existence of dark conformers related to the interconversion of the molecules between different conformers. This might be best investigated by freezing out these interconversions and performing photophysical measurements of absolute quantum yield and time resolved luminescence at low temperature. These measurements are challenging because many solvents can freeze and become scattering at low temperatures. Methyl THF was considered as a candidate for these measurements it forms a transparent glass however it or dissolved impurities were found to react chemically with the HMTP. A further problem with these measurement is a relative method of PLQY measurement cannot be used if there is significant thermal expansion or contraction of the solvent.

Chapters 6 & 7 focused on Iridium based phosphorescent materials for OLEDs. Phosphorescent materials are necessary for achieving the highest efficiencies in

electroluminescence because they can emit from triplet excited states, a large number of which are formed under electrical excitation. In contrast organic materials they do not include heavy metal atoms are fluorescent and cannot harvest these triplet states [9].

Unlike dendrimers, which have previously be used to produce successful solution processable phosphorescent OLEDs with up to 16% external quantum efficiency [10], in this case the materials investigated were phosphorescent polymers. The aim of this work was to increase the viscosity of solution so that phosphorescent devices might be fabricated with ink-jet printing. Many previous attempts used phosphorescent polymers with conjugated backbones, however these sometimes accepted back transfer of the triplet states which then became trapped on the fluorescent backbone and were thus lost [11]. In this work a non-conjugated backbone was used to prevent quenching via back transfer of triplets. The pendant iridium complexes made use of dendrons to reduce intermolecular interactions. By using double dendrons structures with two dendrons per ligand interactions were further reduced. For the homopolymers investigated in Chapter 6, this allowed the production of OLEDs with 9.3% external quantum efficiency. With host guest blending using CBP as a charge transport host the efficiency was increased to 12.1%.

One issue with phosphorescent homopolymers with pedant iridium complexes is that the emissive cores are not sufficiently separated along the chain of the polymer to prevent intra chain concentration quenching. This results in some quenching of the luminescence of the polymers even in dilute solutions. This can be detected from both a reduction in the PLQY values and from non-exponential time-resolved luminescence characteristics indicating there is more than one emissive state. While the monomer's of the more emissive 2-phenylpydridyl (ppy)/phenyltriazolyl (ptz) based materials achieved >90% PLQY in solution these interactions limited the solution PLQY of the homopolymers discussed in Chapter 6 to 61-67%.

In Chapter 7 I investigated the use of co-polymers with high energy gap spacer units to reduce interchormophore interactions along the polymer chain. By using high energy poly(styrene) spacer groups the solution PLQY was increased to 94% and mono-exponential luminescence decay was achieved indicating that intra-molecular

interactions had been eliminated in solution. When blended with the charge transport host CBP this allowed 6.7% EQE OLEDs to be produced. However, the high energy of the poly(styrene) spacer units meant they would not contribute to charge transport and this is undesirable in a material intended for use in OLEDs.

Materials with charge transporting, poly(9-vinylcarbazole) (PVK), spacer units were investigated next with the aim of retaining the desirable photophysics of the poly(styrene) co-polymer while improving charge transport. Although these materials did show only one emissive state in time resolved luminescence the PLQY values were reduced to 64-69% compared to >90% for the emissive monomers. This may have been due to back transfer of triplet excitons from the iridium complexes onto the PVK spacer units. Nevertheless these co-polymers resulted in efficient neat devices with 10-11 % EQE. The best device achieved 14.7% EQE on blending with CBP, which is higher than previous reports for a phosphorescent polymer of 11.8% EQE [12].

Photophysical investigation could determine of the solid state PLQY of these materials was indeed being reduced by back transfer to the PVK units and offer a route to still more efficient materials for devices. Futher optimisation of the OLEDs to achiever lower drive voltages and higher power efficiencies would be desirable. This would involve adjusting layer thicknesses, considering alternative charge transport hosts and possibly improving hole injection by using a PEDOT:PSS layer on the anode. Ideally the charge balance would be optimised by adjusting the transport groups in the co-polymer structure or by adding charge transport dendrons [13]. Optimising the OLED structure would be easier if the carrier transport of the polymers and co-polymers was characterised, perhaps by the time of flight or single carrier device methods, and it would be interesting to see if the charge transport properties were significantly different from in comparable dendrimer films.

The high luminescence efficiency and easy processing of organic semiconductors were used to good effect in Chapter 8 to enhance the UV response of a silicon photodiodes. As silicon photodiodes do not show much response to UV light but are sensitive to longer wavelengths, a luminescent layer was added to the top of the devices to downcovert the energy of incident light. By using a blend of a long

wavelength emitting polymer with a higher energy host efficient absorption in the UV was combined with re-emission at wavelengths were the silicon photodiode was most sensitive achieving 61% external quantum efficiency. The strong absorbance of the enhancement layers allowed thin ~100 nm films to be used which would be thin enough to be used for enhancement of multipixel detectors like CCDs without introducing cross talk between pixels. This is promising because it shows an efficiency significantly better than 20-30% EQE reported for currently used lumogen devices [14, 15], but also it can be solution processed, rather than the normally deposited via thermal evaporation in high vacuum normally used for lumogen.

The next step for this project would be the enhancement of a CCD device and to determined the effects of the enhancement layer on pixel cross talk. Further optimisation of this enhancement layer would also be possible by varying materials, blend ratios and layer thicknesses. Although these devices were shown to be stable in air, their lifetime would need to be investigated and controlled under operating conditions. This would possibly involve making use of UV transparent thin film encapsulation.

Emissive organic light emitting diode displays are already being deployed commercially and in the future solution processable OLEDs, possibly on flexible substrates, may provide low cost, energy efficient portable device displays and large area low-glare lighting and signage [2]. This thesis has contributed to the investigation of high efficiency phosphorescent materials available for solution processed OLEDs. By combing the strengths of organics with inorganics hybrid devices allow us make use of the best of both systems. For example using organic layers as light concentrators for high performance but expensive inorganic solar cells [16] or making compact LED pumped tuneable polymer lasers [17]. In this work I have shown that solution processed organics are versatile and efficient materials for making hybrid UV photodetectors. Taking all of this into account, the future of organic optoelectronics looks bright indeed.

1. Burn, P.L., S.C. Lo, and I.D.W. Samuel, *The development of light-emitting dendrimers for displays.* Advanced Materials, 2007. **19**(13): p. 1675-1688.
2. Forrest, S.R., *The path to ubiquitous and low-cost organic electronic appliances on plastic.* Nature, 2004. **428**: p. 911.

3. Yan, H., et al., *A high-mobility electron-transporting polymer for printed transistors.* Nature, 2009. **457**(7230): p. 679.
4. Shimoda, T., et al., *Inkjet printing of light-emitting polymer displays.* Mrs Bulletin, 2003. **28**(11): p. 821-827.
5. Wang, Y., et al., *1,4,5,8,9,12-hexamethyltriphenylene. A molecule with a flipping twist.* Journal of the American Chemical Society, 2007. **129**(43): p. 13193-13200.
6. Markovitsi, D., et al., *Triphenylene Columnar Liquid-Crystals - Excited States and Energy Transfer.* Journal of Physical Chemistry, 1995. **99**(3): p. 1005-1017.
7. Di Donato, E., et al., *Tuning Fluorescence Lifetimes through Changes in Herzberg-Teller Activities: The Case of Triphenylene and Its Hexamethoxy-Substituted Derivative.* Journal of Physical Chemistry A, 2009. **113**(23): p. 6504-6510.
8. Kokkin, D.L., et al., *Gas phase spectra of all-benzenoid polycyclic aromatic hydrocarbons: Triphenylene.* Journal of Chemical Physics, 2007. **126**(8).
9. Baldo, M.A., et al., *Highly efficient phosphorescent emission from organic electroluminescent devices.* Nature, 1998. **395**(6698): p. 151-154.
10. Lo, S.C., et al., *Green phosphorescent dendrimer for light-emitting diodes.* Advanced Materials, 2002. **14**(13-14): p. 975.
11. Sudhakar, M., et al., *Phosphorescence quenching by conjugated polymers.* Journal of the American Chemical Society, 2003. **125**(26): p. 7796-7797.
12. Suzuki, M., et al., *Highly efficient polymer light-emitting devices using ambipolar phosphorescent polymers.* Applied Physics Letters, 2005. **86**(10): p. 103507.
13. Gambino, S., et al., *Control of Charge Transport in Iridium(III) Complex-Cored Carbazole Dendrimers by Generation and Structural Modification.* Advanced Functional Materials, 2009. **19**(2): p. 317-323.
14. Blouke, M.M., et al., *Ultraviolet Downconverting Phosphor for Use With Silicon CCD Imagers.* Applied Optics, 1980. **19**(19): p. 3318-3321.
15. Garnir, H.P. and P.H. Lefebvre, *Quantum efficiency of back-illuminated CCD detectors in the VUV region (30-200 nm).* Nuclear Instruments & Methods in Physics Research Section B-Beam Interactions with Materials and Atoms, 2005. **235**: p. 530-534.
16. Currie, M.J., et al., *High-efficiency organic solar concentrators for photovoltaics.* Science, 2008. **321**(5886): p. 226-228.
17. Yang, Y., G.A. Turnbull, and I.D.W. Samuel, *Hybrid optoelectronics: A polymer laser pumped by a nitride light-emitting diode.* Applied Physics Letters, 2008. **92**(16): p. 163306.

Appendix: Publications

Chapter 5: Fluorescent Enhancement Using a Twisted Tripheneylene Derivative

J. W. Levell, A. Ruseckas, J. B. Henry, Y. Wang, A. D. Stretton, A. R. Mount, T. H. Galow, I. D. W. Samuel, *Fluorescence Enhancement by Symmetry Breaking in a Twisted Triphenylene Derivative.* Journal of Physical Chemistry A, 2010. **114**(51): p. 13291.

Chapter 6: Poly(dendrimer) Iridium Complexes

Lai, W.Y., et al., *A study on the preparation and photophysical properties of an iridium(III) complexed homopolymer.* Journal of Materials Chemistry, 2009. **19**(28): p. 4952-4959.

W. Y. Lai, J. W. Levell, A. C. Jackson, S. C. Lo, P. V. Bernhardt, I. D. W. Samuel, P. L. Burn, *A Phosphorescent Poly(dendrimer) Containing Iridium(III) Complexes: Synthesis and Light-Emitting Properties.* Macromolecules, 2010. **43**(17): p. 6986-6994.

W. Y. Lai, J. W. Levell, S. C. Lo, P. L. Burn, and I. D. W. Samuel, *The 'Double Dendron' Approach to Host Free Phosphorescent Poly(dendrimer) OLEDs.* Advanced Materials, 2011. **Submitted**

Related Work:

J. P. Gunning, J. W. Levell, M. F. Wyatt, P. L. Burn, J. Robertson, I. D. W. Samuel, *The development of poly(dendrimer)s for advanced processing.* Polymer Chemistry, 2010. **1**(5): p. 730-738.

J. W. Levell, J. P. Gunning, P. L. Burn, J. Robertson, I. D. W. Samuel, *A phosphorescent poly(dendrimer) with increased viscosity for solution-processed OLED devices* Organic Electronics, 2010. **11**(9): p. 1561-1568

Conference Proceedings:

J. P. Gunning, K. A. Knights, J. C. Ribierre, R. E. Harding, J. W. Levell, P. L. Burn, I. D. W. Samuel, *Light-emitting poly(dendrimer)s - art. no. 70511X.* Proceedings of the SPIE, 2008. **7051**: p. X511-X511.

J. W. Levell, W. Y. Lai, S. C. Lo, P. L. Burn and I. D. W. Samuel, *Iridium (III) Complex-based Small Molecules, Dendrimers and Poly(dendrimers) for Organic Light-Emitting Diodes,* Polymer Preprints, 2011. **Submitted**

Chapter 7: Phosphorescent Copolymer Dendrimers

J. W. Levell, W. Y. Lai, R. J. Borthwick, S. C. Lo, P. L. Burn and I. D. W. Samuel, *Efficient phosphorescence by reducing intrachain chromophore interactions in dendrimer containing polymers*, Journal of Physical Chemistry C, 2011. **Submitted**

J. W. Levell, W. Y. Lai, S. C. Lo, P. L. Burn and I. D. W. Samuel, *Carbazoyl /iridium dendrimer based phosphorescent copolymers for efficient light emitting devices,* New Journal of Chemistry, **In Preparation**

Chapter 8: UV Enhanced Hybrid Photodiodes

Levell, J.W., M.E. Giardini, and I.D.W. Samuel, *A hybrid organic semiconductor/silicon photodiode for efficient ultraviolet photodetection.* Optics Express, 2010. **18**(4): p. 3219-3225.

Other Publications

G. C. Fortman, A. Poater, J. W. Levell, S. Gaillard, A. M. Z. Slawin, I. D. W. Samuel, L. Cavallo, S. P. Nolan, *A versatile gold synthon for acetylene C-H bond activation.* Dalton Transactions, 2010. **39**(43): p. 10382-10390.